Relay-Assisted Free-Space Optical Communications

by

Majid Safari

A thesis
presented to the University of Waterloo
in fulfillment of the
thesis requirement for the degree of
Doctor of Philosophy
in
Electrical and Computer Engineering

Waterloo, Ontario, Canada, 2010

AUTHOR'S DECLARATION

I hereby declare that I am the sole author of this thesis. This is a true copy of the thesis, including any required final revisions, as accepted by my examiners.

I understand that my thesis may be made electronically available to the public.

Abstract

The atmospheric lightwave propagation is considerably influenced by the random variations in the refractive index of air pockets due to turbulence. This undesired effect significantly degrades the performance of free-space optical (FSO) communication systems. Interestingly, the severity of such random degradations is highly related to the range of atmospheric propagation. In this thesis, we introduce relay-assisted FSO communications as a very promising technique to combat the degradation effects of atmospheric turbulence. Considering different configurations of the relays, we quantify the outage behavior of the relay-assisted system and identify the optimum relaying scheme. We further optimize the performance of the relay-assisted FSO system subject to some power constraints and provide optimal power control strategies for different scenarios under consideration. Moreover, an application of FSO relaying technique in quantum communications is investigated. The results demonstrate impressive performance improvements for the proposed relay-assisted FSO systems with respect to the conventional direct transmission whether applied in a classical or a quantum communication channel.

Acknowledgements

I would like to take this opportunity to thank those who have helped me to complete this thesis. I would like to foremost thank my supervisor, Professor Murat Uysal. This thesis would not have been possible without his consistent guidance and support. I have had a great opportunity to work with him and have learned a lot from him throughout the course of my PhD studies.

I would like to thank the members of my dissertation committee, Professors Robert Schober, Gregor Weihs, Liang-Liang Xie, Pin-Han Ho, and Amir K. Khandani for taking the time out of their busy schedules to carefully review my thesis, providing me with insightful questions and suggestions. I am also thankful to my colleague, Mohammad Mansouri Rad, for helping with the simulation results of chapter 4 and all other members of our research group for their help and support. As indicated in the introduction of the thesis, we have already reported some of the contributions and the results of the thesis in IEEE journals and conference publications.

I would like to lovingly thank my wife, Afrooz, for her unconditional love, kindness, and patience. My warmest gratitude goes to my parents and siblings who always supported me throughout my life. I would like to specially thank my elder brother, Saeed, who inspired me during the earlier stages of my education. I will be forever indebted to my family for their unlimited trust and willingness to endure with me the difficulties and stresses of my endeavors.

Finally, I would like to thank my wonderful friends with whom I have shared many happy moments of our lives: Maziar Sharbafi, Saeed Kamalinia, Mohammad shakiba, Sattar Taheri, Masoud Koochakzadeh, Vahid Shahmansouri, Hesam Hajimiri, Vahid Pourahmadi, Javad Abdoli, Mahdi Zamani, and Mehdi Torbatian.

This thesis is dedicated

to my love, Afrooz,

and

to my dear parents.

Table of Contents

List of Figures

List of Abbreviations

AF	amplify-and-forward.
APD	avalanche photodiode.
ARDO	asymptotic relative diversity order.
AWGN	additive white Gaussian noise.
BPPM	binary pulse position modulation.
cdf	cumulative distribution function.
CSI	channel state information.
DF	decode-and-forward.
FSO	free-space optical.
IM/DD	intensity modulation direct detection.
IP	internet protocol.
KKT	Karush-Kuhn-Tucker.
LED	light emitting diode.
LEO	low earth orbit.
LTPC	long-term power constraint.

MIMO	multiple-input multiple-output.
MISO	multiple-input single-output.
MLSD	maximum likelihood sequence detection.
OOK	on-off keying.
OSTBC	orthogonal space-time block code.
PBS	polarizing beam splitter.
pdf	probability distribution function.
PPM	pulse position modulation.
PSK	phase shift keying.
QAM	quadrature amplitude modulation.
QBER	quantum bit error rate.
QKD	quantum-key distribution.
RDO	relative diversity order.
RF	radio frequency.
SISO	single-input single-output.
SNR	signal-to-noise ratio.
STPC	short-term power constraint.
XOR	exclusive disjunction.

List of Symbols

$g_{i,j}$	Normalized channel gain of the link connecting i^{th} and j^{th} nodes
α_i	Channel state variable at i^{th} hop
χ	Turbulence-induced log-amplitude fluctuation
$\ell(.)$	Path loss factor
η	Quantum efficiency of photodetector
λ	Wavelength
Ω_{fv}	Field of view of the receiver
$\mathrm{W}_{-1}(\cdot)$	-1^{th} branch of Lambert-W function
σ_χ^2	Fading log-amplitude variance
φ	Turbulence-induced phase fluctuation
$\xi(\vec{\rho})$	Spatial beam pattern
a	Absorption-and-scattering loss coefficient
A_{RX}	Receive pupil area
A_{TX}	Transmit pupil area
f_c	Carrier frequency

h Turbulence-induced fading coefficient

$h(\vec{\rho}, \vec{\rho}')$ Green's function for atmospheric propagation

$I(\alpha_i, \mu_i)$ Maximum mutual information of the i^{th} hop

$I_M(\boldsymbol{\alpha}, \boldsymbol{\mu})$ Maximum mutual information of the multi-hop Poisson channel

K Number of relays

L Distance between the source and destination

R Responsivity of the photodetector

Chapter 1

Introduction

Free-space optical communication refers to terrestrial line-of-sight optical transmission through the atmosphere [1]. This technology has recently attracted a renewed interest within the research community although its roots can be traced back to Alexander Graham Bell's "photophone" [2]. In this first free-space optical (FSO) experiment carried out on February 18, 1880, Bell was able to transmit voice signals through a modulated beam of light via atmosphere for a distance of about 200 m. Although Bell's photophone never came out as a commercial product, it has successfully demonstrated the potential of FSO transmission.

Today's FSO systems use either lasers or light emitting diodes (LEDs) to transmit a modulated beam of visible/infrared light [3]. These systems are license-free with high-bandwidth capacity providing a cost-effective and easy-to-install alternative to fiber optics. They further provide an inherent security due to the nature of their directional and narrow beams which make eavesdropping and jamming nearly impossible. With its unique features, FSO communication is appealing for a number of applications including last-mile access, fiber back-up, back-haul for wireless cellular networks, and disaster recovery [4].

Despite the major advantages of FSO, its widespread use has been hampered by its rather disappointing performance for long-range links. For link ranges longer than 1 km,

atmospheric turbulence-induced fading becomes a major performance limiting factor in FSO systems [5]. Although FSO links are built taking into account a certain dynamic margin, the practical limitations on link budgets do not allow very high margins leaving the link vulnerable to deep fades. Therefore, powerful fading-mitigation techniques need to be employed for FSO links particularly with transmission range of 1 km or longer.

1.1 Previous Works

Error control coding in conjunction with interleaving can be employed in FSO communications to combat fading [6], [7]. However, optical links with their transmission rates of order of gigabits need to deal with highly correlated channel states over a large number of consecutive bits. For most scenarios, this requires large-size interleavers to achieve the promised coding gains. Based on the statistical properties of turbulence-induced fading, maximum likelihood sequence detection (MLSD) is proposed in [8] as another solution for fading mitigation. However, MLSD requires complicated multidimensional integrations and suffers from excessive computational complexity.

Spatial diversity techniques [9, 10, 11, 12, 13], i.e., the employment of multiple transmit/receive apertures, provide an attractive alternative approach for fading compensation with their inherent redundancy. Besides its role as a fading-mitigation tool, multiple-aperture designs significantly reduce the potential for temporary blockage of the laser beam by obstructions (e.g., birds). Further justification for the employment of multiple apertures comes from limitations in transmit power density. The allowable safe laser power depends on the wavelength and obviously a higher power at the transmitter side allows the system to support longer distances and through heavier attenuation while achieving higher data rates.

It is well known from the vast literature on wireless radio frequency (RF) systems that simply sending the same signal from multiple transmit antennas (i.e., repetition coding) does not realize any transmit diversity advantage. This is also the case for FSO links with heterodyne reception and it is indeed demonstrated in [14] that conventional orthogonal space-time block codes (OSTBCs) designed for wireless RF systems can be

employed in heterodyne FSO links with quadrature amplitude modulation (QAM) or phase shift keying (PSK). These codes, however, cannot be employed in the intensity modulation direct detection (IM/DD) FSO systems since they require signal's phase information which is not available in the case of intensity modulation. In [15], Simon and Vilnrotter have proposed a modified version of Alamouti code [16] (i.e., OSTBC for two transmit antennas) for FSO IM/DD links by avoiding the necessity of transmitting the negative of a modulation signal. However, the question arises if we need modified OSTBCs for FSO IM/DD systems where the repetition code is able to extract spatial diversity advantages, [9, 10, 11, 12, 13], unlike RF or heterodyne FSO communications. If yes, how much improvement they can provide with respect to the simple repetition code? The answer is interestingly "No". In [17], we have clearly demonstrated that utilization of OSTBCs is not necessary, even detrimental in some cases, for an FSO IM/DD link.

Cooperative diversity has been recently introduced as an alternative way of realizing spatial diversity advantages [18, 19, 20]. The main idea behind cooperative diversity is based on the observation that in a wireless RF channel, the signal transmitted by the source node is overheard by other nodes, which can be defined as partners or relays. The source and its partners can jointly process and transmit their information, creating a virtual antenna array although each of them is equipped with only one antenna. Multi-hop transmission is an alternative relay-assisted transmission scheme which employs the relays in a serial configuration [21]. Such schemes are typically used to broaden the signal coverage for limited-power transmitters and do not offer performance improvement against fading effects in wireless RF environments, i.e., it does not increase the diversity order [18].

To the best of our knowledge, relay-assisted FSO transmission was first proposed by Acampora and Krishnamurthy in [22]. Their work, however, has a networking perspective and does not address the physical layer aspects which our work aims to focus on. In [23], Akella et al. have studied the bit error rate performance of a decode-and-forward FSO multi-hop scheme. Their channel model considers only path-loss and ignores the fading effects. In [24] and [25], Tsiftsis et al. have considered K and Gamma-Gamma atmospheric-induced fading models without explicitly taking into

account the path-loss and evaluated outage probability for a multi-hop FSO system. Their results demonstrate the usefulness of relay-assisted transmission as a method to broaden the coverage area, but do not highlight its use as a fading-mitigation tool which is demonstrated in our work.

1.2 Relay-Assisted FSO Communications

In this thesis, we introduce relay-assisted FSO communications as a very promising technique to combat the atmospheric turbulence degradations. We present an extensive investigation of the relay-assisted FSO communications based on both the Poisson and Gaussian channel models commonly used in the literature. Furthermore, as an application of FSO communications, we study an FSO quantum-key distribution (QKD) system employing a proposed passive relaying strategy.

The impressive performance of the proposed relay-assisted FSO systems can be mainly described by the distance-dependency of the turbulence-induced fading. This is a major difference between the wireless RF and wireless optical systems and allows multi-hop FSO transmission bring performance improvements against the degrading effects of fading, as reflected by our performance analysis and numerical results. The main contributions and the results of this thesis which have been also reported in [26, 27, 28, 29] can be categorized in three parts as follows.

1.2.1 Relay-Assisted FSO Communication over the Gaussian Channel

In the first part, we consider IM/DD FSO communication systems modeled by an additive white Gaussian noise (AWGN) channel. Relay-assisted FSO systems with Different configurations of the relays are investigated whether they are employed in serial (i.e., multi-hop transmission) or in parallel (i.e., cooperative diversity). Our investigation on multi-hop FSO differs from earlier work in [23, 24, 25] in the sense that we explicitly take into account both path-loss and fading effects. We also consider parallel relaying as

a possible alternative to serial relaying. It is obvious that broadcast nature of wireless RF transmission (i.e., the cost-free possibility of the transmitted signals being received by other than destination nodes) is not present in FSO transmission which is based on line-of-sight transmission through directional beams. Therefore, we create an artificial broadcasting through the use of multiple transmitter apertures directed to relay nodes and propose a parallel relaying transmission scheme.

For both the parallel and serial transmissions under consideration, we derive expressions for outage probability assuming amplify-and-forward (AF) and decode-and-forward (DF) relaying. We present a diversity gain analysis through the derivation of so-called relative diversity order (RDO) particularly applicable to the log-normal channel under consideration [30]. We further present an extensive simulation study to confirm our derivations. In particular, the outage probability analysis demonstrates that an impressive performance improvement of 18.5 dB is possible with the use of a single relay at a target outage probability of 10^{-6} and this improvement enhances by inserting more relays within the link. It is also observed that parallel relaying takes advantage of the distance-dependency of the fading variance to a lesser extent and is outperformed by serial relaying as the number of relays increases.

1.2.2 Relay-Assisted FSO Communication over the Poisson Channel

In this part, we consider shot noise-limited IM/DD FSO systems commonly modeled by the Poisson channel. The outage behavior of the multi-hop atmospheric turbulent Poisson channel with a constant rate and transmission delay constraint is studied. It is assumed that perfect channel state information (CSI) is available at the receiver side; however, it may or may not be available at the transmitter side. We solve the outage probability minimization problem for the decode-and-forward multi-hop Poisson channel subject to a peak power constraint as well as a short- or long-term average sum power constraint. As a result, the optimal power control strategies are provided for different scenarios under consideration. Furthermore, a simple and accurate sup-optimal solution is proposed for the case of perfect CSI at the transmitters with short-

term average power constraint where the calculation of the power control law involves solving a nonlinear equation.

The results show that the relaying strategy significantly improves the outage probability of the system operating over the turbulence-degraded Poisson channel and this improvement enhances as the number of relays increases. Moreover, we observe that available CSI at the transmitters can improve the outage probability of the system under both short- and long-term power constraints except for a single-hop Poisson channel with short-term power constraint.

1.2.3 Relay-Assisted Free-space Quantum-Key Distribution

In the last part of the thesis, we propose a terrestrial relay-assisted scheme for a free-space quantum key distribution system based on BB84 protocol. The QKD scheme uses elementary quantum systems such as polarized photons to transfer secret keys between two points [31, 32]. We consider the deployment of passive relays which simply redirect (i.e., collect and point) the qubits (quantum bits) to the next relay node or to the receiver without performing any measurement or detection process. These relays, which can be implemented by adaptive optics, reconstruct the turbulence-degraded wave-front of the received beam and redirect the resulting collimated beam to the next relay or destination.

We investigate the efficiency of such relay-assisted systems to combat the range limitations in a terrestrial scenario. Based on a near-field analysis, we derive an upper bound on quantum bit error rate (QBER) of the relay-assisted QKD system. Our results demonstrate that, although the relay-assisted QKD scheme increases the average number of background photons collected at the receiver, it is able to significantly decrease the photon loss caused by diffraction and turbulence. The proposed scheme therefore outperforms point-to-point counterparts in long ranges.

1.3 Organization of the Thesis

In the next chapter, we present a brief introduction to the free-space optical communications. In chapter 3, we propose the relay-assisted FSO communications with different relay configurations and analyze their outage performances and diversity gains based on the Gaussian channel model. In chapter 4, we investigate the optimal performance of the multi-hop FSO system modeled by the Poisson channel and provide optimum power control laws for different scenarios. In chapter 5, we introduce a particular application of the relay-assisted FSO systems in quantum cryptography and discuss its advantages. Finally, we summarize the thesis in chapter 6.

Chapter 2

Background

2.1 Optical Communication System

The demand increase for high-speed data communication has been accelerated by the growth of Internet usage, internet protocol (IP) television, and Voice over IP. This strong demand for high-bandwidth communication encourages engineers to design high bit-rate optical communication systems in which the information is transferred using a high frequency ($\sim$ 100 THz) lightwave carrier. The fiber-optic and free-space optical systems are the two common forms of optical communications. In fiber-optic communications, the information-bearing light is guided through an optical fiber. However, it is radiated over the atmosphere in free-space optical communications.

Figure 2.1 illustrates the block diagram of an optical communication system. A source produces information waveforms which are then modulated onto an optical carrier. The generated optical field is radiated through an optical link (turbulent at-

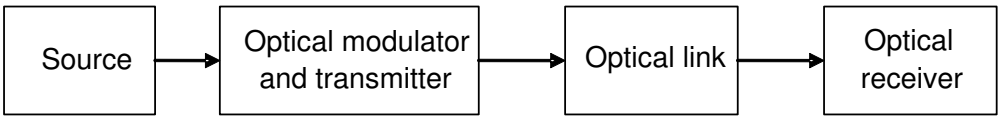

Figure 2.1: The block diagram of an optical communication system.

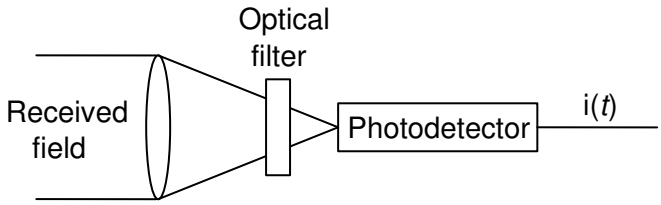

Figure 2.2: The schematic diagram of direct detection receiver.

mosphere or optical fiber) towards a remote destination. At the receiver, the field is optically collected and a photo-detector, located at the focal plane of the collecting lens, transforms the optical field to an electrical current. The receiver processes the detected electrical current to recover the original transmitted information [1].

There are basically two types of optical receivers: Direct detection (non-coherent) receivers and coherent detection receivers. In direct detection receivers (Figure 2.2), the photodetecor directly detect the instantaneous power (or intensity) of the collected field at the receiver aperture. The implementation of such receivers is very simple and cost-effective. However, they can be only employed in intensity-modulation direct-detection systems in which the information is contained in the power variation of the transmitted field.

A form of coherent detection receivers (i.e., heterodyne receiver) is illustrated in Figure 2.3. In this detection technique, the received field is optically mixed before photodetection with a locally generated optical field through a front-end mirror. Amplitude, frequency, or phase modulation can be used in optical communication systems employing coherent reception. However, such receivers are much more difficult to implement in comparison to non-coherent counterparts and require spatially coherent combining of the received field and the locally generated field [1].

Since coherent FSO communication, although possible, is rarely employed in current systems due to technical difficulties and high cost, practical interest lies in the design of IM/DD FSO systems which will be the focus of this thesis. IM/DD communication systems use intensity modulation techniques such as on-off keying (OOK) or pulse position modulation (PPM). In OOK, the optical transmitter is “on” during the whole bit interval when “1” is transmitted, and is “off” when “0” is transmitted. On the

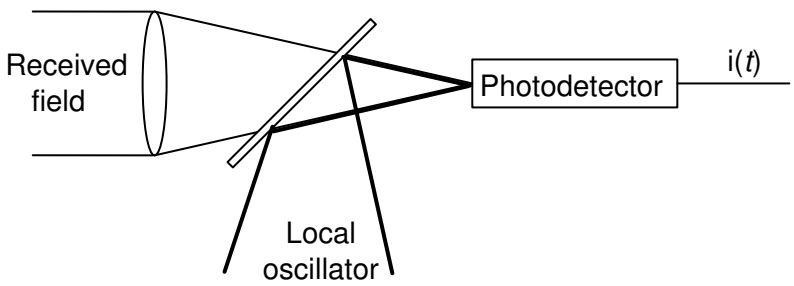

Figure 2.3: The schematic diagram of heterodyne detection receiver.

other hand, in binary pulse position modulation (BPPM), the optical transmitter is "on" during a half of the BPPM bit interval (i.e., "signal slot") and is "off" during the other half (i.e., "non-signal slot"). Although OOK gives a better spectral efficiency with respect to BPPM, it requires threshold detection which needs channel state information. In contrast, the BPPM signal can be easily detected without any need to threshold detection. Nevertheless, the two techniques yield the same error rate performances.

2.2 Atmospheric Turbulence Channel

Atmospheric aerosols and molecules along with bad weather conditions cause absorption and scattering which attenuate the power of the light traveling through atmosphere. Furthermore, the spatial and temporal variations of the air thermal inhomogeneities cause random fluctuations of the refractive index (i.e., atmospheric turbulence) which degrades the performance of optical communication. In this section, we discuss the modeling of an IM/DD free-space optical channel through an atmospheric path.

It is known [33] that the polarization-dependent effects of the turbulent atmosphere which may cause signal distortions due to dispersion effect are negligible especially at the low-loss transmission windows of atmosphere. Therefore, without loss of generality, we assume that the transmitted optical signal is linearly polarized. Using the complex quasi-monochromatic notation, we can then represent the transmitted optical field at $z = 0$ plane as a scalar function of time and space by

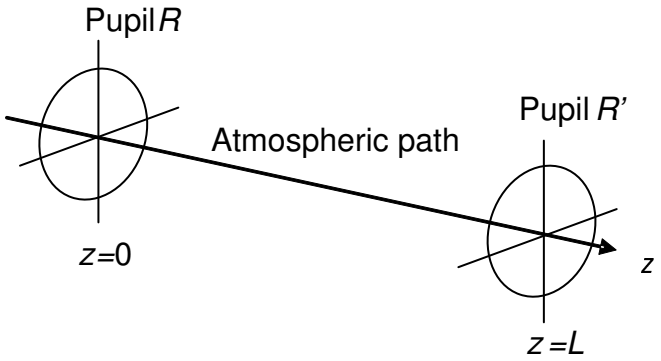

Figure 2.4: The free-space propagation geometry.

$$f(t,\vec{\rho}) = \mathrm{Re}\left\{[\xi(\vec{\rho})x(t)]\, e^{-j2\pi f_c t}\right\} \tag{2.1}$$

where $x(t)$ is the temporal component (modulating signal) and $\xi(\vec{\rho})$ is the spatial component (spatial beam pattern) of the transmitted optical field and f_c is the carrier frequency. Assuming that the beam pattern $\xi(\vec{\rho})$ is transmitted from a circular pupil R located in the plane $z = 0$ as in figure 2.4, the extended Huygens-Fresnel principle [33] yields the received field pattern $\xi'(\vec{\rho}')$ as

$$\xi'(\vec{\rho}') = \int_R \xi(\vec{\rho}) h(\vec{\rho},\vec{\rho}') e^{-aL/2} d\vec{\rho} \tag{2.2}$$

which is collected within the pupil R' in the $z = L$ plane. In (2.2), a is the extinction coefficient which determines the loss due to absorption and scattering and $h(\vec{\rho},\vec{\rho}')$ denotes the paraxial[1] Green's function for atmospheric propagation through clear turbulent air and is given by [33]

$$h(\vec{\rho},\vec{\rho}') = \frac{e^{jkL + jk|\vec{\rho}-\vec{\rho}'|^2/2L}}{j\lambda L} e^{\chi(\vec{\rho},\vec{\rho}') + j\varphi(\vec{\rho},\vec{\rho}')} \tag{2.3}$$

where λ is the wavelength and $k = 2\pi/\lambda$ is the wave number. In (2.3), $\chi(\vec{\rho},\vec{\rho}')$ and

[1]The paraxial assumption is valid here since the propagation of the optical beam is highly directional and the wavelength is much smaller than the spatial scale of the refractive index fluctuations [33].

$\varphi(\vec{\rho},\vec{\rho}')$ are, respectively, the stochastic log-amplitude and phase fluctuation terms describing the atmospheric turbulence of the path connecting the points at $\vec{\rho}$ and $\vec{\rho}'$. Assuming that the transmit beam pattern is normalized such that $\int_R |\xi(\vec{\rho})|^2 d\vec{\rho} = 1$, the optical signal power collected by the receive aperture can be written as

$$P_s = P_t \int_{R'} |\xi'(\vec{\rho}')|^2 d\vec{\rho}' \tag{2.4}$$

where $P_t = \int_R |f(t,\vec{\rho})|^2 d\vec{\rho}$ is the transmitted optical field power. In a far-field scenario which explains most of the practical FSO systems, the received optical power in (2.4) reduces to [9]

$$P_s \approx e^{-aL} \frac{A_{TX} A_{RX}}{(\lambda L)^2} h\, P_t \tag{2.5}$$

where A_{TX} and A_{RX} are respectively the transmit and receive pupil areas and h denotes the turbulence-induced fading coefficient given by

$$h = \left| e^{\chi + j\varphi} \right|^2 = e^{2\chi}. \tag{2.6}$$

We can further define the path loss of the optical link as

$$\ell(L) = e^{-\sigma\, L} \frac{A_{TX} A_{RX}}{(\lambda L)^2} \tag{2.7}$$

which include the atmospheric attenuation caused by diffraction, absorption and scattering.

In the derivation of the received power in (2.5), it is assumed that the transmit and receive apertures are small compared to the spatial coherence length of the turbulent atmosphere. We further consider the far-field assumptions that the distance between source and destination L is much greater than the receive and transmit aperture diameters, i.e., $\lambda L >> A_{RX}, A_{TX}$.

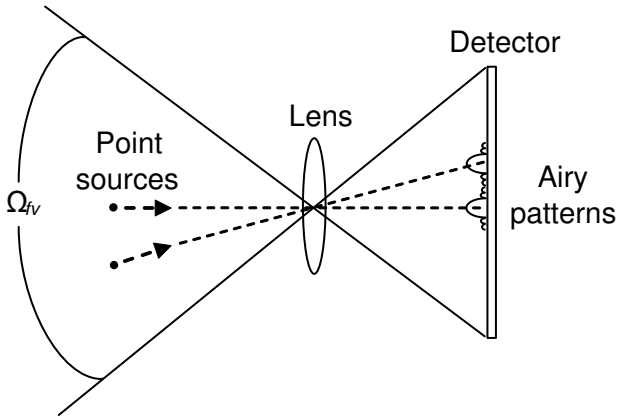

Figure 2.5: The Airy pattern image of two separated point sources on the detector.

At the receiver side, the field collected at the receive aperture is focused by an optical lens onto the detecting surface which is located at the focal plane of the optical lens. The field produced in the focal plane called as diffracted field, is related to the two-dimensional spatial Fourier transform of the received field. The diffracted field forms a familiar pattern known as "Airy pattern" in optical diffraction theory. The Airy pattern occupies a width of about 2λ which is on the order of microns in size [1]. In fact, the Airy pattern is the *image* of point source produced by the lens on its focal plane.

Figure 2.5 illustrates the Airy pattern image of two separated point sources produced by a lens on the detector located at the lens focal plane. The individual Airy patterns superimpose in the focal plane since the optical lens performs a linear transformation. The two patterns can be resolved only if the corresponding point sources are sufficiently separated. In figure 2.5, the solid angle Ω_{fv} represents the *field of view* of the receiver which determines how much of incoming light field is actually detected.

In free-space optical systems, in addition to the desired signal power, a strong background light radiation is also collected by the receive aperture. The background noise is modeled as a uniformly radiating source. The amount of the background noise collected by the receiver is proportional to the receiver field of view and the receiver aperture area as [1]

$$P_b = N(\lambda)\Delta\lambda\Omega_{fv}A_{RX} \tag{2.8}$$

where $N(\lambda)$ and $\Delta\lambda$ are respectively the spectral radiance function and the receiver optical filter bandwidth.

2.2.1 Turbulence-Induced fading

An optical beam traveling through the atmosphere experiences random phase and amplitude fluctuations (scintillation) due to atmospheric turbulence. Turbulence is a chaotic state of the atmospheric flows which is caused by temperature variations in the atmosphere. An atmospheric turbulent medium consists of many spherical regions or eddies with randomly varying diameters and different indexes of refraction. The propagating optical beam experiences random spatial and temporal fluctuations in this randomly-varying-refractive-index medium.

According to Rytov's theory [34], the turbulent medium is assumed to consist of a series of thin slabs. Each slab modulates the optical field from the previous slab's perturbation by some incremental amount e^{ψ_i}. Therefore, the received field can be expressed in terms of the transmitted field U_0 as

$$U = U_0 e^{\psi} = U_0 \prod_i e^{\psi_i} = U_0 e^{\sum_i \psi_i} \tag{2.9}$$

where $e^{\psi} = e^{\chi + j\varphi}$ represents the effect of turbulence-induced fading as a complex multiplicative term. According to the central limit theorem, $\psi = \sum_i \psi_i$ is a complex Gaussian random variable and therefore, the fading log-amplitude (χ) and phase (φ) are normally distributed [34]. As a result, the turbulence-induced fading amplitude ($h_a = |e^{\chi + j\varphi}| = e^{\chi} = \sqrt{h}$) is a log-normal random variable with log-amplitude mean and variance of (μ_x, σ_x^2) and the probability distribution function (pdf) given by

$$f\left(h_a\right) = \frac{1}{h_a\sqrt{2\pi\sigma_x^2}} \exp\left(-\frac{\left(\ln\left(h_a\right) - \mu_x\right)^2}{2\sigma_x^2}\right). \tag{2.10}$$

We normalize the fading coefficient such that $E[h_a^2] = E[h] = 1$ implying $\mu_x = -\sigma_x^2$. This ensures that the fading does not attenuate or amplify the average power [35]. Assuming spherical wave propagation through a horizontal atmospheric path, the log-amplitude variance σ_x^2 can be expressed in terms of wave number (k), refractive index structure constant (C_n^2), and the distance between transmitter and receiver (L) as [34]

$$\sigma_\chi^2 = 0.124 k^{7/6} C_n^2 L^{11/6}. \tag{2.11}$$

As demonstrated in the next chapters, the distance-dependency of the turbulence-induced fading described by (2.11) plays a major role in the performance analysis of FSO communication systems. As reflected by our performance analysis and numerical results, this inherent characteristic allows multi-hop relaying technique bring performance improvements against the degrading effects of turbulence-induce fading in FSO systems, unlike wireless RF communications where the fading effects are not distance-dependent.

In order to describe the spatial correlation of the turbulence-induced fluctuations, we need to establish a statistical relationship between separated points on a turbulent wavefront. For this purpose, we consider the phase and log-amplitude structure functions, respectively, given by [34, 35]

$$D_\phi(r) = \left\langle [\varphi(\vec{\rho}') - \varphi(\vec{\rho})]^2 \right\rangle, \tag{2.12}$$

$$D_\chi(r) = \left\langle [\chi(\vec{\rho}') - \chi(\vec{\rho})]^2 \right\rangle \tag{2.13}$$

where $\vec{\rho}'$ and $\vec{\rho}$ are position vectors on a plane perpendicular to the direction of the propagation of the turbulent wave and the angle brackets denote the ensemble average. Since the turbulent phase and log-amplitude are locally stationary, their structure functions depend only on the distance between the separated points $r = |\vec{\rho}' - \vec{\rho}|$. Therefore, the sum of the phase and log-amplitude structure functions which is called wave structure function can be described using a well-known expression as [35]

$$D(r) = D_\chi(r) + D_\varphi(r) = 6.88 \left(\frac{r}{r_0}\right)^{5/3} \tag{2.14}$$

where r_0 is the Fried parameter which can be written for the spherical waves as

$$r_0 = 0.331 \left(\frac{\lambda^2}{C_n^2 L}\right)^{3/5} \tag{2.15}$$

which yields a measure of spatial coherence length of the atmospheric turbulence fluctuations.

Various experiments have confirmed the validity of log-normal model under weak turbulence conditions [34]. These weak turbulence conditions occur at the linear region of scintillation index which saturates at $\sigma_\chi^2 = 0.5$[9][2]. Although early measurements proposed log-normal statistics even for the saturated turbulence regime but later it was theoretically and experimentally shown that this assumption is only partially true.

It is generally accepted that for very large values of σ_χ^2, the irradiance (i.e. optical intensity fluctuation) statistics approach negative exponential distribution [34]. There are also other turbulence models including Log-normal-Rician distribution [36], I-K distribution [37], and gamma-gamma distribution [3] which take into account stronger turbulence effects. In this thesis, we study weak turbulence conditions where the turbulence-induced fading can be precisely modeled by log-normal distribution.

2.3 Optical Detection and Receiver Noise

Optical receivers employ photodetector to transform the received optical power to an electrical signal. If the frequency of the light (energy of the photons) is sufficiently high, the photosensitive surface of the photodetector responds to incident light (photon streams) by releasing free electrons from its inner surface. The released electrons are then accumulated at a collecting anode and produce an electrical current.

[2]Some references reported the saturating point at $\sigma_\chi^2 = 0.3$.

One of the most important problems occurs during the reception of photon streams is shot effect. The emission of photons on to the photosensitive surface releases electrons in random time instances. The average rate of the electron releases (Λ electron/second) is proportional to the incident field intensity (i.e. optical power). Since the electrons are released independently, the probability of an electron release occurrence in a very short time interval (Δt) can be calculated as the average rate multiplied by the time interval (i.e. $\Lambda\Delta t$). Under these assumptions, the electron count in a time interval of $\tau = n\Delta t$ is described by an n-Bernoulli trial event which is governed by "binomial distribution". For $n \to \infty$ and $\Delta t \to 0$, the electron count process can be described by the Poisson distribution as a limiting case of Binomial distribution. Therefore, the electron count during a certain time interval of τ with the average count rate of Λ can be characterized by a Poisson process $\nu(t)$ as [1]

$$\Pr(\nu(t+\tau) - \nu(t) = j) = e^{-\Lambda}\frac{\Lambda^j}{j!} \qquad j = 0,\ 1,\ 2,\ \ldots. \tag{2.16}$$

This count distribution is indeed conditional Poisson, conditioned on a known value for Λ. Therefore, for a random Λ, the counting process is a conditional Poisson or doubly stochastic Poisson process. The quantity Λ can be expressed as the time average of instantaneous received optical power as

$$\Lambda = \frac{\eta}{\hbar\omega}\int_{t}^{t+\tau} P(t')dt' = \frac{\eta}{\hbar\omega}\int_{t}^{t+\tau} (P_s(t') + P_n(t'))dt' \tag{2.17}$$

where η is quantum efficiency of the photodetector, $\hbar$ is the reduced Planck constant, ω is the optical angular frequency, P_s is the instantaneous optical signal power collected by the receiver lens. In (2.17), P_n is the noise power which corresponds to the sum of background noise level (P_b) and the "dark current" level (P_d). Dark current corresponds to the random emission of electrons at a fixed rate, when no field is being emitted.

A released electron at a random time instance t_i produces a response pulse $Q(t-t_i)$ such that $\int_{-\infty}^{\infty} Q(t')dt' = q$ where q is the electron charge. The superposition of the response pulses of all the released electrons constitutes an electric current $i(t)$ at the

output of the photodetector which can be described by the shot noise process as

$$i(t) = \sum_{i=1}^{\nu(t)} Q(t - t_i) \tag{2.18}$$

with mean μ_i and variance σ_i^2 which are, respectively, given by

$$\mu_i = \Lambda \int_{-\infty}^{\infty} Q(t')dt' = q\Lambda, \tag{2.19}$$

$$\sigma_i^2 = \Lambda \int_{-\infty}^{\infty} Q^2(t')dt'. \tag{2.20}$$

The characteristic function of this shot noise process can be expressed as

$$C_i(jy) = \exp\left(\Lambda \int_{-\infty}^{\infty} \left[\exp(jyQ(t')) - 1\right] dt'\right). \tag{2.21}$$

Considering an ideal photodetector with an impulse response function, the shot noise process reduces to the original photon counting process (i.e., Poisson process). Integrating the photodetection current over the signal duration, the received signal can be expressed in terms of the Poisson process $\nu(t)$ as

$$P_r = \int_0^T i(t)dt = \sum_{i=1}^{k} \int_0^T q\delta(t - t_i)dt = \sum_{i=1}^{k} q = q\left[\nu(T) - \nu(0)\right] \tag{2.22}$$

with mean μ_r and variance σ_r^2 given by

$$\mu_r = \frac{\eta q}{\hbar\omega} \int_0^T (P_s(t') + P_n(t'))dt', \tag{2.23}$$

$$\sigma_r^2 = \frac{\eta q^2}{\hbar\omega} \int_0^T (P_s(t') + P_n(t'))dt'. \tag{2.24}$$

This photon counting model of the optical receiver referred as the shot-noise-limited receiver leads to a Poisson channel for our FSO communication system which will be the focus of chapter 4 of the thesis. As an alternative to this model, we can consider the high-count-rate regime (many counts expected at each t) of the shot noise process. This model is well suited to the shot-noise-limited receivers when significant background noise is collected by the receiver (i.e., $P_b >> 1 \Rightarrow P = P_s + P_b + P_d >> 1 \Rightarrow \Lambda >> 1$). Inserting the normalized random variable $x = (i - \mu_i)/\sigma_i$ in (2.21) and then expanding the argument of the exponential in power series, we obtain

$$C_x(jy) = \exp\left(-\frac{y^2\Lambda}{2\sigma_i^2} \int_{-\infty}^{\infty} Q^2(t')dt' - j\frac{y^3\Lambda}{6\sigma_i^3} \int_{-\infty}^{\infty} Q^3(t')dt' + \frac{y^4\Lambda}{24\sigma_i^4} \int_{-\infty}^{\infty} Q^4(t')dt' + \cdots \right) \tag{2.25}$$

Since $\sigma_i \propto \sqrt{\Lambda}$, the terms of higher order than y^2 vanishes as $\Lambda \to \infty$. Therefore, the characteristic function of the normalized random variable reduces to

$$C_x(jy) = \exp\left(-\frac{y^2}{2}\right) \tag{2.26}$$

which is the characteristic function of the Gaussian distribution. Therefore, we can describe FSO communication systems degraded by strong background radiation using a Gaussian channel model which is the focus of chapter 3.

2.4 Quantum-Key Distribution

Cryptosystems are an indispensable part of modern telecommunication networks to secure the privacy of data transmission and to protect it from electronic copying, cloning,

and destroying, and to also deter unauthorized entry into the network. Vast majority of today's cryptosystems are able to offer only computational security within the limitations of conventional computing power. Moreover, the realization of quantum computers would, for example, make electronic money instantly worthless. Based on the firm laws of quantum mechanics rather than some unproven foundations of mathematical complexity, quantum cryptography provides a radically different solution for key distribution promising unconditional security.

Quantum cryptography builds on a well-known quantum physics rule that no measurement can be taken without perturbing the quantum system, unless the quantum state and the measurement are compatible. It guarantees a provenly-secure communication between a transmitting party (conventionally named as Alice) and a receiving party (conventionally named as Bob). This comes from the fact that a potential eavesdropper (conventionally named as Eve) cannot get any information about the communicated quantum system without introducing perturbations that would reveal her presence. In fact, Alice and Bob can check whether someone was eavesdropping or not by simply comparing a randomly chosen subset of their data using a public channel. If the subset received by Bob was unperturbed, then they can conclude that no measurement has been taken and thus no eavesdropper was present. An end-to-end quantum cryptosystem includes an initial phase of quantum key distribution (QKD) generating a fully secure key between Alice and Bob and a subsequent one-time pad encryption process.

In the one-time pad process proposed by Vernam in 1926 [38], Alice encrypts her message (m) using the randomly generated key (k) through QKD. She adds each bit of the message to the corresponding bit of the key using modulo 2 binary addition to obtain a scrambled text ($s = m \oplus k$). Then she sends the scrambled text to Bob through a public communication channel. Bob can then simply decrypt the message by adding again the shared key ($s \oplus k = m \oplus k \oplus k = m$). Note that the scrambled text is as random as the key and thus it does not contain any information. Therefore, the cryptosystem is provably secure according to the fundamentals of information theory. In fact, this is the only provably secure cryptosystem known today [32].

The first QKD protocol proposed by Bennett and Brassard [39] is today widely known as BB84 which uses elementary quantum systems such as polarized photons to

transfer secret keys between two points. As an alternative to BB84, Ekert [40] has proposed another protocol which involves the emission of two qubits (quantum bits) from a source to Alice and Bob instead of transmitting a single qubit from Alice to Bob. Assuming that the two emitted qubits from the source are in a maximally entangled state, Ekert's protocol avoids trusting the source which can be targeted by eavesdropping attacks. Despite rather different implementation structures, both protocols guarantee equivalently secured QKD systems. A number of other protocols also exist in the literature [32], but they essentially build on these two main protocols.

2.4.1 BB84 Protocol

Figure 2.6 illustrates a schematic diagram of a free-space QKD system which uses BB84 protocol [39] for key distribution. In this system, for each qubit, Alice randomly chooses a polarization basis from two known polarization bases (e.g., $0°/90°$ and $-45°/+45°$). She then sends the qubit with a random bit value of 0 or 1 using polarization encoding of photons based on the randomly chosen basis. Note that the first polarization in each basis ($0°$ and $-45°$) represents 0 and the second one ($90°$ and $+45°$) represents 1.

At the receiver side, Bob also chooses a random basis from the two bases using a passive beam splitter. At the outputs of the beam splitter, two polarization detection units measure the quantum state of the possibly coming photon based on the two different bases. Each of these units includes a polarizing beam splitter (PBS) to decide between two orthogonal polarization states of the corresponding basis and two single-photon Geiger-mode avalanche photodiodes (APDs) at the output of the PBS for photon count.

To avoid uncorrelated measurement results due to incompatibility of the chosen bases, Alice and Bob construct the secure key only based on the qubits received at the *sift* events. Sift events correspond to the bit intervals in which exactly one of the APDs registers a count and both Alice and Bob have chosen the same basis. According to BB84 protocol, Alice and Bob can identify the sift events by exchanging information in a public communication channel. After identifying the sifted qubits, Alice and Bob follow a standard set of operations to identify and correct errors which have occurred

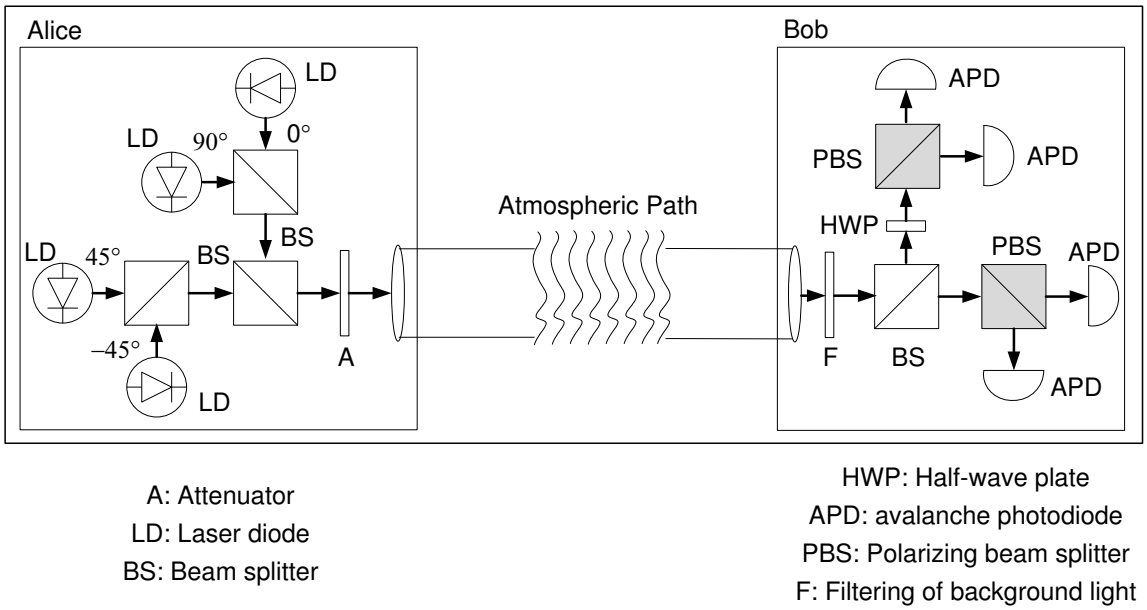

Figure 2.6: The schematic diagram of a free-space QKD system based on BB84 protocol.

in the sifted bits. These errors are caused by dark counts or background noise as well as by potential eavesdropper's intervention. Then, Alice and Bob perform a procedure called *privacy amplification* to prevent Eve from keeping useful information about the key and finally establish a shared one-time pad key to use for secure communication [32].

Chapter 3

Relay-Assisted FSO Communication over the Gaussian Channel

In this chapter, we consider relay-assisted FSO communication over IM/DD optical channels modeled by additive white Gaussian noise (AWGN). We study both serial (i.e., multi-hop transmission) and parallel (i.e., cooperative diversity) relaying encoupled with amplify-and-forward (AF) and decode-and-forward (DF) modes. We consider an aggregated channel model which takes into account both the path loss and turbulence-induced log-normal fading. Since the fading variance is distance dependent in free-space optical systems, relay-assisted transmission takes advantage of the resulting shorter hops and yields significant performance improvements. We derive the outage probability of the relaying schemes under consideration, which are further confirmed through Monte-Carlo simulations. We also present a diversity gain analysis for the relay-assisted FSO systems operating in log-normal atmospheric turbulence channels.

3.1 Relay-Assisted FSO Transmission

We consider a relay-assisted FSO communication system in which the transmitted signal from a source node propagates through K serial or parallel relays before detection

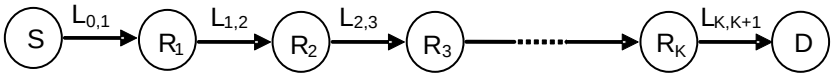

Figure 3.1: The FSO serial relaying configuration.

at the destination node. The system under consideration uses intensity-modulation direct-detection (IM/DD) employing binary pulse position modulation (BPPM). In such systems, optical transmitter is "on" during a half of the BPPM bit interval (i.e., "signal slot") and is "off" during the other half (i.e., "non-signal slot"). The receiver integrates the detected photocurrent over both the signal and non-signal slots of the BPPM pulse and obtains the resulting electrical signal vector given by

$$\mathbf{r} = \begin{bmatrix} r^s \\ r^n \end{bmatrix} = \begin{bmatrix} RT_b(P_s + P_b) + n^s \\ RT_bP_b + n^n \end{bmatrix} \tag{3.1}$$

where r^s and r^n are the received electrical signals which correspond to signal and non-signal slots of the BPPM pulse. In (3.1), P_s and P_b are, respectively, the optical signal power and background power incident on the photodetector, T_b is the duration of the signal and non-signal slots, and $R = \eta q/\hbar\omega$ is responsivity of the photodetector. n^s and n^n in (3.1) denote the additive noise terms for the signal and non-signal slots. We assume that the noise terms are modeled as signal-independent additive white Gaussian noise with zero mean and variance of $\sigma_n^2 = N_0/2$. This is a good approximation for FSO systems in which the receiver signal-to-noise ratio (SNR) is limited by the shot noise caused by background light much stronger than signal (c.f. (2.26)) and/or by the electronics thermal noise [5, 10].

In figures 3.1 and 3.2, we illustrate the serial and parallel relaying schemes under consideration. In serial relaying (figure 3.1), the source transmits an intensity-modulated signal to the relay node. Under the assumption of DF relaying, the relay decodes the signal after direct detection, modulates it with BPPM, and retransmits it to the next relay. If AF relaying is employed, the relay does not perform any decoding on the received signal and, after multiplication with a proper energy scaling term, simply forwards it to the next relay. This continues until the source's data arrives at the destination node.

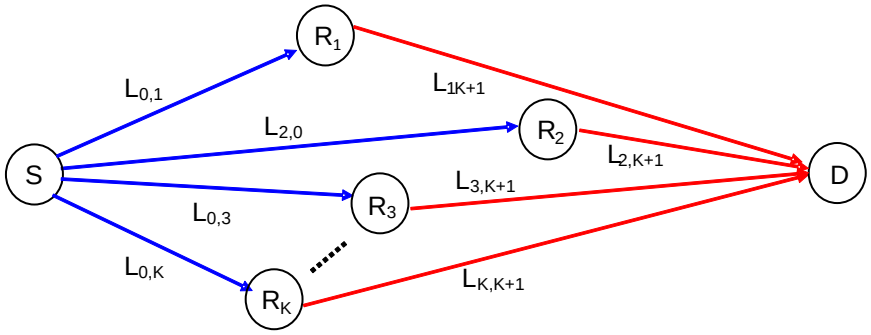

Figure 3.2: The FSO parallel relaying configuration.

Figure 3.2 illustrates a parallel relaying scheme. Since broadcasting is not possible in a line of site FSO communication system, the source is equipped with a multi-laser transmitter with each of the transmitter pointing out in the direction of a corresponding relay node. The source node transmits the same signal to K relays. Based on the AF or DF relaying method, the relays either decode and retransmit the signal or scale the received signal and forward it to the destination. It should be noted that, different from wireless RF communication, distributed space-time block coding across relays is not required because of the ensured orthogonality of the received diffraction patterns from sufficiently separated transmit apertures (cf., section 2.2 and [11, 17]).

3.1.1 Decoded-and-Forward Relaying

In DF relaying, the relay decodes the signal after direct detection, modulates it with BPPM, and retransmits it to the next relay or the destination only if the received SNR exceeds a given decoding threshold γ_{th} defined in section 3.2. Such a threshold is required to avoid error propagation and provide reliable communication [19].

In serial relaying, the received signal at i^{th} node ($i = 1, 2..K+1$) can be expressed using (3.1) as[1]

[1]Throughout this chapter, indexes $i = 0$ and $i = K+1$ refer to the source and the destination nodes respectively, and indexes $i = 1, 2, \cdots, K$ refer to the relay nodes.

$$\mathbf{r}_i = \begin{bmatrix} r_i^s \\ r_i^n \end{bmatrix} = \begin{bmatrix} RT_b(Pg_{i-1,i} + P_b) + n_i^s \\ RT_bP_b + n_i^n \end{bmatrix} \tag{3.2}$$

where r_i^s and r_i^n are the received signals which correspond to signal and non-signal slots of the BPPM pulse. In (3.2), P is the transmitted optical power per transmit aperture which is related to the total transmitted power (P_t) by $P = P_t/(K+1)$ for serial relaying. It is obvious that the optical signal power incident on the photodetector defined in (3.1) is now given as $P_s = Pg_{i-1,i}$ where $g_{i-1,i}$ is the normalized channel gain of the link connecting $(i-1)^{\text{th}}$ and i^{th} nodes. Considering an aggregated FSO channel model where both distance-dependant path loss and turbulence-induced fading are taken into account as discussed in chapter 2, we define a normalized channel gain $g_{i,j}$ as

$$g_{i,j} = \frac{\ell(L_{i,j})}{\ell(L_{0,K+1})} h_{i,j} = \ell_{i,j} h_{i,j} \tag{3.3}$$

where $L_{i,j}$ is the range of the link connecting i^{th} and j^{th} nodes. Furthermore, the log-normal fading coefficient $h_{i,j}$ and the path loss factor $\ell(\cdot)$ are, respectively, given by (2.6) and (2.7). In (3.3), the path loss factor is normalized with respect to the path loss of the direct link connecting the source and destination, i.e., $\ell(L_{0,K+1})$. This normalization simplifies our performance analysis where the performances of FSO links with different lengths are compared.

In parallel relaying, each of the relay nodes receives the transmitted signal from the corresponding transmit apertures pointed in their direction. The received signal at i^{th} relay ($i = 1, 2, ...K$) is given by

$$\mathbf{r}_i = \begin{bmatrix} r_i^s \\ r_i^n \end{bmatrix} = \begin{bmatrix} RT_b(Pg_{0,i} + P_b) + n_i^s \\ RT_bP_b + n_i^n \end{bmatrix} \tag{3.4}$$

where the average optical power per transmit aperture P can be obtained by dividing the total transmitted power by the number of the transmit apertures in parallel relaying

configuration[2] , i.e., $P = P_t/(2K)$. The relay nodes decode their received signals after direct detection, modulate them with BPPM, and simultaneously retransmit to the destination. At the destination, we assume a large receiver field of view which allows all of the optical fields transmitted from different relay nodes are simultaneously detected. Let D denote the *decoded set* which is the set of relays having successfully decoded the signal (i.e., the received SNR exceeds the threshold). The received signal at the destination can be written as the superposition of the transmitted optical signals from the decoded set as

$$\mathbf{r}_{K+1} = \begin{bmatrix} r^s_{K+1} \\ r^n_{K+1} \end{bmatrix} = \begin{bmatrix} RT_b \left(\sum_{i \in D} P g_{i,K+1} + P_b \right) + n^s_{K+1} \\ RT_b P_b + n^n_{K+1} \end{bmatrix}. \tag{3.5}$$

3.1.2 Amplify-and-Forward Relaying

In AF relaying, the relay first scales the received signals by an amplification factor which keeps the average optical transmit power fixed and then retransmits it to the next relay (or to the destination within the last hop). As illustrated in figure 3.3, after photodetection, the power efficiency of the electrical signal can be improved through a debiasing operation where the background noise bias level (i.e., RT_bP_b) is mostly removed from the received signal without any loss of signal information. This debaising operation should preserve the positivity of the electrical signal as it is used to modulate the intensity of transmit laser beam after scaling by an amplifier. To achieve the maximum power efficiency, the debiasing component decreases the level of both signal and non-signal BPPM slots such that one of them reaches zero.

Considering the amplification and debiasing operations, the received signal at i^{th} node ($i = 1, 2..K+1$) for serial relaying is given as

[2]Recall that the source is equipped with K transmitters and each of K relay nodes has one transmitter resulting in a total of $2K$ transmit apertures for this scheme.

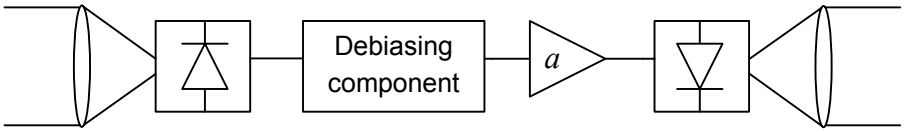

Figure 3.3: The block diagram of the amplify-and-forward relay.

$$\begin{aligned}\mathbf{r}_i = \begin{bmatrix} r_i^s \\ r_i^n \end{bmatrix} &= \begin{bmatrix} a_{i-1}g_{i-1,i}r_{i-1}^s + RT_bP_b - A_i' + n_i^s \\ a_{i-1}g_{i-1,i}r_{i-1}^n + RT_bP_b - A_i' + n_i^n \end{bmatrix} \\ &= \begin{bmatrix} a_{i-1}g_{i-1,i}r_{i-1}^s + A_i + n_i^s \\ a_{i-1}g_{i-1,i}r_{i-1}^n + A_i + n_i^n \end{bmatrix}\end{aligned} \tag{3.6}$$

where $A_i = RT_bP_b - A_i' = -\min\{a_{i-1}g_{i-1,i}r_{i-1,1} + n_i^s, n_i^n\}$ is the bias term included to improve power efficiency. Depending on the additive noise terms and fading amplitudes, the bias term A_i can be positive or negative. In (3.6), the amplification factor at the $(i-1)^{\text{th}}$ node a_{i-1}, $i = 2, 3..K+1$, is defined as

$$a_{i-1} = \frac{RT_bP}{\Gamma_{i-1}}. \tag{3.7}$$

In (3.7), we have normalization term, i.e., $\Gamma_{i-1} = E[r_{i-1}^s + r_{i-1}^n]$, to ensure that the average optical transmitted power from each node remains constant as P. Note that for the signal transmitted from the source, normalization is obviously not required (i.e., $a_0 = RT_bP$). The received signal at the destination for serial relaying is therefore given by

$$\mathbf{r}_{K+1} = \begin{bmatrix} r_{K+1}^s \\ r_{K+1}^n \end{bmatrix} = \begin{bmatrix} \prod_{i=0}^{K} a_i g_{i,i+1} + \sum_{j=1}^{K} (n_j^s + A_j) \prod_{i=j}^{K} a_i g_{i,i+1} + n_{K+1}^s \\ \sum_{j=1}^{K} (n_j^n + A_j) \prod_{i=j}^{K} a_i g_{i,i+1} + n_{K+1}^n \end{bmatrix}. \tag{3.8}$$

In parallel relaying, the relays receive the transmitted signals from the corresponding transmit apertures pointed in the direction of their locations and simultaneously retransmit them with proper amplification and debiasing operations. The received signal at i^{th} relay $(i = 1, 2, ...K)$ is therefore given by

$$\mathbf{r}_i = \begin{bmatrix} r_i^s \\ r_i^n \end{bmatrix} = \begin{bmatrix} RT_bPg_{0,i} + A_i + n_i^s \\ A_i + n_i^n \end{bmatrix} \tag{3.9}$$

and the received signal at the destination is

$$\mathbf{r}_{K+1} = \begin{bmatrix} r_{K+1}^s \\ r_{K+1}^n \end{bmatrix} = \begin{bmatrix} RT_bP\sum_{i=1}^{K} a_i g_{i,K+1} g_{0,i} + \sum_{i=1}^{K} a_i g_{i,K+1}(n_i^s + A_i) + n_{K+1}^s \\ \sum_{i=1}^{K} a_i g_{i,K+1}(n_i^n + A_i) + n_{K+1}^n \end{bmatrix}. \tag{3.10}$$

3.1.3 Calculation of the Normalization Term

The normalization term at i^{th} relay $(i = 1, 2, ...K)$ is given by

$$\Gamma_i = E[r_i^s + r_i^n]. \tag{3.11}$$

After the insertion of the bias term, either r_i^s or r_i^n becomes zero. Therefore, we can rewrite the normalization term as

$$\Gamma_i = E[|r_i^s - r_i^n|]. \tag{3.12}$$

Conditioned on $\bar{g}_i = \{g_{0,1}, g_{1,2}..., g_{i-1,i}\}$, the term $r_i^s - r_i^n$ is real Gaussian with mean $m_i = \prod_{j=0}^{i-1} a_j g_{j,j+1}$ and variance $s_i^2 = \left(1 + \sum_{j=1}^{i-1} \prod_{k=j}^{i-1} a_k g_{k,k+1}\right) N_0$ for serial AF relaying and with mean $m_i = RT_bPg_{0,i}$ and variance $s_i^2 = N_0$ for parallel AF relaying. Its magnitude, therefore, follows a *folded-normal* distribution [41]. Hence, the normalization term conditioned on $\bar{g}_i$ is given by [41]

$$E[r_i^s + r_i^n|\bar{g}_i] = s_i(\bar{g}_i)\sqrt{\frac{2}{\pi}} \exp\left(-\frac{m_i^2(\bar{g}_i)}{2s_i^2(\bar{g}_i)}\right) + m_i(\bar{g}_i)\left(2Q\left(-\frac{m_i(\bar{g}_i)}{s_i(\bar{g}_i)}\right) - 1\right). \tag{3.13}$$

Performing an expectation over $\bar{g}_i$, we obtain

$$\Gamma_i = \int_{\bar{g}_i} f_{\bar{g}_i}(\bar{g}_i) \left(s_i(\bar{g}_i)\sqrt{\frac{2}{\pi}} \exp\left(-\frac{m_i^2(\bar{g}_i)}{2s_i^2(\bar{g}_i)}\right) + m_i(\bar{g}_i)\left(2Q\left(-\frac{m_i(\bar{g}_i)}{s_i(\bar{g}_i)}\right) - 1\right)\right) d\bar{g}_i \tag{3.14}$$

where $f_{\bar{g}_i}(\bar{g}_i)$ is the joint pdf of the log-normal vector $\bar{g}_i$.

The calculation of (3.14) requires numerical computation, but it can be also precisely approximated which is particularly useful for practical implementation. The normalization factor can be rewritten by the law of total probability as

$$\Gamma_i = E[|r_i^s - r_i^n|] = \Pr(r_i^s > r_i^n)E[r_i^s - r_i^n] + \Pr(r_i^n > r_i^s)E[r_i^n - r_i^s]. \tag{3.15}$$

Let P_e denote the average error probability for BPPM modulation scheme. We can then write $\Pr(r_i^s > r_i^n) = 1 - P_e \cong 1$ and $\Pr(r_i^n > r_i^s) = P_e << 1$. Inserting these in (3.15), we find

$$\Gamma_i = E[|r_i^s - r_i^n|] \cong E[r_i^s - r_i^n] = E[m_i] = \begin{cases} \prod_{j=0}^{i-1} a_j \ell_{j,j+1}, & \text{serial relaying} \\ RT_b P \ell_{0,i}, & \text{parallel relaying} \end{cases} \tag{3.16}$$

Inserting (3.16) in (3.7), the amplification factor (for $i > 0$) can be approximated as

$$a_i \cong \begin{cases} \frac{RT_bP}{\prod_{j=0}^{i-1} a_j \ell_{j,j+1}} = \frac{1}{\ell_{i-1,i}}, & \text{serial relaying} \\ \frac{RT_bP}{RT_bP\ell_{0,i}} = \frac{1}{\ell_{0,i}}, & \text{parallel relaying} \end{cases} \tag{3.17}$$

Equation (3.17) shows that the amplification factor in AF relays is only related to the deterministic path loss factor. In other words, to keep the relays' average optical power consumption fixed, the AF relays should approximately compensate only for the average link loss (i.e., path loss factor). We can then obtain the normalization term using (3.16) in (3.17) as

$$\Gamma_i \cong \begin{cases} RT_bP\ell_{i-1,i}, & \text{serial relaying} \\ RT_bP\ell_{0,i}, & \text{parallel relaying} \end{cases} \tag{3.18}$$

It is obvious that the resulting normalization terms in (3.18) are very simple in comparison to (3.14) and can be easily implemented at the relay terminals. Our simulation results further indicate that these approximations result in a negligible difference within the line thickness.

3.2 Outage Probability Analysis

Atmospheric turbulence results in a very slowly-varying fading in FSO systems. The channel coherence time is about 1-10 ms, therefore fading remains constant over hundreds of thousands up to millions of consecutive bits for typical transmission rates [9]. For such quasi-static channels where the errors caused by fading are no longer independent, outage probability is an appropriate metric to evaluate the performance of the system. Denote $C(h')$ as the instantaneous capacity corresponding to a channel realization $h = h'$ which is a function of instantaneous electrical SNR γ. For a Gaussian channel where the mean values of received signal components for the signal and non-signal slots are given by m^s and m^n, we have $r^s \sim N(m^s, \sigma_n^2/2)$ and $r^n \sim N(m^n, \sigma_n^2/2)$. Instantaneous electrical SNR can be then defined as [42]

$$\gamma = \frac{(m^s - m^n)^2}{\sigma_n^2}. \tag{3.19}$$

The outage probability at the transmission rate of R_0 is given by [43]

$$P_{out}(R_0) = \Pr\{C(\gamma) < R_0\}. \tag{3.20}$$

Since $C(\cdot)$ is monotonically increasing with respect to γ, (3.20) can be rewritten as

$$P_{out}(R_0) = \Pr\{\gamma < \gamma_{th}\} \tag{3.21}$$

where $\gamma_{th} = C^{-1}(R_0)$ is the threshold SNR. If SNR exceeds γ_{th}, no outage happens and signal can be decoded with arbitrarily low error probability at the receiver. We note that this threshold SNR is also considered as the DF relaying decoding threshold introduced earlier in 3.1.1.

3.2.1 Outage Probability for DF Relaying

In DF relaying, an outage at each intermediate link may lead to the outage of the relaying scheme. Therefore, the calculation of outage probability for each intermediate link is required to evaluate the end-to-end performance. We first calculate the outage probability of an intermediate single-input single-output (SISO) link which is the building block of both serial and parallel relaying schemes.

Using (3.19), the received electrical SNR for an intermediate SISO link connecting i^{th} and j^{th} nodes can be obtained as

$$\gamma = \frac{R^2 T_b^2 P^2 g_{i,j}^2}{N_0}. \tag{3.22}$$

Inserting (3.22) in (3.21), the outage probability of the SISO link is

$$P_{out,SISO} = \Pr\left\{ g_{i,j} < \sqrt{\frac{\gamma_{th} N_0}{R^2 T_b^2 P^2}} \right\}. \tag{3.23}$$

We replace the definition of $g_{i,j} = \ell_{i,j} h_{i,j}$ in (3.23) and obtain

$$P_{out,SISO} = \Pr\left\{ h_{i,j} < \frac{1}{\ell_{i,j}} \frac{N}{P_M} \right\} \tag{3.24}$$

where $N = K + 1$ for serial relaying and $N = 2K$ for parallel relaying. In (3.24), P_M denotes power margin [10] and is defined as $P_M = P_t / P_{th}$ where P_{th} denotes a threshold transmit power required to guarantee that no outage happens in a direct fading-free transmission from the source to the destination. Thus the power margin can be expressed as

$$P_M = \sqrt{\frac{P_t^2 (RT_b)^2}{N_0 \gamma_{th}}}. \tag{3.25}$$

In (3.24), $h_{i,j}$ is a log-normal random variable with mean $2\mu_\chi(L_{i,j})$ and variance $4\sigma_\chi^2(L_{i,j})$. Therefore the outage probability can be written using the cumulative distribution function (cdf) of the log-normal distribution a

$$P_{out,SISO}(L_{i,j}) = Q\left(\frac{\ln\left(\ell_{i,j} P_M/N\right) + 2\mu_\chi(L_{i,j})}{2\sigma_\chi(L_{i,j})}\right). \tag{3.26}$$

Once we obtain the outage probability of the SISO link, we can now return our attention to end-to-end outage probability for serial and parallel relaying.

Serial DF relaying: In serial relaying, an outage occurs when any of the intermediate SISO links fails. Hence the outage probability for the end-to-end scheme can be given as

$$P_{out} = \Pr\left\{\bigcup_{i=0}^{N} \{\gamma_i < \gamma_{th}\}\right\} \tag{3.27}$$

where $\gamma_0, \gamma_1, \cdots, \gamma_K$ are the SNRs of the intermediate SISO links with the lengths of $L_{0,1}, L_{1,2}, ...L_{K,K+1}$. Eq. (3.27) can be rewritten as

$$P_{out} = 1 - \Pr\left\{\bigcap_{i=0}^{K} \{\gamma_i > \gamma_{th}\}\right\} = 1 - \prod_{i=0}^{K} (1 - P_{out,SISO}(L_{i,i+1})). \tag{3.28}$$

Replacing (3.26) in (3.28), the end-to-end outage probability for serial relaying scheme is obtained as

$$P_{out} = 1 - \prod_{i=0}^{K} \left(1 - Q\left(\frac{\ln\left(\ell_{i,i+1} P_M/(K+1)\right) + 2\mu_\chi(L_{i,i+1})}{2\sigma_\chi(L_{i,i+1})}\right)\right). \tag{3.29}$$

Parallel DF Relaying: In parallel relaying, outage occurrence in one of the intermediate SISO links does not necessarily lead to an outage of the relaying scheme. In this scheme, an outage occurs if either the decoded set D is empty or the multiple-input single-output (MISO) link between the decoding relays and the destination fails. The received SNR for the MISO link can be written as

$$\gamma = \frac{R^2 T_b^2 P^2 \left(\sum_{i \in D} g_{i,K+1} \right)^2}{N_0}. \tag{3.30}$$

Inserting (3.30) in (3.21), the outage probability of the MISO link is obtained as

$$\begin{aligned} P_{out,MISO} &= \Pr \left\{ \sum_{i \in D} g_{i,K+1} < \sqrt{\frac{\gamma_{th} N_0}{R^2 T_b^2 P^2}} \right\} \\ &= \Pr \left\{ \sum_{i \in D} \ell_{i,K+1} h_{i,K+1} < \frac{2K}{P_M} \right\}. \end{aligned} \tag{3.31}$$

We approximate the weighted sum of log-normal random variables in (3.31) as a log-normal random variable using moment matching method [44], i.e., $\beta = \exp(\xi) \approx \sum_{i \in D} \ell_{i,K+1} h_{i,K+1}$. The log-amplitude factor ξ is defined as a normal random variable with mean μ_ξ and variance σ_ξ^2 which can be respectively written as

$$\mu_\xi(\mathbf{L}_D) = \ln \sum_{i \in D} \ell_{i,K+1} - \sigma_\xi^2(\mathbf{L}_D)/2, \tag{3.32}$$

$$\sigma_\xi^2(\mathbf{L}_D) = \ln \left(1 + \sum_{i \in D} \ell_{i,K+1}^2 \left(\exp(4\sigma_\chi^2(L_{i,K+1})) - 1 \right) \Big/ \left(\sum_{i \in D} \ell_{i,K+1} \right)^2 \right). \tag{3.33}$$

The mean and variance of ξ are functions of $\mathbf{L}_D$ which is the set of distances between the decoding relays and the destination (i.e., $L_{i,K+1} \in \mathbf{L}_D$, $\forall i \in D$). Using the cdf of log-normal distribution, (3.31) is approximated as

$$P_{out,MISO}(\mathbf{L}_D) \approx \Pr\left\{\beta < \frac{2K}{P_M}\right\} = Q\left(\frac{\ln\left(P_M/2K\right) + \mu_\xi(\mathbf{L}_D)}{\sigma_\xi(\mathbf{L}_D)}\right). \tag{3.34}$$

For a parallel relaying scheme with K relays, the decoded set consists of 2^K possibilities. Let $\mathrm{S}(i)$ denote the i^{th} possible set and $\Pr\{\mathrm{S}(i)\}$ denote the probability of the event $\{D = \mathrm{S}(i)\}$. The outage probability for parallel relaying scheme can be then obtained as

$$P_{out} = \sum_{i=1}^{2^K} P_{out,MISO}(\mathbf{L}_{\mathrm{S}(i)}) \Pr\{\mathrm{S}(i)\}. \tag{3.35}$$

Noting $\Pr\{\mathrm{S}(i)\} = \Pr\{(\cap_{j\in\mathrm{S}(i)} j \in \mathrm{S}(i)) \cap (\cap_{j\notin\mathrm{S}(i)} j \notin \mathrm{S}(i))\}$, $\Pr\{i \in \mathrm{S}(i)\} = 1 - P_{out,SISO}$, and $\Pr\{i \notin \mathrm{S}(i)\} = P_{out,SISO}$, we can rewrite (3.35) as

$$P_{out} = \sum_{i=1}^{2^K} \left(\prod_{j\in\mathrm{S}(i)} \left(1 - P_{out,SISO}(L_{0,j})\right) \prod_{j\notin\mathrm{S}(i)} P_{out,SISO}(L_{0,j}) \right) P_{out,MISO}(\mathbf{L}_{\mathrm{S}(i)}). \tag{3.36}$$

Replacing (3.26) and (3.34) in (3.36), the end-to-end outage probability for parallel relaying scheme is obtained as

$$\begin{aligned} P_{out} \approx \sum_{i=1}^{2^K} \Bigg[\prod_{j\in\mathrm{S}(i)} \left(1 - Q\left(\frac{\ln\left(\ell_{0,j}P_M/2K\right) + 2\mu_\chi(L_{0,j})}{2\sigma_\chi(L_{0,j})}\right)\right) \\ \times \prod_{j\notin\mathrm{S}(i)} Q\left(\frac{\ln\left(\ell_{0,j}P_M/2K\right) + 2\mu_\chi(L_{0,j})}{2\sigma_\chi(L_{0,j})}\right) \Bigg] Q\left(\frac{\ln\left(P_M/2K\right) + \mu_\xi(\mathbf{L}_{\mathrm{S}(i)})}{\sigma_\xi(\mathbf{L}_{\mathrm{S}(i)})}\right). \end{aligned} \tag{3.37}$$

3.2.2 Outage Probability for AF Relaying

In AF relaying, the intermediate relay nodes forward the signal without any decoding. Thus, instead of considering SNRs in intermediate SISO links, the total received SNR at the destination should be calculated for outage analysis.

Serial AF Relaying: Recall that the received signal at the destination node for serial AF relaying is given by (3.8). Equation (3.8) can be rewritten as

$$\mathbf{r}_{K+1} = \begin{bmatrix} r^s_{K+1} \\ r^n_{K+1} \end{bmatrix} = \begin{bmatrix} \prod_{i=0}^{K} a_i g_{i,i+1} + A_{acc} + n^s_{acc} \\ A_{acc} + n^n_{acc} \end{bmatrix} \tag{3.38}$$

where we define the accumulated noise terms as $n^s_{acc} = \sum_{j=1}^{K} n^s_j \prod_{i=j}^{K} a_i g_{i,i+1} + n^s_{K+1}$, and $n^n_{acc} = \sum_{j=1}^{K} n^n_j \prod_{i=j}^{K} a_i g_{i,i+1} + n^n_{K+1}$. In (3.38), A_{acc} denotes the accumulated bias term and is given by $A_{acc} = \sum_{j=1}^{K} A_j \prod_{i=j}^{K} a_i g_{i,i+1}$. Using (3.19) and (3.38), the received SNR at the destination node is given by

$$\gamma = \frac{\prod_{i=0}^{K} a_i^2 g_{i,i+1}^2}{N_0 \left(\prod_{i=1}^{K} a_i^2 g_{i,i+1}^2 + \prod_{i=2}^{K} a_i^2 g_{i,i+1}^2 + \cdots + a_K^2 g_{K,K+1}^2 + 1 \right)}. \tag{3.39}$$

Defining

$$\upsilon_j = \frac{\prod_{i=0}^{j} a_i^2 g_{i,i+1}^2}{(RT_b)^2 P^2}, \tag{3.40}$$

we can rewrite (3.39) as

$$\gamma = \frac{(RT_b)^2 P^2 \left(\upsilon_0^{-1} + \upsilon_1^{-1} + \cdots + \upsilon_K^{-1} \right)^{-1}}{N_0} \tag{3.41}$$

where υ_j's are log-normal random variables since any product of independent log-normal

random variables is also log-normally distributed. Let $\upsilon_j = \exp(\kappa_i)$, then κ_i is a normal random variable with mean

$$\mu_\kappa(i) = \ln\left(\ell_{0,1}^2 \prod_{j=1}^{i} a_j^2 \ell_{j,j+1}^2\right) - 4\sum_{j=0}^{i} \sigma_\chi^2(L_{j,j+1}) \tag{3.42}$$

and variance

$$\sigma_\kappa^2(i) = 16\sum_{j=0}^{i} \sigma_\chi^2(L_{j,j+1}). \tag{3.43}$$

Moreover, the covariance between κ_i and κ_j can be obtained as $\Sigma_\kappa(i,j) = \sigma_\kappa^2(\min(i,j))$. Since any power (positive or negative) of a log-normal random variable is also log-normally distributed, the sum of υ_j^{-1}'s can be approximated as a log-normal random variable, i.e., $\exp(\varepsilon) \approx \sum_{j=0}^{K} \upsilon_j^{-1}$. Therefore, γ can be approximated in terms of a single log-normal random variable as

$$\gamma \approx (RT_b)^2 P^2 \exp(-\varepsilon)/N_0 \tag{3.44}$$

where the mean and variance of the normally distributed random variable ε are

$$\mu_\varepsilon = \ln\left(\sum_{i=0}^{K} \exp(\sigma_\kappa^2(i)/2 - \mu_\kappa(i))\right) - \sigma_\varepsilon^2/2, \tag{3.45}$$

$$\sigma_\varepsilon^2 = \ln\left(1 + \frac{\left(\sum_{i=0}^{K}\sum_{j=0}^{K} e^{\sigma_\kappa^2(i)/2+\sigma_\kappa^2(j)/2-\mu_\kappa(i)-\mu_\kappa(j)}\left(e^{\Sigma_\kappa(i,j)} - 1\right)\right)}{\left(\sum_{i=0}^{K} \exp(\sigma_\kappa^2(i)/2 - \mu_\kappa(i))\right)^2}\right). \tag{3.46}$$

Replacing (3.44) in (3.21), the end-to-end outage probability of the serial AF relaying scheme is obtained as

$$
\begin{aligned}
P_{out} &\approx \Pr\left\{\exp(-\varepsilon) < \frac{\gamma_{th} N_0}{(RT_b)^2 P^2}\right\} \\
&= \Pr\left\{\exp(-\varepsilon) < \frac{(K+1)^2}{P_M^2}\right\} \\
&= Q\left(\frac{\ln\left(P_M^2/(K+1)^2\right) - \mu_\varepsilon}{\sigma_\varepsilon}\right).
\end{aligned} \tag{3.47}
$$

Parallel AF Relaying: Recall that the received signal at the destination node for parallel AF relaying is given by (3.10). Equation (3.10) can be rewritten as

$$
\mathbf{r}_{K+1} = \begin{bmatrix} r_{K+1}^s \\ r_{K+1}^n \end{bmatrix} = \begin{bmatrix} \sum_{i=1}^{K} P a_i g_{i,K+1} g_{0,i} + A_{acc} + n_{acc}^s \\ A_{acc} + n_{acc}^n \end{bmatrix} \tag{3.48}
$$

where we define the accumulated noise terms as $n_{acc}^s = \sum_{i=1}^{K} a_i g_{i,K+1} n_i^s + n_{K+1}^s$, and $n_{acc}^n = \sum_{i=1}^{K} a_i g_{i,K+1} n_i^n + n_{K+1}^n$, and the accumulated bias term as $A_{acc} = \sum_{i=1}^{K} a_i g_{i,K+1} A_i$. Using (3.19) and (3.48), the received SNR at the destination node is given by

$$
\gamma = \frac{\left(RT_b P \sum_{i=1}^{K} a_i g_{i,K+1} g_{0,i}\right)^2}{N_0\left(\sum_{i=1}^{K} a_i^2 g_{i,K+1}^2 + 1\right)}. \tag{3.49}
$$

The summation terms in the numerator and denominator of (3.49) can be approximated as single log-normal random variables, i.e. $\exp(\omega_1) \approx \sum_{i=1}^{K} a_i g_{i,K+1} g_{0,i}$, and $\exp(\omega_2) \approx \sum_{i=1}^{K} a_i^2 g_{i,K+1}^2$. Therefore, (3.49) reduces to

$$
\gamma \approx \frac{R^2 T_b^2 P^2 \exp(2\omega_1)}{N_0\left(\exp(\omega_2) + 1\right)}. \tag{3.50}
$$

The log-amplitude pair (ω_1, ω_2) follows a correlated bivariate normal distribution. Their mean and covariance matrix are defined respectively as

$$\mu_1 = \ln \sum_{i=1}^{K} a_i \ell_{0,i} \ell_{i,K+1} - \sigma_1^2/2, \tag{3.51}$$

$$\mu_2 = \ln \sum_{i=1}^{K} a_i^2 \ell_{i,K+1}^2 e^{4\sigma_\chi^2(L_{i,K+1})} - \sigma_2^2/2, \tag{3.52}$$

$$\mathbf{\Sigma} = \begin{bmatrix} \sigma_1^2 & \sigma_{12} \\ \sigma_{12} & \sigma_2^2 \end{bmatrix} \tag{3.53}$$

where σ_1^2, σ_2^2, and σ_{12} are given by

$$\sigma_1^2 = \ln \left(1 + \sum_{i=1}^{K} a_i^2 \ell_{0,i}^2 \ell_{i,K+1}^2 \left(e^{4\sigma_\chi^2(L_{0,i}) + 4\sigma_\chi^2(L_{i,K+1})} - 1 \right) \Bigg/ \left(\sum_{i=1}^{K} a_i \ell_{0,i} \ell_{i,K+1} \right)^2 \right), \tag{3.54}$$

$$\sigma_2^2 = \ln \left(1 + \sum_{i=1}^{K} a_i^4 \ell_{i,K+1}^4 \left(e^{24\sigma_\chi^2(L_{i,K+1})} - e^{8\sigma_\chi^2(L_{i,K+1})} \right) \Bigg/ \left(\sum_{i=1}^{K} a_i^2 \ell_{i,K+1}^2 e^{4\sigma_\chi^2(L_{i,K+1})} \right)^2 \right), \tag{3.55}$$

$$\sigma_{12} = \ln \left(1 + \frac{\sum_{i=1}^{K} a_i^3 \ell_{0,i} \ell_{i,K+1}^3 \left(e^{12\sigma_\chi^2(L_{i,K+1})} - e^{4\sigma_\chi^2(L_{i,K+1})} \right)}{\left(\sum_{i=1}^{K} a_i^2 \ell_{i,K+1}^2 e^{4\sigma_\chi^2(L_{i,K+1})} \right) \left(\sum_{i=1}^{K} a_i \ell_{0,i} \ell_{i,K+1} \right)} \right). \tag{3.56}$$

Replacing (3.50) in (3.21), the end-to-end outage probability is obtained using pdf of the bivariate normal distribution as

$$\begin{aligned} P_{out} &= \Pr \left\{ \frac{\exp(2\omega_1)}{\exp(\omega_2) + 1} < \frac{2K}{P_M} \right\} \\ &= \int_{-\infty}^{\infty} \int_{-\infty}^{\omega_0} \frac{\exp\left(-\frac{\left(\sigma_2^2(\omega_1 - \mu_1)^2 + \sigma_1^2(\omega_2 - \mu_2)^2 - 2\sigma_{12}(\omega_1 - \mu_1)(\omega_2 - \mu_2) \right)}{2|\mathbf{\Sigma}|} \right)}{2\pi\sqrt{|\mathbf{\Sigma}|}} d\omega_2 d\omega_1 \end{aligned} \tag{3.57}$$

where the upper limit of the inner integration is defined as $\omega_0 = \ln(\sqrt{\exp(\omega_2)+1}) + \ln(\sqrt{2K/P_M})$. A closed-form expression for (3.57) is unfortunately not available. However, it can be easily calculated through multi-dimensional integration routines such as Gauss-Hermite quadrature formula [45].

3.3 Diversity Gain Analysis

Diversity order is conventionally defined as the negative asymptotic slope of the performance metric (e.g., probability of error or outage probability) versus SNR on a log-log scale. Unfortunately, the conventional definition of diversity order is useless for log-normal fading channels [30]. In this section, we adopt relative diversity order (RDO), which we have recently introduced in the context of indoor RF log-normal channels [30], for FSO communication systems operating in turbulence-induced fading channels.

Based on the conventional definition, the diversity order of the FSO SISO transmission is given as

$$d = -\lim_{SNR\to\infty} \frac{\partial \ln P_{out}}{\partial \ln SNR} = -\lim_{P_M\to\infty} \frac{\partial \ln P_{out}}{\partial \ln P_M}. \tag{3.58}$$

Using (3.26) and applying the Chernoff bound on the Q function (i.e., $Q(x) \leq 0.5\exp(x^2/2)$), the outage probability of the FSO SISO transmission can be bounded by

$$P_{out} = Q\left(\frac{\ln(P_M) + 2\mu_\chi(L)}{2\sigma_\chi(L)}\right) \leq \frac{1}{2}\exp\left(\frac{\left(\ln(P_M) + 2\mu_\chi(L)\right)^2}{8\sigma_\chi^2(L)}\right). \tag{3.59}$$

Inserting (3.59) in (3.58), the diversity order for the direct transmission is obtained as

$$d = -\lim_{P_M\to\infty} \frac{\partial\left(-\frac{\left(\ln(P_M)+2\mu_\chi(L)\right)^2}{8\sigma_\chi^2(L)} + \ln\left(\frac{1}{2}\right)\right)}{\partial \ln P_M} = \lim_{P_M\to\infty} \frac{\ln(P_M)}{4\sigma_\chi^2(L)} = \infty. \tag{3.60}$$

As observed in (3.60), the conventional definition of diversity order yields infinity [30] and does not provide a meaningful measure for diversity order. To overcome this problem, we define the so-called relative diversity order (RDO) [30] to quantify the diversity gain of FSO diversity systems. Based on the outage probability, RDO is given as

$$\mathrm{RDO}(P_M) = \frac{\partial \ln P_{out} / \partial \ln P_M}{\partial \ln P_{out,\mathrm{benchmark}} / \partial \ln P_M} \tag{3.61}$$

where $P_{out,\mathrm{benchmark}}$ is the outage probability of a benchmark scheme. We consider the benchmark scheme as the direct (SISO) transmission to keep compatibility with the conventional definition of the diversity order in Rayleigh fading channels [30]. The asymptotic relative diversity order (ARDO) is further given by [30]

$$\mathrm{ARDO} = \lim_{P_M \to \infty} \mathrm{RDO}(P_M). \tag{3.62}$$

3.3.1 Diversity Gain Analysis for Serial DF Relaying

Inserting (3.29) and (3.59) in (3.61), the RDO of FSO serial relaying scheme is obtained as

$$\mathrm{RDO}(P_M) = \frac{\partial \ln \left(1 - \prod_{i=1}^{K+1} \left(1 - Q\left(\frac{\ln\left(\ell_{i,i+1} P_M/(K+1)\right) + 2\mu_\chi(L_{i,i+1})}{2\sigma_\chi(L_{i,i+1})}\right)\right)\right) \Big/ \partial \ln P_M}{\partial \ln \left(Q\left(\left(\ln(P_M) + 2\mu_\chi(L)\right)/2\sigma_\chi(L)\right)\right) / \partial \ln P_M}. \tag{3.63}$$

Expanding the product in the numerator and neglecting the terms of the same or higher order than $Q^2(.)$, (3.63) can be well approximated as

$$\mathrm{RDO}(P_M) = \frac{\partial \ln \left(\sum_{i=1}^{K+1} Q\left(\frac{\ln\left(\ell_{i,i+1} P_M/(K+1)\right) + 2\mu_\chi(L_{i,i+1})}{2\sigma_\chi(L_{i,i+1})}\right)\right) \Big/ \partial \ln P_M}{\partial \ln \left(Q\left(\left(\ln(P_M) + 2\mu_\chi(L)\right)/2\sigma_\chi(L)\right)\right) / \partial \ln P_M}. \tag{3.64}$$

Assuming that the nodes in serial relaying configuration are equidistant, i.e., $L_{i,i+1} = L' = L/(K+1)$, and using the Chernoff bound on Q function, ARDO of DF serial relaying can obtained by taking the limit of (3.64) as

$$\begin{aligned}\text{ARDO} &= \lim_{P_M\to\infty} \frac{\partial\left(\frac{\left(\ln\left(\ell_{0,1}P_M/(K+1)\right)+2\mu_\chi(L')\right)^2}{8\sigma_\chi^2(L')}+\ln\left(\frac{(K+1)}{2}\right)\right)\Big/\partial\ln P_M}{\partial\left(\left(\ln(P_M)+2\mu_\chi(L)\right)^2\Big/8\sigma_\chi^2(L)+\ln(0.5)\right)\Big/\partial\ln P_M} \\ &= \lim_{P_M\to\infty}\frac{\ln(P_M)/4\sigma_\chi^2(L/(K+1))}{\ln(P_M)/4\sigma_\chi^2(L)} \\ &= \frac{\sigma_\chi^2(L)}{\sigma_\chi^2(L/(K+1))}. \end{aligned} \tag{3.65}$$

Inserting (2.11) in (3.65), we find ARDO as

$$\text{ARDO} = \frac{\sigma_\chi^2(L)}{\sigma_\chi^2(L/(K+1))} = \frac{L^{11/6}}{(L/(K+1))^{11/6}} = (K+1)^{11/6}. \tag{3.66}$$

From (3.66), it is interesting to note that, unlike wireless RF communication, serial relaying (multi-hop transmission) can extract diversity advantage in FSO systems. The fact that fading variance is distance-dependent in FSO systems (cf. Eq. (2.11)) constitutes a major difference between wireless RF and wireless optical systems. This inherent characteristic lets multi-hop FSO transmission smartly exploit the shorter distance in the resulting hops and take advantage of the artificially induced diversity gain resulting from distance-dependency of fading variance.

3.3.2 Diversity Gain Analysis for Parallel DF Relaying

Inserting (3.37) and (3.59) in (3.61), the RDO of FSO parallel relaying scheme is obtained as

$$\mathrm{RDO}(P_M) = \frac{\partial \ln \left(\sum_{i=1}^{2^K} P_{out}(S(i)) \right) \Big/ \partial \ln P_M}{\partial \ln \left(Q\left(\left(\ln(P_M) + 2\mu_{\chi} \right) / 2\sigma_{\chi} \right) \right) / \partial \ln P_M}. \tag{3.67}$$

The numerator of (3.67) can be written as

$$I = \frac{\partial \ln \left(\sum_{i=1}^{2^K} P_{out}(S(i)) \right)}{\partial \ln P_M} = \frac{\sum_{i=1}^{2^K} \frac{\partial P_{out}(S(i))}{\partial \ln P_M}}{\sum_{i=1}^{2^K} P_{out}(S(i))} = \frac{\sum_{i=1}^{2^K} P_{out}(S(i)) \frac{\partial \ln P_{out}(S(i))}{\partial \ln P_M}}{\sum_{i=1}^{2^K} P_{out}(S(i))}. \tag{3.68}$$

Assuming that the relays are located at the halfway point, i.e., $L_{0,i} = L_{i,K+1} = L/2$, and using the Chernoff bound on Q functions in $P_{out}(S(i))$, we can rewrite (3.68) as

$$I = \sum_{j=1}^{K} \frac{\binom{K}{j} P_{out}(S(j))}{\sum_{i=1}^{2^K} P_{out}(S(i))} \Bigg[j \frac{\partial \left(\frac{\left(\ln(\ell_{0,1} P_M / 2K) + 2\mu_{\chi}(L/2) \right)^2}{8\sigma_{\chi}^2(L/2)} \right)}{\partial \ln P_M} + (K-j) \frac{\partial \ln(\Gamma)}{\partial \ln P_M} + \partial \left(\frac{\left(\ln(P_M/2K) + \mu_{\xi}(\mathbf{L}_{\mathrm{S}(i)}) \right)^2}{2\sigma_{\xi}^2(\mathbf{L}_{\mathrm{S}(i)})} \right) \Big/ \partial \ln P_M \Bigg] \tag{3.69}$$

where $\Gamma = 1 - Q\left(\left(\ln\left(\ell_{0,1} P_M / 2K \right) + 2\mu_{\chi}(L/2) \right) / 2\sigma_{\chi}(L/2) \right)$. Noting $\ln(\Gamma) \to 0$ for $P_M \to \infty$, and inserting (3.69) in (3.67), ARDO of the DF parallel relaying can obtained by taking the limit of (3.67) as

$$\mathrm{ARDO} = \lim_{P_M \to \infty} \frac{\frac{1}{\sum_{i=1}^{2^K} P_{out}(S(i))} \sum_{j=1}^{K} \binom{K}{j} P_{out}(S(j)) \left(j \frac{\ln(P_M)}{4\sigma_{\chi}^2(L/2)} + \frac{\ln(P_M)}{\sigma_{\xi}^2(j, L/2)} \right)}{\ln(P_M)/4\sigma_{\chi}^2(L)} \tag{3.70}$$

where $\sigma_{\xi}^2(j, L/2) = \sigma_{\xi}^2(\mathbf{L}_{\mathrm{S}(i)})|_{L_{0,j}=L_{j,K+1}} = \ln(1+(\exp(4\sigma_{\chi}^2(L/2))-1)/(K-j))$. Assume that the fading variance $\sigma_{\chi}^2(L)$ is sufficiently small, we can approximate $\sigma_{\xi}^2(j, L/2) \approx 4\sigma_{\chi}^2(L/2)/(K-j)$. Therefore, we can rewrite (3.70) as

$$\mathrm{ARDO} = \lim_{P_M \to \infty} \frac{1}{\sum_{i=1}^{2^K} P_{out}(S(i))} \sum_{j=1}^{K} \left(\begin{array}{c} K \\ j \end{array} \right) P_{out}(S(j)) \left(j \frac{\sigma_{\chi}^2(L)}{\sigma_{\chi}^2(L/2)} + (K-j) \frac{\sigma_{\chi}^2(L)}{\sigma_{\chi}^2(L/2)} \right). \tag{3.71}$$

Inserting (2.11) in (3.71), we obtain

$$\begin{aligned} \mathrm{ARDO} &= \lim_{P_M \to \infty} \frac{2^{11/6} K}{\sum_{i=1}^{2^K} P_{out}(S(i))} \sum_{j=1}^{K} \left(\begin{array}{c} K \\ j \end{array} \right) P_{out}(S(j)) \\ &= \lim_{P_M \to \infty} \frac{2^{11/6} K}{\sum_{i=1}^{2^K} P_{out}(S(i))} \sum_{j=1}^{2^K} P_{out}(S(j)) = 2^{11/6} K. \end{aligned} \tag{3.72}$$

Comparing (3.66) and (3.72), we can express the ARDO of the relay-assisted FSO systems with DF relaying in a general form as

$$\mathrm{ARDO} = N_H^{11/6} N_D \tag{3.73}$$

where N_H and N_D are respectively the number of hops and the number of diversity paths in the relaying configuration. In (3.73), we observe that the serial relaying factor (i.e., $N_H^{11/6}$) is stronger than the parallel relaying factor (i.e., N_D). Therefore, we can conclude that a parallel relaying scheme ($N_D \geq N_H$) takes advantage of the distance-dependency of fading log-normal variance less than a serial relaying scheme ($N_H \geq N_D$). Therefore, the serial relaying outperforms the parallel relaying as the number of relays increases.

3.4 Numerical Results and Discussions

In this section, we present numerical results for the outage and diversity analysis obtained through the derived expressions and Monte-Carlo simulations. We consider an FSO system with $\lambda = 1550$ nm operating in clear weather conditions with visibility of 10 km. We assume an atmospheric attenuation of 0.43 dB/km (i.e., $a \approx 0.1$) and structure constant of $C_n^2 = 1 \times 10^{-14}\mathrm{m}^{-2/3}$. The link range (i.e., distance between the source and the destination) is $L_{0,K+1} = L = 5\,\mathrm{km}$. For serial relaying, we assume the consecutive nodes are equidistant along the path from the source to the destination. In parallel relaying, the relays are located on the halfway point.

Figure 3.4 demonstrates the end-to-end outage probability of an FSO DF system for serial relaying assuming $K = 1, 2, 3$. We present analytical results which have been obtained through (3.29) along with the Monte-Carlo simulation of (3.21). As clearly seen from figure 3.4, our exact closed-form expressions provide an identical match to simulation results. As a benchmark, outage probability of the direct transmission is also included in this figure.

Figure 3.4 shows that serial relaying significantly improves the performance. Particularly, for a target outage probability of 10^{-6}, we observe performance improvements of 18.5 dB, 25.4 dB, and 29.2 dB for $K = 1, 2$, and 3 with respect to the direct transmission. We should emphasize that these impressive performance gains are a result of relay-assisted transmission's ability to exploit the distance-dependency of the log-amplitude variance. As reported in [12], spatial diversity, through the use of co-located apertures, in an FSO communication system scales down the effective log-amplitude variance by the number of apertures. A similar effect is observed in serial relaying where the fading log-amplitude variance of each intermediate SISO link decreases as the intra-distance decreases through the insertion of relaying nodes. Therefore, diversity advantage is artificially induced in the relaying scheme by shortening the distance between communicating nodes. This diversity advantage can be also observed in the figure by comparing the slopes of the performance curves for the relay-assisted and direct transmission systems.

Figure 3.5 demonstrates the end-to-end outage probability of an FSO DF system for

parallel relaying assuming $K = 1, 2, 3$. We present analytical results which have been obtained through (3.37) along with the Monte-Carlo simulation of (3.21). Although the derived expression is based upon an approximation, we have found nearly identical match between analytical and simulation results. We also note that for $K = 1$ the performance of serial and parallel relaying coincide as expected which can be readily confirmed through the comparison of (3.21) and (3.37). We observe from figure 3.5 that parallel relaying improves the outage performance with respect to direct transmission. Specifically, we obtain performance improvements of 18.5 dB, 20.3 dB, 20.7 dB for

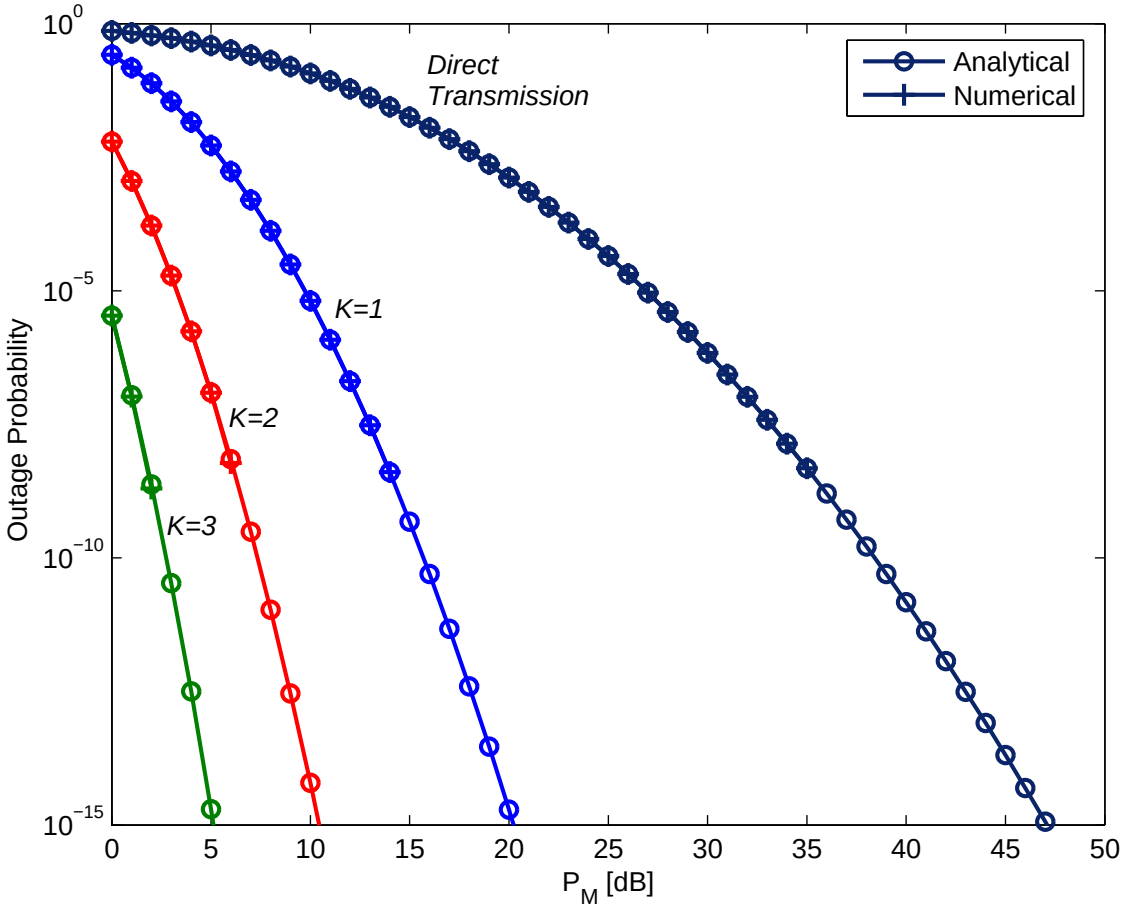

Figure 3.4: The outage probability of the FSO serial decode-and-forward relaying scheme.

$K = 1, 2$ and 3 with respect to the direct transmission for a target outage probability of 10^{-6}. We note that performance gains are less than those observed in serial relaying since parallel relaying (with only two hops) exploits distance-dependency of fading variance to a lesser extent.

Figure 3.6 demonstrates the end-to-end outage probability of an FSO AF system for serial relaying assuming $K = 1, 2, 3$. We present approximate analytical results which have been obtained through (3.47) along with the Monte-Carlo simulation of (3.21). For $K = 1$, we observe a very good match between analytical and simulation results. The

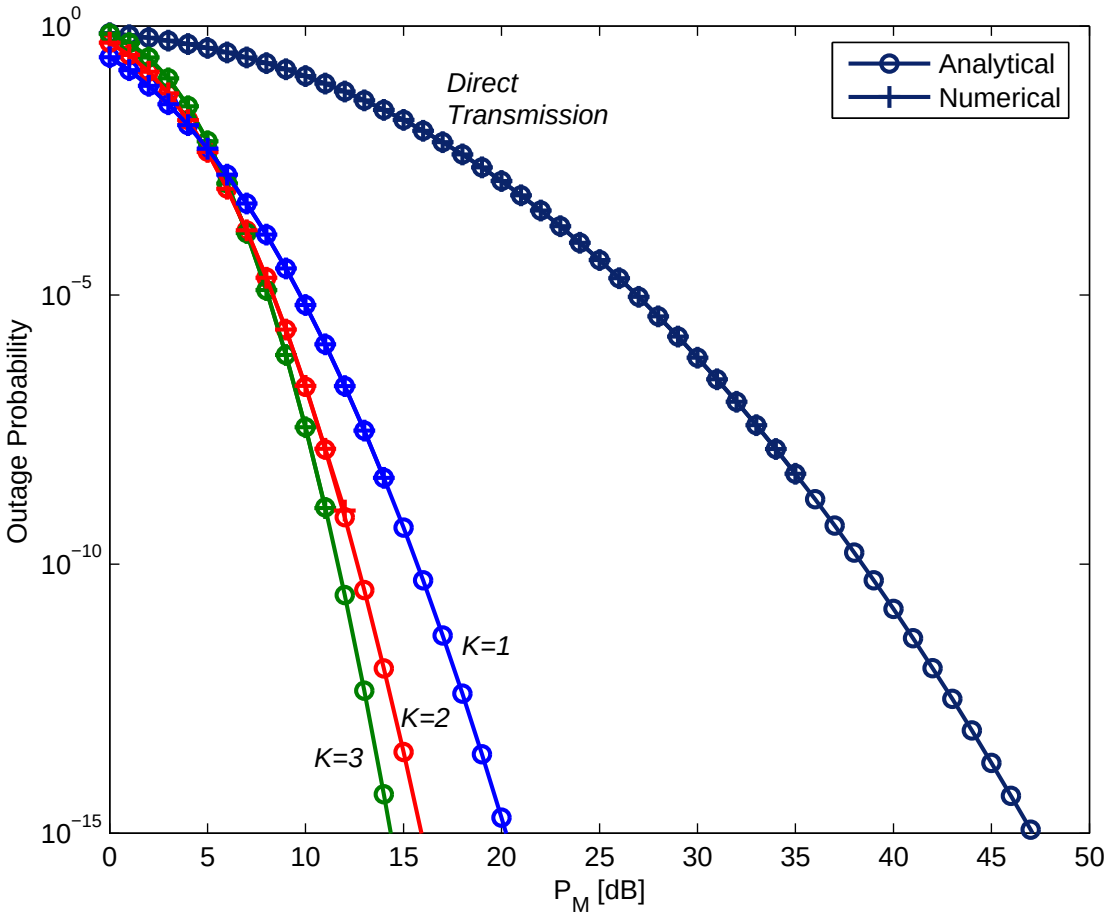

Figure 3.5: The outage probability of the FSO parallel decode-and-forward relaying scheme.

discrepancy gets larger for $K = 2$ and $K = 3$. Recall that closed-form expressions for this case are built upon an approximation of the sum of correlated log-normal random variables as a single log-normal term. Comparison with direct transmission reveals that performance improvements are 12.2 dB, 17.7 dB, 21 dB for $K = 1, 2$ and 3 for a target outage probability of 10^{-6}. It is observed that the performance gains are less than those observed in DF relaying. However, AF relays enjoy a lower complexity in comparison with DF counterparts since it does not require any decoding process.

Figure 3.7 demonstrates the end-to-end outage probability of an FSO AF system

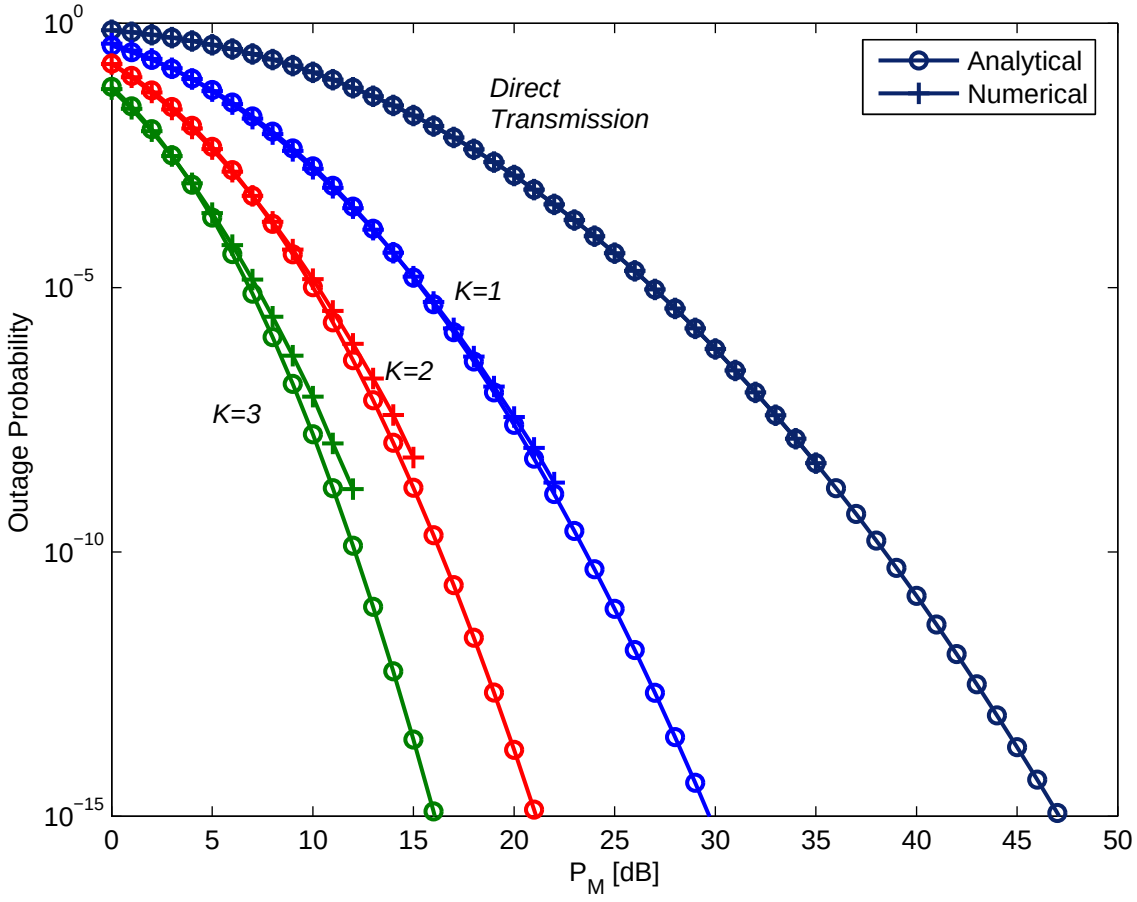

Figure 3.6: The outage probability of the FSO serial amplify-and-forward relaying scheme.

for parallel relaying assuming $K = 1, 2, 3$. We present analytical results which have been obtained through (3.57) along with the Monte-Carlo simulation of (3.21). Similar to figure 3.6, they provide a good match for $K = 1$ while some discrepancy is observed for $K = 2, 3$ due to the log-normal approximation. At a target outage probability of 10^{-6}, FSO DF parallel relaying system yields performance gains of 12.2 dB, 18.1 dB, 20.2 dB for $K = 1, 2$, and 3. It is observed that these are lower than those observed for its counterpart with DF relaying.

Figure 3.8 demonstrates the RDO of an FSO DF system with serial relaying for

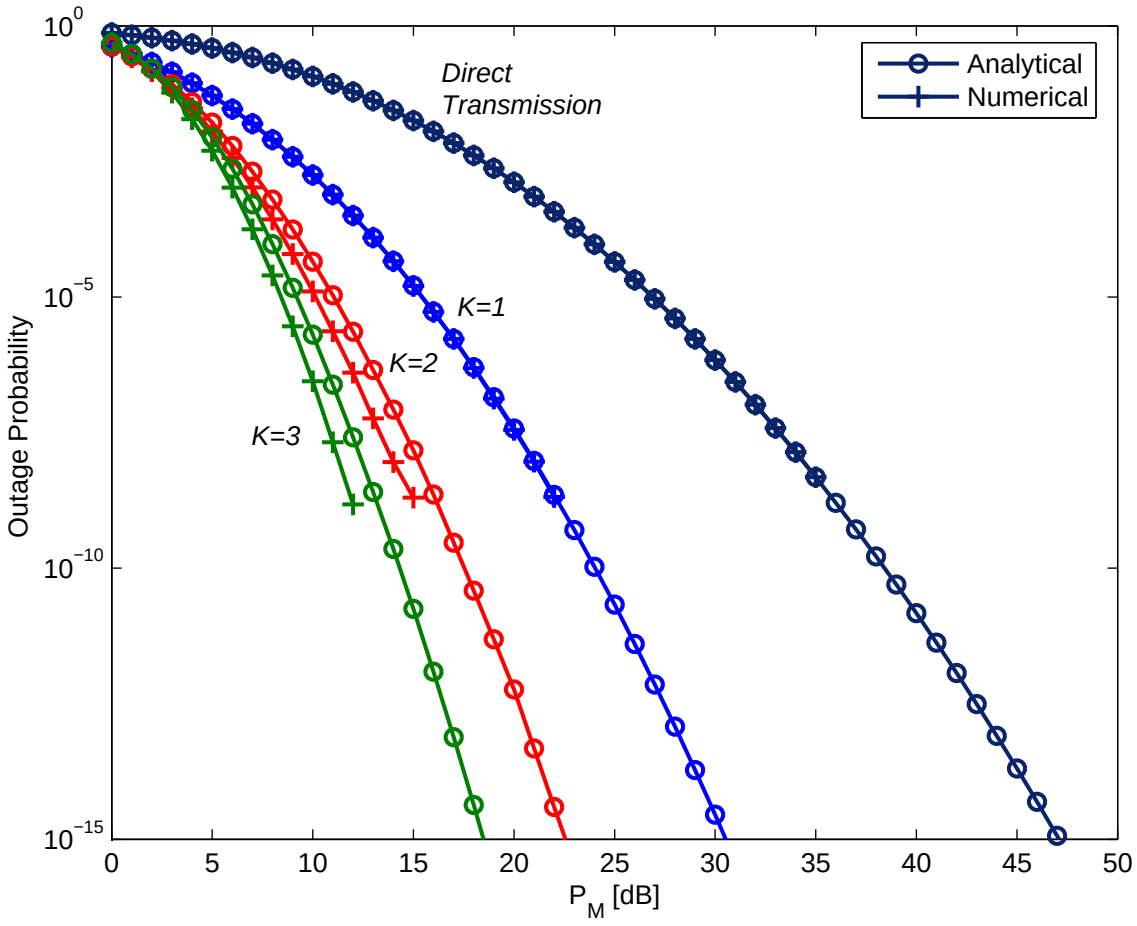

Figure 3.7: The outage probability of the FSO parallel amplify-and-forward relaying scheme.

different number of relays (i.e., $K = 1, 2, 3$). At very high power margin, we observe RDO values of 3.7, 7.9, and 13.5 respectively for $K = 1, 2$, and 3. These provide a good match to analytical ARDOs (i.e. $P_M \to \infty$) calculated as $(K+1)^{11/6} = 3.6, 7.5$, and 12.7 for $K = 1, 2$, and 3. We also observe that RDOs for lower P_M values are higher than those for higher P_M values. This can be explained by the advantage of serial relaying configuration in reduction of path loss effects which is more pronounced in lower power margin values.

Figure 3.9 demonstrates the RDO of an FSO DF system with parallel relaying for

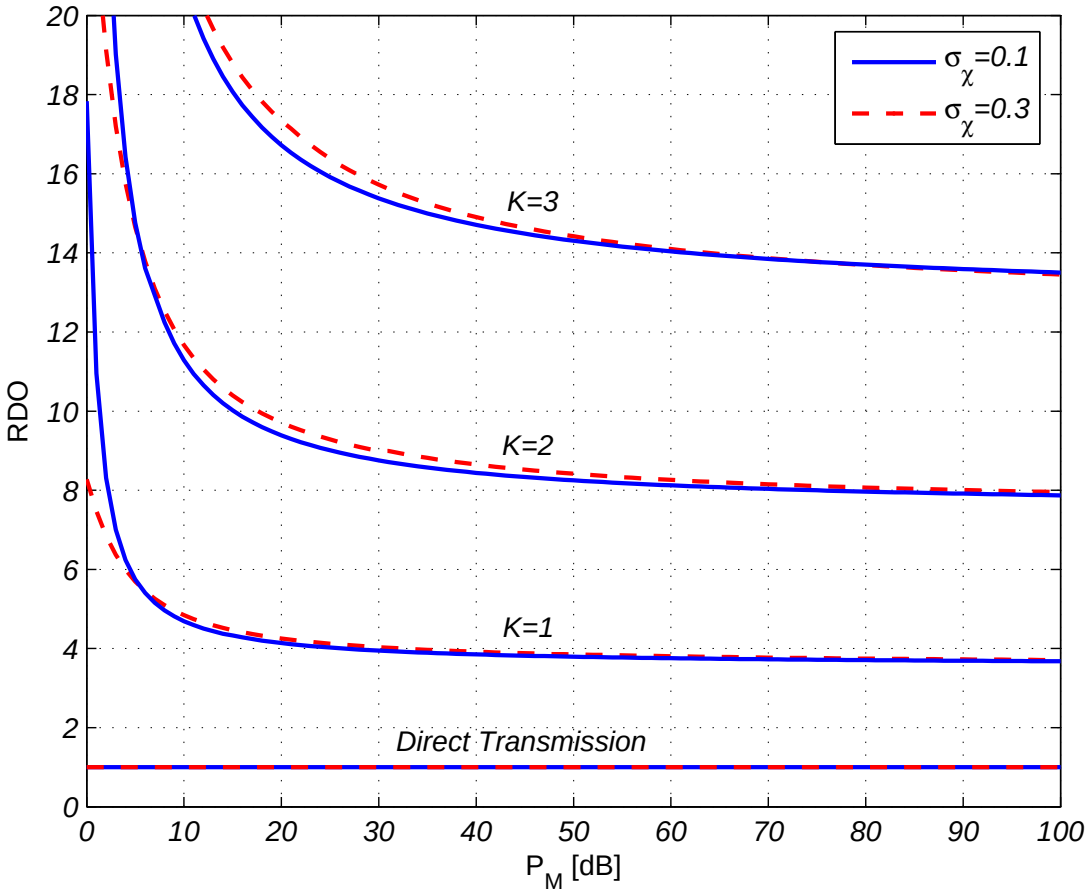

Figure 3.8: The diversity gain of the serial DF relaying scheme with different number of relays.

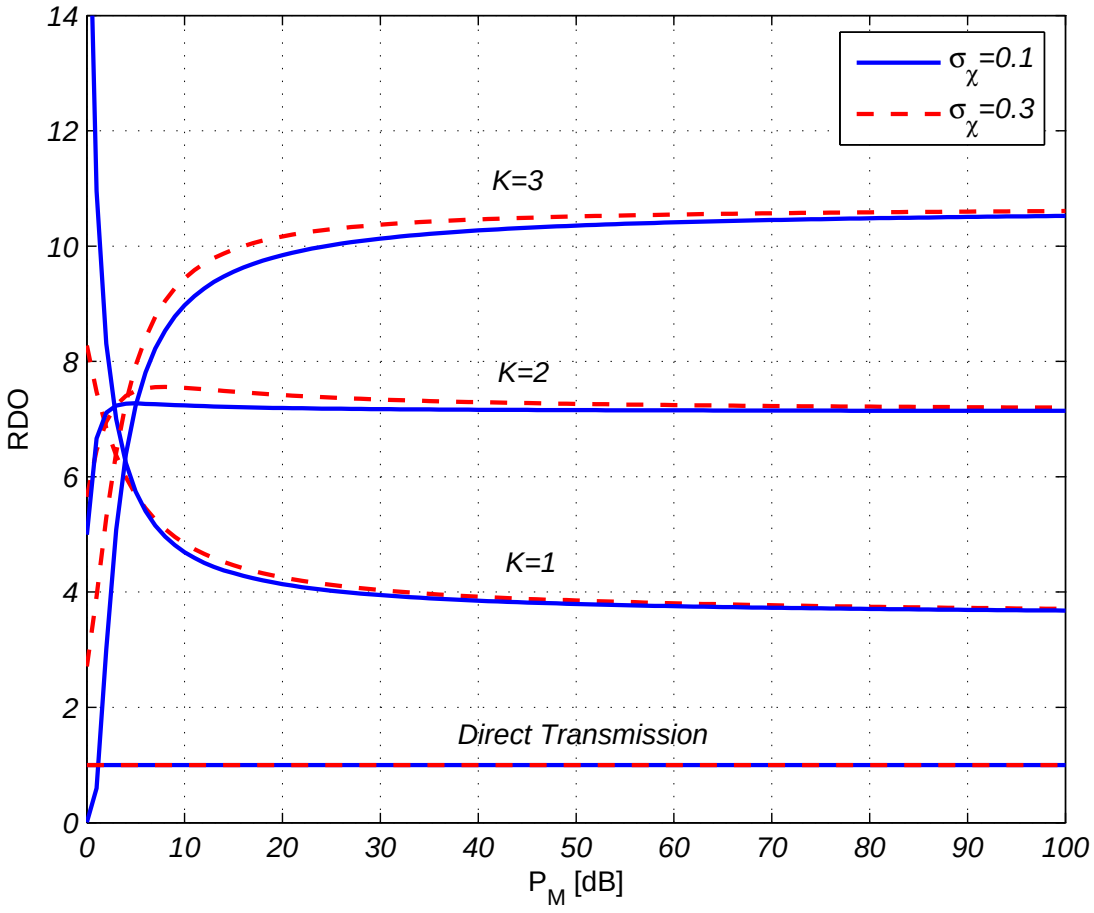

Figure 3.9: The diversity gain of the parallel DF relaying scheme with different number of relays.

different number of relays (i.e., $K = 1, 2, 3$). At very high power margin, we observe RDO values of 3.7, 7.17, and 10.6 for $K = 1, 2$, and 3. These values are very close to analytical ARDOs (i.e. $P_M \to \infty$) which are obtained as $2^{11/6}K = 3.6, 7.12$, and 10.7 for $K = 1, 2$, and 3.

Chapter 4

Relay-Assisted FSO Communication over the Poisson Channel

In this chapter, we study the outage behavior of a constant-rate multi-hop FSO system over the Poisson channel degraded by turbulence-induced fading. This is the suitable model for multi-hop FSO communication with shot-noise-limited direct detection receivers. In the previous chapter, under a Gaussian channel model, we showed that such multi-hop relaying can significantly outperform the parallel relaying and direct transmission counterparts. In fact, the multi-hop FSO system takes advantage of shorter individual intermediate hops with much weaker turbulence and effectively mitigates the fading degradation.

A decode-and-forward relaying strategy is employed for the multi-hop FSO transmission where the turbulence-induced degradation is described by a block fading model. We assume delay-limited transmission waveforms spanning over a single fading block where the fading level remains constant. It is further assumed that perfect channel state information (CSI) is available at the receiver side; however, it may or may not be available at the transmitter side. We formulate an outage probability minimization problem subject to a peak power constraint as well as a short- or long-term average sum power constraint. As a result, optimal power control strategies are presented for different scenarios under consideration. A sub-optimal yet low-complexity solution is

further proposed under short-term power constraint.

4.1 Multi-Hop Poisson channel Model

The Poisson channel has been extensively studied in the literature (e.g., see [46] and references therein). In [47], Kabanov derived the capacity of a single-user Poisson channel subject to a peak power constraint using martingale techniques. Davis extended Kabanov's results in [48] by considering both peak and average power constraints and introducing an additional parameter which represents background noise level. In [49], Wyner derived the Poisson channel capacity and error exponent based on a discrete memoryless channel approximation.

Shamai (Shitz) and Lapidoth [50] studied the Poisson channel with spectral constraints on the optical channel. In [51], Haas et al. derived upper and lower bounds on the capacity of the multiple-input multiple-output (MIMO) Poisson channel degraded by atmospheric turbulence-induced fading. In [52], Chakraborty and Narayan studied the capacity of the single-input single-output Poisson channel in the presence of atmospheric turbulence. Furthermore, Chakraborty et al. investigated the outage probability of the turbulence-degraded MIMO Poisson channel assuming perfect CSI available at both transmitter and receiver [53].

In this chapter, we study the multi-hop Poisson channel degraded by atmospheric turbulence. We consider a relay-assisted IM/DD FSO communication system in which the transmitted signal from a source node propagates through K DF relays before detection at the destination node. We assume strict transmission delay constraint and constant transmission rate of R. The transmitter sends information by modulating the intensity of the transmitted optical beam using a non-negative waveform $\lambda_i(t)$ spanning over a fading block, i.e., $0 \leq t \leq T$. The input waveform in the i^{th} hop $(1 \leq i \leq K+1)$ satisfies the peak power and average sum power constraints[1] given by

[1]Noting that the optical communication bandwidth is license-free and plentiful, we neglect the spectral constraints on the system model. In effect, a more tractable model is considered rather than a complicated one which fully takes into account the optical transmitter and receiver spectral limitations.

$$0 \leq \lambda_i(t) \leq A, \tag{4.1}$$

$$\sum_{n=1}^{K+1} \frac{1}{T_c} \int_0^{T_c} \lambda_i(t')dt' \leq \sigma A \tag{4.2}$$

where the peak power ($A > 0$) and the average-to-peak power ratio ($0 \leq \sigma \leq K+1$) are fixed. In (4.2), T_c is the average power constraint period and is equal to the fading block duration under short-term average power constraint (i.e., $T_c = T$) and is much greater than the fading block duration under long-term average power constraint (i.e., $T_c \gg T$).

The atmospheric channel within each hop is described by a block fading channel which models the slowly-varying nature of atmospheric turbulence. The channel state variable α_i ($i = 1, 2 \ldots K+1$) for each hop is assumed to remain constant within each fading block and randomly change between two consecutive fading blocks according to a known turbulence-induced fading distribution[2]. Considering both effects of path loss (ℓ_i) and turbulence-induced fading (h_i), the channel state variable is defined as

$$\alpha_i = \ell_i h_i. \tag{4.3}$$

Different statistical distributions for the turbulence-induced fading have been proposed in the literature. Although the solution of the optimization problem discussed in the next section does not depend on the fading distribution, a specific fading type is required for outage probability calculations. In our numerical results, we assume the log-normally distributed fading coefficient as defined in (2.6). In (4.3), $\ell_i = \ell(L_i)/\ell(L)$ denotes the normalized path loss of the i^{th} hop where L_i and L are respectively the length of the i^{th} hop and the length of the multi-hop link and the path loss factor $\ell(\cdot)$ is given by (2.7).

[2]Note that, for the notation simplicity, both random channel state variable and its realization (instantaneous channel state) have been denoted by α. However, they can be easily distinguished from the context.

In the multi-hop Poisson channel model, the relay and destination nodes employ shot-noise-limited direct detection receivers which count the individual photon arrivals at the photodetector. Therefore, the received signal at the i^{th} hop can be well described [54] by a doubly-stochastic Poisson process $\nu_i(t)$ with rate

$$\Psi_i(t) = \alpha_i \lambda_i(t) + \lambda_0 \tag{4.4}$$

where $\lambda_0 \geq 0$ is the background noise rate. Assuming the reception of many spatial and/or temporal modes of light, the background noise can be well described by a constant rate [54]. Therefore, for $t, \tau \geq 0$ and $j = 0, 1, 2, ...$, the Poisson process $\nu_i(t)$ is defined as

$$\Pr\left\{\nu_i(t+\tau) - \nu_i(t) = j | \Psi_i(t) = \psi_i(t)\right\} = \frac{e^{-\Lambda_i(t,\tau)} \left[\Lambda_i(t,\tau)\right]^j}{j!} \tag{4.5}$$

where $\Lambda_i(t,\tau) = \int_t^{t+\tau} \psi_i(t')dt'$.

4.2 Outage Analysis and Optimization

As mentioned earlier, for typical FSO transmission rates, fading remains constant over hundreds of thousands up to millions of consecutive bits. For such channels where the errors caused by fading are no longer independent, outage probability is an appropriate performance criterion. Outage probability is defined as the probability of the channel instantaneous mutual information being below the transmission rate [43].

In this section, we investigate the outage behavior of multi-hop IM/DD FSO system under consideration. Due to the slowly varying nature of the channel, an estimate of CSI can be accurately obtained by the receiver and, if required, can be sent to the transmitter via feedback. Therefore, we assume that perfect CSI is always available at the receiver side and consider both cases of perfect CSI and no CSI at the transmitter side. Specifically, in the following, we solve the problem of minimizing the outage probability in three cases: i) No CSI at the transmitters, ii) Perfect CSI at the transmitters

under short-term average power constraint, and iii) Perfect CSI at the transmitters under long-term average power constraint.

In the DF multi-hop transmission systems, the received signal at each relay is fully decoded, re-encoded and then retransmitted to the next relay or destination. The directed propagation of light and the isolation capability between the optical transmitter and receiver in an FSO communication system prevent any inter- or intra-node interference. Therefore, we consider full-duplex relaying and assume no interference between individual FSO channels. The maximum instantaneous mutual information of such multi-hop Poisson fading channel can be expressed in terms of the individual hops' mutual information as

$$I_M(\boldsymbol{\alpha}, \boldsymbol{\mu}) = \min\{I(\alpha_1, \mu_1), I(\alpha_2, \mu_2), \cdots, I(\alpha_{K+1}, \mu_{K+1})\} \tag{4.6}$$

where $\boldsymbol{\alpha} = \{\alpha_1, \alpha_2, \cdots, \alpha_{K+1}\}$ is a given realization of the channel state vector and $\boldsymbol{\mu} = \{\mu_1, \mu_2, \cdots, \mu_{K+1}\}$ is the duty cycle vector. In (4.6), $I(\alpha_i, \mu_i)$ is the maximum instantaneous mutual information of the i^{th} hop which can be expressed using the maximum mutual information of the single-hop Poisson fading channel as [49, 52]

$$I(\alpha_i, \mu_i) = A[\mu_i \zeta(\alpha_i, s) - \zeta(\mu_i \alpha_i, s)] \tag{4.7}$$

where the multi-variable function $\zeta(\cdot, \cdot)$ is defined as $\zeta(x, y) \triangleq (x+y)\ln(x+y) - y\ln(y)$. The maximum mutual information in (4.7) can be achieved by piecewise-constant input waveforms taking only the values 0 and A. In (4.7), μ_i is the probability of the input waveform taking the value A (i.e., duty cycle of the input waveform), and $s = \lambda_0/A$ is the reciprocal of the peak-signal-to-noise-ratio (SNR) denoted as SNR$= A/\lambda_0$. It can be noted that, in the two special cases of high SNR (i.e., $\lambda_0 \to 0$) and low SNR (i.e., $\lambda_0 \to \infty$) regimes, the mutual information function in (4.7) tends respectively to [49]

$$I(\alpha_i, \mu_i) = A\mu_i \alpha_i \ln(1/\mu_i), \tag{4.8}$$

$$I(\alpha_i, \mu_i) = \frac{A\alpha_i^2 \mu_i (1-\mu_i)}{2s}. \tag{4.9}$$

Note that the peak power constraint in (4.1) is already applied to the achievable mutual information function in (4.7). Furthermore, applying the average power constraint in (4.2) to the maximizing input waveform, the short and long-term average power constraints can be expressed in terms of the duty cycle as

$$\sum_{i=1}^{K+1} \mu_i(\boldsymbol{\alpha}) \leq \sigma, \tag{4.10}$$

$$\mathrm{E}\left\{\sum\nolimits_{i=1}^{K+1} \mu_i(\boldsymbol{\alpha})\right\} \leq \sigma. \tag{4.11}$$

4.2.1 Short-Term Power Constraint

The outage minimization problem under short-term average power constraint can be expressed as

$$\begin{aligned} \min \quad & P_{\text{out}} = \Pr\left\{I_M(\boldsymbol{\alpha}, \boldsymbol{\mu}) < R\right\} \\ \text{s.t.} \quad & \sum_{i=1}^{K+1} \mu_i(\boldsymbol{\alpha}) \leq \sigma \quad \text{with probability 1} \end{aligned} \tag{4.12}$$

where $R = rA/e$ [nats/s] is the constant transmission rate, e is the Euler's number, and r is the unitless relative rate with respect to the ultimate capacity of the peak-power-constrained fading-free Poisson channel with background noise tending to zero (i.e., A/e [49, 50]).

It is intuitive and easily provable that the outage probability minimization problem in (4.12) can be reduced to a multi-hop mutual information maximization problem at any channel state realization of $\boldsymbol{\alpha}$ (e.g., see proposition 3 of [55]) as

$$\begin{aligned} \max \quad & I_M(\boldsymbol{\alpha}, \boldsymbol{\mu}) = \min\{I(\alpha_1, \mu_1), \cdots, I(\alpha_{K+1}, \mu_{K+1})\} \\ \text{s.t.} \quad & \sum_{i=1}^{K+1} \mu_i(\boldsymbol{\alpha}) \leq \sigma \end{aligned} \tag{4.13}$$

The mutual information function given in (4.7), $I(\alpha, \cdot)$, for all $\alpha \in \mathbb{R}$ is concave and its maximum occurs at a critical point within $1/e \leqslant \mu < 1/2$ given by [49, 52]

$$\mu_0(\alpha) = \frac{s}{\alpha}\left[\frac{1}{e}\left(1 + \frac{\alpha}{s}\right)^{\left(1+\frac{s}{\alpha}\right)} - 1\right]. \tag{4.14}$$

Therefore, the solution to (4.13) can be attained either on an interior point of the feasible region where the smallest individual mutual information function attains its maximum or on the boundary of the feasible region. We first consider the former case where the constraint of the problem in (4.13) becomes inactive and therefore we have the unconstrained problem as

$$\max\, I_M(\boldsymbol{\alpha}, \boldsymbol{\mu}) = \max \;\; \min\{I(\alpha_1, \mu_1), \cdots, I(\alpha_{K+1}, \mu_{K+1})\} \tag{4.15}$$

which can be solved as in Lemma 4.1.

Lemma 4.1: Eq. (4.15) attains its maximum at the maximum mutual information of the hop with minimum fading level, i.e.,

$$\max\, I_M(\boldsymbol{\alpha}, \boldsymbol{\mu}) \equiv C_m = I(\alpha_m, \mu_0(\alpha_m)) \tag{4.16}$$

where $\alpha_m = \min\{\alpha_1, \cdots, \alpha_{K+1}\}$. The duty cycle vector at which this maximum is attained is not unique. However, the maximizing duty cycle vector which attains minimum average sum power (or minimum duty cycle sum) can be stated as

$$\tilde{\mu}_i = \begin{cases} \mu_0(\alpha_m), & i = m \\ I^{-1}(\alpha_i, C_m), & i = 1, \cdots, K+1 \text{ and } i \neq m \end{cases} \tag{4.17}$$

where $I^{-1}(\alpha,\cdot)$ is the inverse of the mutual information function given in (4.7). It can be calculated as

$$I^{-1}(\alpha,R_0)=\frac{\alpha s\ln s-\alpha R_0/A-s\zeta(\alpha,s)}{\alpha^2\,\mathrm{W}_{-1}\left(\left[s\ln s-\frac{R_0}{A}-\frac{s\zeta(\alpha,s)}{\alpha}\right]e^{-\frac{\zeta(\alpha,s)}{\alpha}}\right)}-\frac{s}{\alpha} \tag{4.18}$$

where $\mathrm{W}_{-1}(\cdot)$ is -1^{th} branch of Lambert-W function which is a solution of the well-known equation $\mathrm{W}(z)e^{\mathrm{W}(z)}=z$ [56].

Proof: See section 4.4.1.

Any solution of (4.15) might be a solution of the constrained problem in (4.13) as well, if and only if that solution satisfies the constraint in (4.13). Therefore, an immediate result of Lemma 4.1 is that the power control law in (4.17) gives the solution of the constrained maximization problem in (4.13), if and only if

$$\sum_{i=1}^{K+1}\tilde{\mu}_i=\sum_{i=1}^{K+1}I^{-1}(\alpha_i,C_m)\leqslant\sigma. \tag{4.19}$$

On the other hand, if the solution of (4.15) does not belong to the feasible region of (4.13), then the problem in (4.13) can be solved by a water-filling approach [57] as stated in Lemma 4.2.

Lemma 4.2: If the inequality in (4.19) does not hold, the solution to the constrained maximization problem in (4.13) is attained at a boundary point of the feasible region (i.e., points that satisfy the constraint with equality) where the mutual information of all the individual hops are equal or below their maximum. Therefore, the solution can be obtained by solving the following equations

$$\begin{aligned}&I(\alpha_1,\mu_1^*)=I(\alpha_2,\mu_2^*)=\cdots=I(\alpha_{K+1},\mu_{K+1}^*)=C^*,\\&\mu_i^*\leqslant\mu_0(\alpha_i)\ \forall 1\leqslant i\leqslant K+1,\\&\sum_{i=1}^{K+1}\mu_i^*=\sigma.\end{aligned} \tag{4.20}$$

Proof: See section 4.4.2.

The inverse of mutual information function given by (4.18) always yields the duty cycles below the maximizing duty cycle, i.e., $I^{-1}(\alpha, \cdot) \leqslant \mu_0(\alpha)$. Therefore, the equations in (4.20) can be combined and reduced to a single equation as

$$I^{-1}(\alpha_1, C^*) + I^{-1}(\alpha_2, C^*) + \cdots + I^{-1}(\alpha_{K+1}, C^*) = \sigma. \tag{4.21}$$

Let $C_{MS}(\boldsymbol{\alpha})$ denote the maximum of objective function in the constrained optimization problem of (4.13). Considering Lemmas 4.1 and 4.2, it can be stated as

$$C_{MS}(\boldsymbol{\alpha}) = \begin{cases} C_m = I(\alpha_m, \mu_0(\alpha_m)), & \text{if } \sum_{i=1}^{K+1} I^{-1}(\alpha_i, C_m) \leqslant \sigma \\ C^*, & \text{otherwise} \end{cases} \tag{4.22}$$

where C^* can be calculated by solving (4.21). Furthermore, the power control law which optimizes both the optimization problems in (4.12) and (4.13) is obtained for the i^{th} hop as

$$\hat{\mu}_i(\boldsymbol{\alpha}) = I^{-1}(\alpha_i, C_{MS}(\boldsymbol{\alpha})) \tag{4.23}$$

and the minimum outage probability can be then calculated as

$$\hat{P}_{out} = \Pr\{C_{MS}(\boldsymbol{\alpha}) < R\} \tag{4.24}$$

For a sanity check, it can be noted that for the case of single-hop Poisson fading channel (i.e., direct transmission), the solution to the outage minimization problem in (4.12) reduces to

$$\hat{\mu}(\alpha) = \min\{\mu_0(\alpha), \sigma\} \tag{4.25}$$

which was earlier reported in [52, 53].

Furthermore, note that for the channel states realizations belonging to the outage region $\Omega(R) = \{\boldsymbol{\alpha} \in \mathbb{R}_+^{K+1} : I_M(\boldsymbol{\alpha}, \hat{\boldsymbol{\mu}}(\boldsymbol{\alpha})) < R\}$, an outage happens whether or not

the optimal power control law (i.e., $\hat{\boldsymbol{\mu}}(\alpha)$) is employed. Therefore, the solution to the optimization problem in (4.12) can be expressed in a more general form as

$$\hat{\boldsymbol{\mu}}_g(\boldsymbol{\alpha}) = \begin{cases} \hat{\boldsymbol{\mu}}(\boldsymbol{\alpha}), & \text{if } \boldsymbol{\alpha} \notin \Omega(R) \\ \mathbf{g}(\boldsymbol{\alpha}), & \text{if } \boldsymbol{\alpha} \in \Omega(R) \end{cases} \tag{4.26}$$

where $\mathbf{g}(\boldsymbol{\alpha})$ is an arbitrary function such that $\mathbf{g}(\boldsymbol{\alpha}) \leqslant \sigma$ with probability 1 and $\hat{\boldsymbol{\mu}}(\boldsymbol{\alpha})$ is the solution of the mutual information maximization problem in (4.13) which is given by (4.23) and (4.25).

4.2.2 A Sup-Optimal Solution

When the inequality in (4.19) is not satisfied, the calculation of power control law under the short-term power constraint involves solving the nonlinear equation in (4.21). To reduce the complexity of the associated numerical procedure that is required at the beginning of each fading block, we introduce a simple sub-optimal solution in this subsection.

Although a general closed-form solution is not available for (4.21), it can be solved for the case of low SNR regime, (c.f., equation (4.9) for single-hop channel). This solution implies that the optimal duty cycle for high fading levels (low optimal duty cycle) is mainly related to the fading level through $\mu_i \propto 1/\alpha_i^2$. Furthermore, it is inferred that when the fading level decreases (the optimal duty cycle increases), the inverse relationship between the fading level and optimal duty cycle becomes weaker. Therefore, we assume

$$\mu_i \propto 1/\alpha_i^k \tag{4.27}$$

where $0 < k < 2$ must be chosen appropriately based on the system parameters. Inserting (4.27) in the short-term average constraint in (4.12) with equality, we can calculate a sub-optimal yet simple power control law for the i^{th} hop as

$$\mu_i = \frac{\sigma}{\sum_{j=1}^{K+1} \frac{\alpha_i^k}{\alpha_j^k}}. \tag{4.28}$$

Let $S_>$ denote the set of all individual duty cycles that exceed their optimum values, i.e., $\mu_0(\alpha_i)$. We can improve the sub-optimal duty cycle vector given by (4.28) by letting $\mu_i = \mu_0(\alpha_i), \forall i \in S_>$ and modifying the rest of the duty cycles as

$$\mu_i = \frac{\sigma - \sum\limits_{l \in S_>} \mu_l}{\sum\limits_{\substack{j=1 \\ j \notin S_>}}^{K+1} \frac{\alpha_i^k}{\alpha_j^k}} \tag{4.29}$$

If $S_>$ is still non-empty, we repeat the above procedure until $S_>$ becomes empty.

4.2.3 Long-Term Power Constraint

The outage minimization problem under long-term average power constraint can be expressed as

$$\begin{array}{ll} \min & P_{out} = \Pr\left\{I_M(\alpha, \mu) < R\right\} \\ \text{s.t.} & E\left\{\sum_{i=1}^{K+1} \mu_i(\alpha)\right\} \leqslant \sigma \end{array} \tag{4.30}$$

To present the solution of this problem, we first need to introduce the following minimization problem

$$\begin{array}{ll} \min & \sum\limits_{i=1}^{K+1} \mu_i(\alpha) \\ \text{s.t.} & I_M(\alpha, \mu) \geqslant R \end{array} \tag{4.31}$$

which is the dual of the problem in (4.13) and can be solved by Lemma 4.3 given in the following.

Lemma 4.3: Assuming $I(\alpha_m, \mu_0(\alpha_m)) \geqslant R$ where $\alpha_m = \min\{\alpha_1, \cdots, \alpha_{K+1}\}$ and $\mu_0(\cdot)$ is given by (4.14), the solution to the minimization problem in (4.31) is given by

$$\mu_i^*(\alpha_i) = I^{-1}(\alpha_i, R), \text{ for } i = 1, 2, \cdots, K+1 \tag{4.32}$$

where $I^{-1}(\alpha, \cdot)$ is given by (4.18).

Proof: See section 4.4.3.

Note that if for a channel state vector $\boldsymbol{\alpha}$, the assumption $I(\alpha_m, \mu_0(\alpha_m)) \geqslant R$ does not hold, then the multi-hop mutual information falls necessarily below the transmission rate (i.e., $I_M(\boldsymbol{\alpha}, \boldsymbol{\mu}) < R$) and the feasible set of problem in (4.31) would be empty. In such a channel state, outage happens regardless of the allocated input power and thus we call them *unavoidable* outage states. We can now present the solution of the outage probability minimization problem in (4.30) using the following Proposition.

Proposition 4.1: The i^{th} element of the optimized duty cycle vector is given by

$$\hat{\mu}_i(\boldsymbol{\alpha}) = \begin{cases} \mu_i^*(\alpha_i) = I^{-1}(\alpha_i, R), & \text{if } \boldsymbol{\alpha} \in \Re(\varsigma^*) \\ 0, & \text{otherwise} \end{cases} \tag{4.33}$$

where $\mu_i^*(\alpha_i)$ is the solution of (4.31) given by Lemma 4.3. For $\varsigma \in \mathbb{R}_+$, we define the region

$$\Re(\varsigma) = \left\{ \boldsymbol{\alpha} \in \mathbb{R}_+^{K+1} : \sum\nolimits_{i=1}^{K+1} \mu_i^*(\alpha_i) \leqslant \varsigma \wedge I(\alpha_m, \mu_0(\alpha_m)) \geqslant R \right\}. \tag{4.34}$$

The threshold value ς^* in (4.33) can be defined as $\varsigma^* = \sup\{\varsigma : P(\varsigma) < \sigma\}$ where

$$P(\varsigma) = \int\limits_{\Re(\varsigma)} \sum\nolimits_{i=1}^{K+1} I^{-1}(\alpha_i, R) dF(\alpha) \tag{4.35}$$

and $F(\alpha)$ is the continuous[3] cdf of the fading parameter α.

[3]The commonly used fading distributions for atmospheric turbulence are continuous. Interested readers may refer to [55] for more details on required modifications in the case of discrete fading distributions.

Proof: See section 4.4.4.

The resulting minimum outage probability is then given by

$$\hat{P}_{out} = 1 - \Pr\{\boldsymbol{\alpha} \in \Re(\varsigma^*)\}. \tag{4.36}$$

The power control law given by (4.33) constitutes a threshold ς^* such that if the sum of the optimal duty cycles exceeds the threshold or an unavoidable outage state occurs, transmission is turned off. Otherwise, transmission is turned on with an outage-preventive power control law with minimum power consumption given by (4.32). In fact, the power control law turns off the transmission in unavoidable outage states or very bad fading conditions to save power therefore avoiding outage in the better channel states.

4.2.4 No CSI at the Transmitters

The outage probability minimization problem for the case of no CSI at the transmitters can be expressed as

$$\begin{array}{ll} \min & P_{out} = \Pr\{I_M(\alpha, \mu) < R\} \\ \text{s.t.} & \sum\limits_{i=1}^{K+1} \mu_i \leqslant \sigma \text{ with probability 1} \end{array} \tag{4.37}$$

where the optimizing duty cycles are constant rather than a function of the fading parameters. Noting that individual channel coefficients are statistically independent, the objective function in (4.37) can be written as

$$\begin{aligned} P_{out} &= \Pr\left\{\bigcup_{i=0}^{K+1} I(\alpha_i, \mu_i) < R\right\} = 1 - \Pr\left\{\bigcap_{i=0}^{K+1} I(\alpha_i, \mu_i) < R\right\} \\ &= 1 - \prod_{i=0}^{K+1} (1 - \Pr\{I(\alpha_i, \mu_i) < R\}). \end{aligned} \tag{4.38}$$

We assume identical distributions for the individual channel coefficients. Therefore, the outage probability in (4.38) is a symmetric function of individual duty cycles and this implies that the individual optimal duty cycles are equal to each other in the optimal solution. Furthermore, from (4.38), it is apparent that minimizing the objective function of (4.37) is equivalent to minimizing the outage probability of the individual hops. Therefore the problem in (4.37) reduces to

$$\begin{array}{ll} \min & P_{out} = \Pr\left\{I(\alpha,\mu) < R\right\} \\ \text{s.t.} & \mu \leqslant \frac{\sigma}{K+1} \end{array} \tag{4.39}$$

In (4.39), we deliberately eliminate the index of α and μ, since the solution of (4.39) as stated in Proposition 4.2 below does not depend on the characteristics of the individual channel states.

Proposition 4.2: The solution to the problem in (4.39) is given by

$$\hat{\mu} = \min\left\{\mu^*, \sigma/(K+1)\right\} \tag{4.40}$$

where μ^* can be obtained by solving

$$\mu^* \zeta(\beta/\mu^*, s) = \frac{R}{A} - \zeta(\beta, s) \tag{4.41}$$

with

$$\beta = -s\left[\mathrm{W}_{-1}\left(-\exp\left(-1-\frac{R}{As}\right)\right)+1\right]. \tag{4.42}$$

Proof: See section 4.4.5.

Based on Proposition 4.2, the solution of minimization problem in (4.37) can be stated as

$$\hat{\mu}_i = \min\left\{\mu^*, \sigma/(K+1)\right\},\ \forall i \in \{1,2,\cdots,K+1\} \tag{4.43}$$

where μ^* is obtained by solving (4.41).

4.3 Numerical Results and Discussions

In this section, we present numerical results of our outage analysis. We assume an absorption and scattering loss of 0.43 dB/km (i.e., $a \approx 0.1$) and a log-normal fading strength of $\sigma_\chi^2 = 0.3$ for the direct link connecting the source and destination ($L = 10$ km). It is assumed that the relays are evenly distributed along the path from the source to the destination. Before we discuss the performance of multi-hop system, we

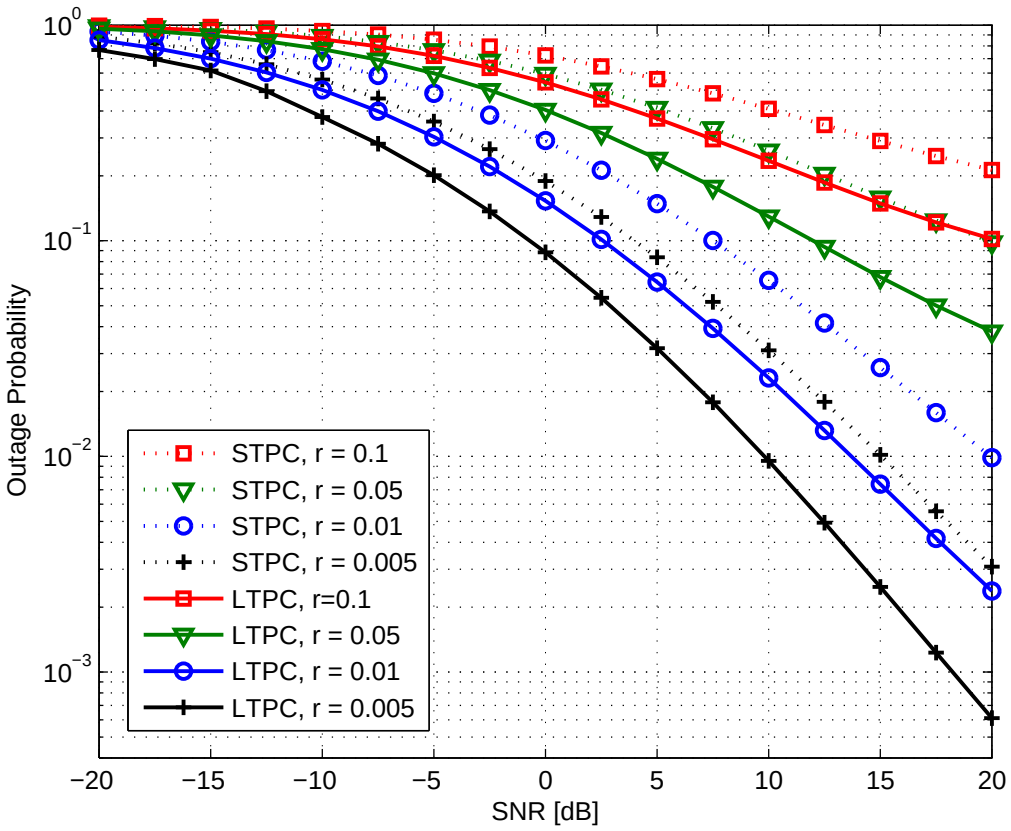

Figure 4.1: The outage probability of the single-hop Poisson fading channel with CSI available at the transmitters ($\sigma = 0.1$).

first present the performance of single-hop system which will be used as a benchmark. Figure 4.1 demonstrates the outage probability of a single-hop Poisson channel (i.e., direct transmission) over log-normal fading. CSI is available at the transmitters and subject to either a short or long-term power constraint. The outage probability is calculated for $\sigma = 0.1$ and at different data rates with relative rates in the range of $r = 0.005$ to $r = 0.1$. As expected, the single-hop system performs better under the long-term power constraint (LTPC) rather than the short-term power constraint (STPC). We further observe that this improvement is independent of the data rate variations.

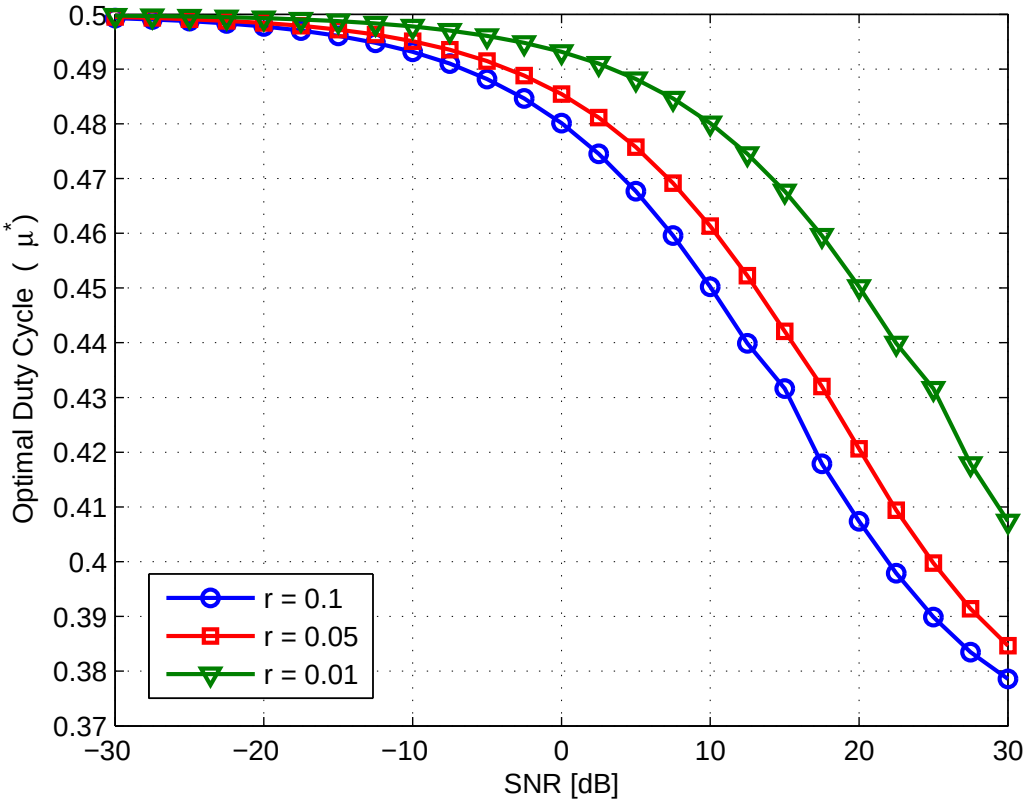

Figure 4.2: The optimal duty cycle of a single-hop Poisson fading channel with no CSI at the transmitter as a function of SNR ($\sigma = 0.5$).

Figure 4.2 shows the variation of the optimal duty cycle for a single-hop system

with no CSI (i.e., μ^*) as a function of SNR. The optimal duty cycle given by (4.41) is calculated at different data rates. We observe from figure 4.2 that the constant optimal duty cycle, μ^*, for the case of no CSI varies from $1/e$ at very high SNR to 0.5 at very low SNR. These asymptotic values can be also confirmed by the earlier results on the optimal duty cycle at high SNR (i.e., $\lambda_0 \to 0$) and low SNR (i.e., $\lambda_0 \to \infty$) regimes [49, 52].

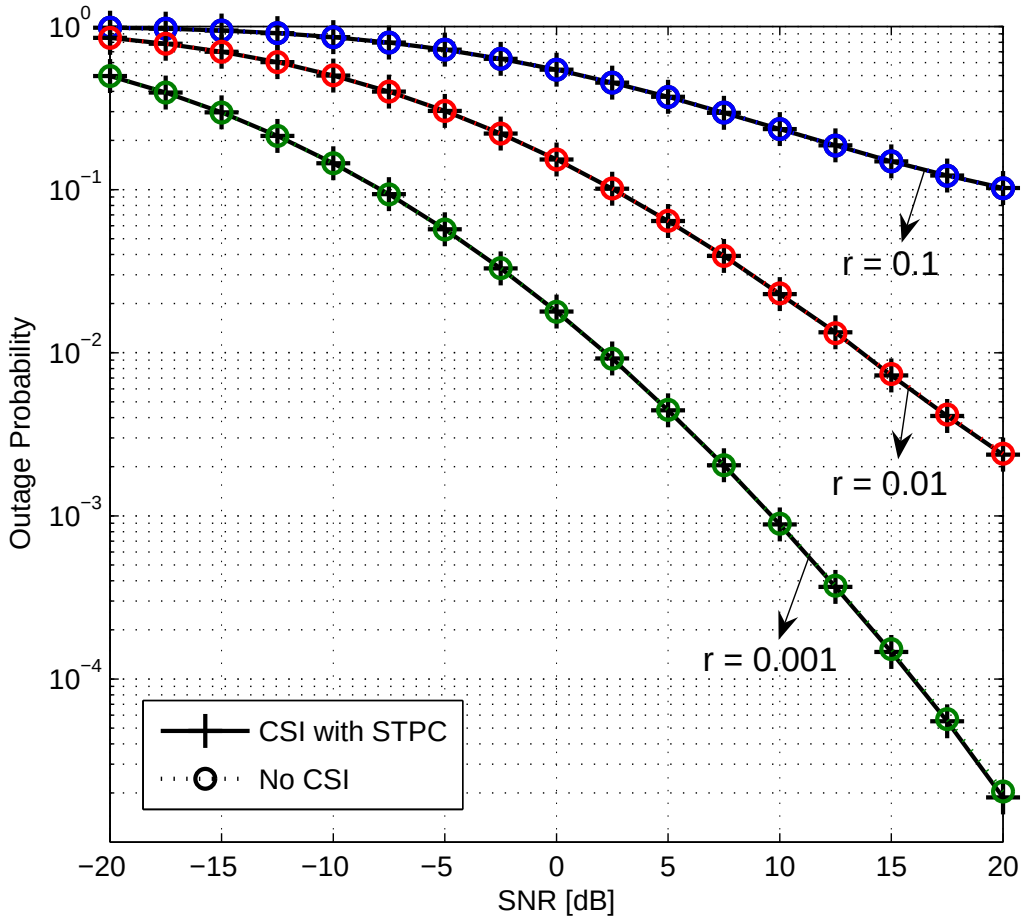

Figure 4.3: The outage probability comparison of the single-hop Poisson fading channel for no CSI case and CSI case with STPC ($\sigma = 0.5$).

Figure 4.3 demonstrates the outage probability for the single-hop system under

short-term power constraint with and without CSI available at the transmitter assuming $\sigma = 0.5$ and different data rates. It is observed that the single-hop system, even at $\sigma = 0.5$, cannot take advantage of the available CSI at the transmitter. In fact, for the single-hop system under the short-term power constraint, knowing the perfect CSI and optimizing the duty cycle accordingly at the beginning of each fading block does not lead to a better outage probability than using the constant optimal duty cycle of the no CSI case given by (4.41). Note that the variation of data rate does not affect this result. This result is somewhat expected if one notes that the power control law for these two cases actually converge at $\hat{\mu} = \min\{1/e, \sigma\}$ for high SNR and $\hat{\mu} = \min\{1/2, \sigma\}$ for low SNR.

Figures 4.4 and 4.5 plot the outage probability of a dual-hop system for the cases of i) perfect CSI with short-term power constraint (STPC) assuming optimal solution), ii) perfect CSI with STPC assuming sub-optimal solution, iii) perfect CSI with long-term power constraint (LTPC), and iv) no CSI assuming a relative rate of $r = 0.01$ and average-to-peak power ratios $\sigma = 0.1$ and 0.25.

We observe from figures 4.4 and 4.5 that the dual-hop system with long-term constraint outperforms the system with short-term constraint. Furthermore it can be seen that unlike the single-hop system (figure 4.3), the dual-hop system can take advantage of available CSI at the transmitters even under short-term constraint and outperforms the system with no CSI for different average-to-peak power ratios. The proposed sub-optimal solution (assuming $k = 0.9$) yields an outage probability very close to the optimum values under short-term constraint for both values of σ. The sub-optimal power control law with a much less complexity can perform almost the same as the more complicated optimal power control law. Comparison of figures 4.1 and 4.5 reveals that the relay-assisted transmission can significantly improve the outage rate of direct transmission at $r = 0.01$. For example, an impressive performance gain of more than 30 dB is observed at the outage probability of 10^{-2} for the dual-hop system with or without CSI.

We observe from the comparison of figures 4.4 and 4.5 that for both cases of no CSI and perfect CSI with short-term constraint, reduction in the average-to-peak power ratio from $\sigma = 0.25$ to $\sigma = 0.1$ increases the outage probability. However, this is not

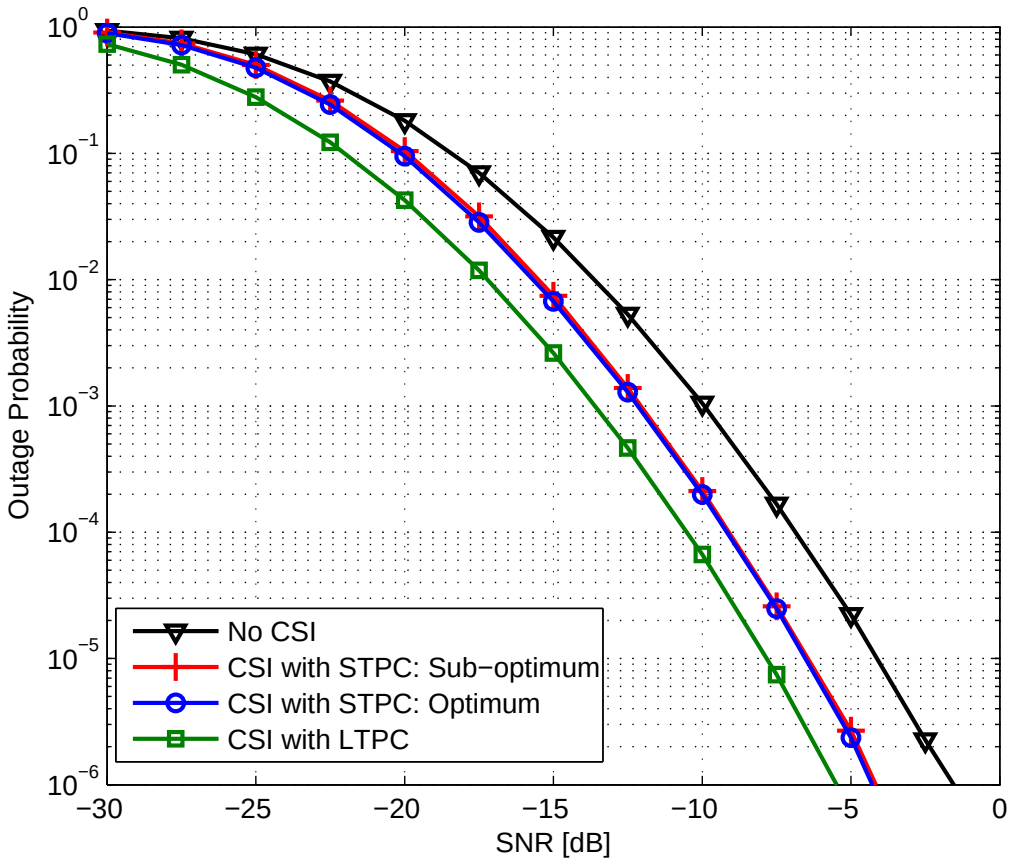

Figure 4.4: The outage probability of the dual-hop Poisson fading channel for cases of i) perfect CSI with STPC assuming optimal solution, ii) perfect CSI with STPC assuming sub-optimal solution, iii) perfect CSI with LTPC, and iv) no CSI ($\sigma = 0.5$ and $r = 0.01$).

observed in quite the same way for the case of perfect CSI with long-term constraint. In fact, although we observe some outage increase in the SNR range[4]of about -18 dB to -8 dB caused by reduction of average-to-peak power ratio, the outage probability

[4]It should be emphasized that some transformations on the SNR values are required before we can compare them with common practical SNR values. This is because we defined SNR in this chapter as the peak-signal-to-noise-ratio at the transmitter (source) rather than the commonly employed average-signal-to-noise-ratio at the receiver which may attain much higher values.

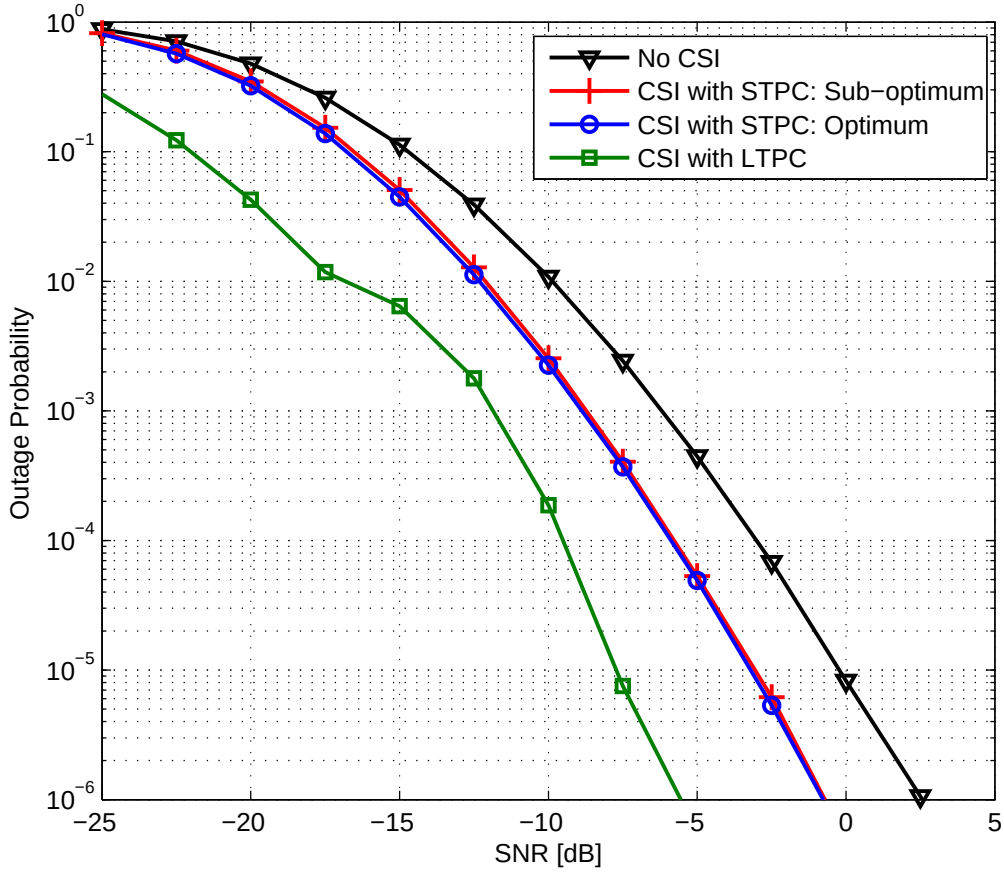

Figure 4.5: The outage probability of the dual-hop Poisson fading channel for cases of i) perfect CSI with STPC assuming optimal solution, ii) perfect CSI with STPC assuming sub-optimal solution, iii) perfect CSI with LTPC, and iv) no CSI ($\sigma = 0.1$ and $r = 0.01$).

remains the same in lower and higher SNR values. This phenomenon can be explained by examining the outage region of the dual-hop system with long-term constraint. Assuming $r = 0.01$ and $\sigma = 0.1$, we plot the boundary of the outage region (when the transmission is turned off) and its complement region, $\Re(\varsigma^*)$, in figure 4.6.

In figure 4.6, the illustrated region $\Re(\varsigma^*)$ which is defined in (4.34) is limited by

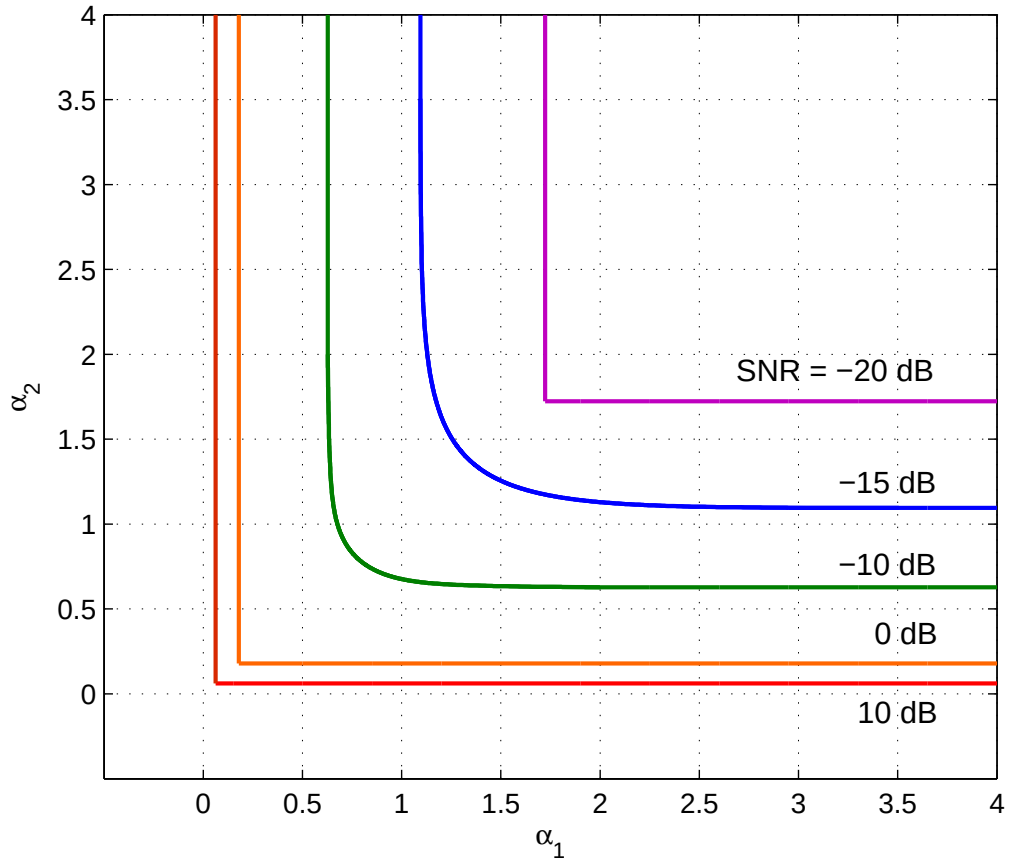

Figure 4.6: The boundary of the outage region and its complement region $\Re(\varsigma^*)$ for the dual-hop system with LTPC ($\sigma = 0.1$ and $r = 0.01$).

both the average sum power constraint (associated with the first condition in (4.34)) and unavoidable outage threshold (associated with the second condition in (4.34)). We observe from figure 4.6 that, for SNR values of -15 dB and -10 dB, not only the unavoidable outage threshold effect is involved but also the average sum power constraint is active. However, for higher and lower SNR values, the long-term average sum power constraint is inactive. Therefore, decreasing the average-to-peak power ratio does not affect the outage probability in these SNR values.

Figure 4.7 illustrates the effect of parameter k in the accuracy of the sub-optimal

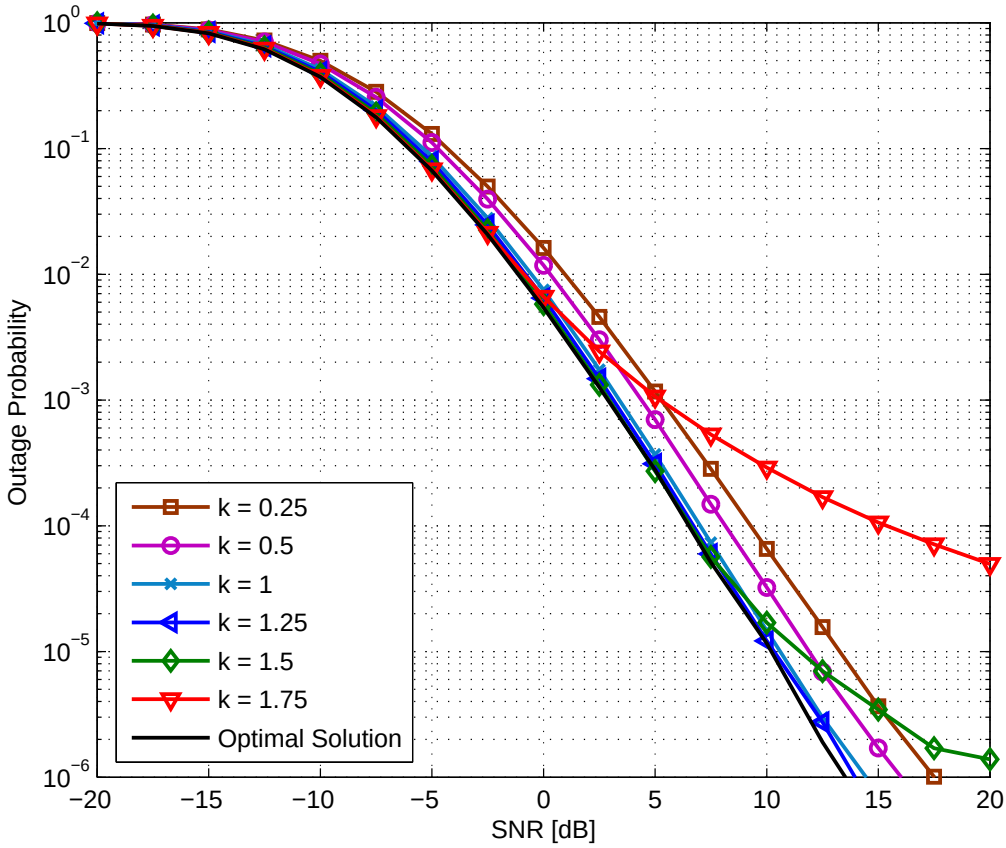

Figure 4.7: The effect of parameter k on the sub-optimal solution for a dual-hop system with $\sigma = 0.1$ and $r = 0.1$.

solution for a dual-hop system with $r = 0.1$ and $\sigma = 0.1$. We observe that an inappropriate choice of k can significantly affect the accuracy of sub-optimal solution particularly at higher SNR. However, it also shows that the performance of the sub-optimal solution is not so sensitive to the small variations around the optimal selection.

Figure 4.8 demonstrates the outage probability of the multi-hop system with different number of hops ($K = 0, 1, 2$) for the cases of i) perfect CSI with STPC assuming optimal solution, ii) perfect CSI with STPC assuming sub-optimal solution, iii) perfect CSI with LTPC, and iv) no CSI assuming $r = 0.1$ and $\sigma = 0.1$. We observe that the

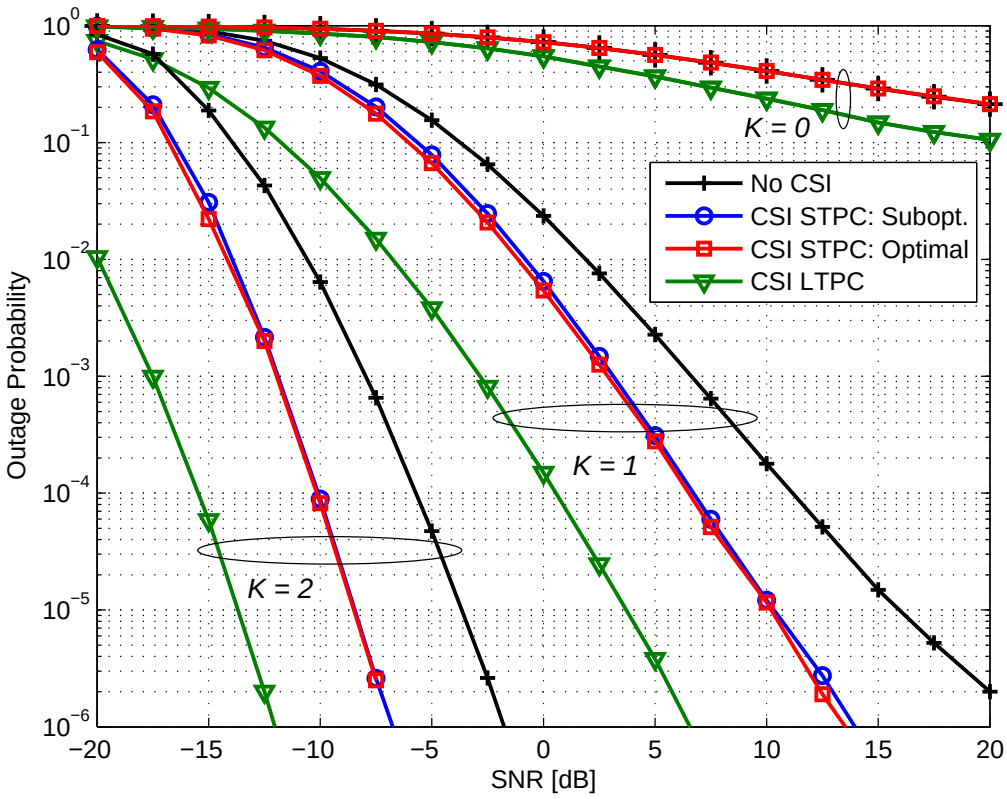

Figure 4.8: The outage probability of the Poisson fading channel for different number of relays for cases of i) perfect CSI with STPC assuming optimal solution, ii) perfect CSI with STPC assuming sub-optimal solution, iii) perfect CSI with LTPC, and iv) no CSI ($\sigma = 0.1$ and $r = 0.1$).

sub-optimal solution can perform very close to the optimal solution for both dual-hop ($k = 1.25$) and triple-hop ($k = 1.75$) systems. It is further observed that CSI available at the transmitter is useful for the multi-hop relaying particularly for the system under long-term constraint.

Moreover, figure 4.8 demonstrates that increasing the number of relays results in significant improvement in the outage probability. For example, an additional performance gain of about 18 dB is observed at the outage probability of 10^{-5} when the

second relay is inserted. In fact, this is a result of the fact that multi-hop FSO system exploits the distance-dependency of the turbulence-induced fading variance by lowering the fading strength of the individual intermediate hops through the insertion of relay nodes.

4.4 Proofs of Lemmas and Propositions

In this section, we present the proofs of lemmas and propositions stated in section 4.2.

4.4.1 Proof of Lemma 4.1

Proof. It is apparent that the duty cycle vector $\tilde{\boldsymbol{\mu}}$ in (4.17) attains the value of $C_m = I(\alpha_m, \mu_0(\alpha_m))$ in (4.16). In order to prove that $\tilde{\boldsymbol{\mu}}$ is a solution of (4.15), we need to show that any other duty cycle vector $\boldsymbol{\mu'}$ attains mutual information of less than or equal to C_m, i.e., $I_M(\boldsymbol{\alpha}, \boldsymbol{\mu'}) \leqslant C_m,\ \forall \boldsymbol{\mu'} \in \mathbb{R}_+^{K+1}$. In fact, we have

$$\begin{aligned} I_M(\boldsymbol{\alpha}, \boldsymbol{\mu'}) &\leqslant I(\alpha_m, \mu'_m) \\ &\leqslant I(\alpha_m, \mu_0(\alpha_m)) \\ &= C_m \end{aligned} \tag{4.44}$$

where the first inequality follows by the definition of multi-hop mutual information function and the second inequality follows by noting that $\mu_0(\alpha_m)$ maximizes $I(\alpha_m, \cdot)$. However, $\tilde{\boldsymbol{\mu}}$ is not the only solution of the unconstrained problem in (4.15). For example, letting $\mu_m = \mu_0(\alpha_m)$, we can obtain many other solutions to (4.15) by selecting μ'_is $(\forall i = 1, \cdots, K+1, i \neq m)$ within the interval of $(I^{-1}(\alpha_i, C_m),\ \mu_0(\alpha_i))$. This is implied by knowing that $I(\alpha_i, \cdot)$ is monotonically increasing in those intervals.

Now, we need to show that $\tilde{\boldsymbol{\mu}}$ which maximizes (4.15) attains the minimum duty cycle sum as well. Let $\boldsymbol{\mu''}$ be any arbitrary duty cycle vector such as $\sum \mu''_i < \sum \tilde{\mu}_i$.

Then, there must be at least one hop with index j for which $\mu''_j < \tilde{\mu}_j$. Therefore, we have

$$\begin{aligned} I_M(\boldsymbol{\alpha}, \boldsymbol{\mu''}) &\leqslant I(\alpha_j, \mu''_j) \\ &< I(\alpha_j, \tilde{\mu}_j) \\ &= I(\alpha_j, I^{-1}(\alpha_j, C_m)) \\ &= C_m \end{aligned} \tag{4.45}$$

where the first inequality follows by the definition of multi-hop mutual information function and the second inequality follows by noting that $I(\alpha_j, \cdot)$ is strictly increasing within $(0,\ \mu_0(\alpha_j)]$ and the fact that the inverse of mutual information function given by (4.18) always returns duty cycles below the maximizing duty cycle, i.e., $I^{-1}(\alpha, \cdot) \leqslant \mu_0(\alpha)$. Equation(4.45) implies that any arbitrary $\boldsymbol{\mu''}$ such that $\sum \mu''_i < \sum \tilde{\mu}_i$ cannot be a solution of (4.15) and therefore $\tilde{\boldsymbol{\mu}}$ is the solution with minimum duty cycle sum. □

4.4.2 Proof of Lemma 4.2

Proof. First, we need to show that the equations in (4.20) have a solution. When (4.19) does not hold, the global solution of unconstrained problem even with minimum duty cycle sum (i.e., $\tilde{\boldsymbol{\mu}}$ given by Lemma 4.1) does not belong to the feasible region of optimization problem in (4.13). Note that the solution of constrained problem cannot exceed this global solution. Therefore, by considering the continuity of the mutual information function, the solution to the equations in (4.20) is available and can be written as $\boldsymbol{\mu^*} = \tilde{\boldsymbol{\mu}} - \boldsymbol{\varepsilon}$ for some $\boldsymbol{\varepsilon} \in \mathbb{R}_+^{K+1}$ such that $\sum \varepsilon_i = \sum I^{-1}(\alpha_i, C_m) - \sigma$.

To complete the proof, we show that $\boldsymbol{\mu^*}$, i.e., the solution of the equations in (4.20), maximizes (4.13). In fact, for any arbitrary power control law $\boldsymbol{\mu'}$ which satisfies the constraint of (4.13), we know that there is at least one individual duty cycle μ'_k such that $\mu'_k \leqslant \mu^*_k$. This is because $\boldsymbol{\mu^*}$ satisfies the constraint with equality. Therefore, we have

$$
\begin{aligned}
I_M(\boldsymbol{\alpha}, \boldsymbol{\mu'}) &\leqslant I(\alpha_k, \mu'_k) \\
&\leqslant I(\alpha_k, \mu^*_k) \\
&= C^* \\
&= I_M(\boldsymbol{\alpha}, \boldsymbol{\mu}^*) \qquad (4.46)
\end{aligned}
$$

where the first inequality follows by the definition of multi-hop mutual information function and the second inequality follows by noting that $I(\alpha_k, \cdot)$ is increasing within $(0,\ \mu_0(\alpha_k)]$. Equation (4.46) implies that any arbitrary $\boldsymbol{\mu'}$ attains multi-hop mutual information of less than or equal to the resulting mutual information by $\boldsymbol{\mu^*}$ and thus $\boldsymbol{\mu^*}$ is the solution of the constrained maximization problem in (4.13). □

4.4.3 Proof of Lemma 4.3

Proof. Inserting $I_M(\boldsymbol{\alpha}, \boldsymbol{\mu})$ given by (4.6) in the constraint of equation (4.31), we can rewrite the problem (4.31) as

$$
\begin{aligned}
\min \quad & \sum_{i=1}^{K+1} \mu_i(\boldsymbol{\alpha,}) \\
\text{s.t.} \quad & I(\alpha_1, \mu_1) \geqslant R, I(\alpha_2, \mu_2) \geqslant R, \cdots, I(\alpha_{K+1}, \mu_{K+1}) \geqslant R. \qquad (4.47)
\end{aligned}
$$

Assuming η_i's $(1 < i < K+1)$ are Lagrange multipliers, the Lagrange function can be expressed as

$$
\mathrm{L}(\boldsymbol{\mu}) = \sum_{i=1}^{K+1} [\mu_i - \eta_i(I(\alpha_i, \mu_i) - R)]. \qquad (4.48)
$$

To find the minimum, we set the gradient of (4.48) to zero and obtain

$$1 - \eta_i I'(\alpha_i, \mu_i) = 0, \ \forall 1 \leqslant i \leqslant K+1 \tag{4.49}$$

where $I'(\alpha_i, \mu_i)$ is the first derivative of mutual information function with respect to the duty cycle variable. Furthermore, noting that the mutual information function is concave, it is easy to verify that the second derivative of (4.48) is always positive. The Karush-Kuhn-Tucker (KKT) conditions enforce that the minimum point satisfies

$$\begin{aligned} \eta_i &\geqslant 0, \ \forall 1 \leqslant i \leqslant K+1 \\ \eta_i(I(\alpha_i, \mu_i) - R) &= 0, \ \forall 1 \leqslant i \leqslant K+1 \ . \end{aligned} \tag{4.50}$$

Inserting (4.49) in the first condition of (4.50), we obtain $I'(\alpha_i, \mu_i) \geqslant 0, \ \forall 1 \leqslant i \leqslant K+1$. This implies that the minimum point can be only attained in the increasing region of the mutual information function. Furthermore, from (4.49), it is obvious that $\eta_i \neq 0, \ \forall 1 \leqslant i \leqslant K+1$. Therefore, the second condition in (4.50) implies that the minimum is obtained when the constraints are satisfied with equality, i.e., $I(\alpha_i, \mu_i) = R, \ \forall 1 \leqslant i \leqslant K+1$. Based on the assumption of the Lemma (i.e., $I(\alpha_m, \mu_0(\alpha_m)) \geqslant R$), we know for all $1 \leqslant i \leqslant K+1$ the equality equations have solutions. Therefore, we can write the solution to the problem in (4.31) using the inverse mutual information function as

$$\mu_i^*(\alpha_i) = I^{-1}(\alpha_i, R), \ \forall 1 \leqslant i \leqslant K+1 \tag{4.51}$$

where the inverse mutual information function, $I^{-1}(\alpha_i, R)$, is given by (4.18). Note that the inverse function is expressed in terms of -1^{th} branch of the Lambert-W function. Therefore, the calculated optimal duty cycle values by (4.51) are always within the increasing region of the mutual information function and hence (4.51) satisfy the KKT conditions. □

4.4.4 Proof of Proposition 4.1

Proof. This proof is based on the approach proposed in [55]. Accordingly, we first introduce the following lemmas.

Lemma 4.4: Let u be a nonnegative real random variable with continuous cdf $F(u)$ and χ_ε denote the indicator function of a subset of $\left\{u \in \mathbb{R}_+\right\}$. We consider the following maximization problem

$$\begin{aligned} &\max \quad \mathrm{E}\{\chi_\varepsilon w(u)\}, \\ &\text{s.t.} \quad 0 \leqslant w(u) \leqslant 1 \text{ and } \mathrm{E}\{\chi_\varepsilon u w(u)\} \leqslant \sigma \ . \end{aligned} \tag{4.52}$$

Then the solution is given by

$$\hat{w}(u) = \begin{cases} 1, & \text{for } u \leqslant \varsigma^* \\ 0, & \text{for } u > \varsigma^* \end{cases} \tag{4.53}$$

where, for $\varsigma \in \mathbb{R}_+$, we let $P(\varsigma) = \int_0^\varsigma \chi_\varepsilon u dF(u)$ and $\varsigma^* = \sup\{\varsigma : P(\varsigma) < \sigma\}$.

Proof. By definition of $\hat{w}(u)$, it is apparent that $\hat{w}(u)$ satisfies the constraints. Therefore, one of the two conditions below will apply

$$\mathrm{E}\{\chi_\varepsilon u \hat{w}(u)\} = P(\varsigma^*) < \sigma, \tag{4.54}$$

$$\mathrm{E}\{\chi_\varepsilon u \hat{w}(u)\} = P(\varsigma^*) = \sigma. \tag{4.55}$$

If (4.54) holds, it is immediate that $\varsigma^* \to \infty$ and therefore (4.53) reduces to a trivial solution as $\hat{w}(u) = 1$ which obviously maximizes (4.52). Now we consider the nontrivial case where the solution in (4.53) satisfies the constraint with equality. Inserting $\hat{w}(u)$ in the objective function, we have

$$\mathrm{E}\{\chi_\varepsilon \hat{w}(u)\} = \int_0^{\varsigma} \chi_\varepsilon dF(u). \tag{4.56}$$

We need to show that if for any other weight function $0 \leqslant w(u) \leqslant 1$ such that $\mathrm{E}\{\chi_\varepsilon w(u)\}$ is larger than (4.56), then it must violate the constraint. For any such $w(u)$, we have

$$\begin{aligned}
\mathrm{E}\{\chi_\varepsilon u w(u)\} - \sigma &= \mathrm{E}\{\chi_\varepsilon u w(u)\} - \mathrm{E}\{\chi_\varepsilon u \hat{w}(u)\} \\
&= \int_{\varsigma^*}^{\infty} \chi_\varepsilon u w(u) dF(u) - \int_0^{\varsigma^*} \chi_\varepsilon u (1 - w(u)) dF(u) \\
&\geqslant \varsigma^* \left[\int_{\varsigma^*}^{\infty} \chi_\varepsilon w(u) dF(u) - \int_0^{\varsigma^*} \chi_\varepsilon (1 - w(u)) dF(u) \right] \\
&= \varsigma^* \left[\mathrm{E}\{\chi_\varepsilon w(u)\} - \mathrm{E}\{\chi_\varepsilon \hat{w}(u)\} \right].
\end{aligned} \tag{4.57}$$

Equation (4.57) shows that if $\mathrm{E}\{\chi_\varepsilon w(u)\} > \mathrm{E}\{\chi_\varepsilon \hat{w}(u)\}$, then $\mathrm{E}\{\chi_\varepsilon u w(u)\} > \sigma$ and therefore $w(u)$ violates the constraint. □

Lemma 4.5: The solution of (4.30) is in the form of

$$\hat{\boldsymbol{\mu}}(\boldsymbol{\alpha}) = \begin{cases} \chi_\rho \boldsymbol{\mu}^*(\boldsymbol{\alpha}), & \text{with probability } \hat{w}(\boldsymbol{\alpha}) \\ 0, & \text{with probability } [1 - \hat{w}(\boldsymbol{\alpha})] \end{cases} \tag{4.58}$$

where $\boldsymbol{\mu}^*(\boldsymbol{\alpha})$ is the solution of (4.31) and χ_ρ denotes the indicator function of region $\rho(R) = \left\{ \boldsymbol{\alpha} \in \mathbb{R}_+^{K+1} : I(\alpha_m, \mu_0(\alpha_m)) \geqslant R \right\}$ for which the problem in (4.31) has a solution. Furthermore, $\hat{w}(\boldsymbol{\alpha})$ is a weight function $\mathbb{R}_+^{K+1} \to [0,\ 1]$ and is obtained by solving the following problem

$$\begin{aligned}
&\max \quad \mathrm{E}\{\chi_\rho w(\boldsymbol{\alpha})\}, \\
&\text{s.t.} \quad 0 \leqslant w(\boldsymbol{\alpha}) \leqslant 1 \text{ and } \mathrm{E}\left\{ \chi_\rho \sum\nolimits_{i=1}^{K+1} \mu_i^*(\alpha_i) w(\boldsymbol{\alpha}) \right\} \leqslant \sigma.
\end{aligned} \tag{4.59}$$

Proof. The resulting outage probability of the power control law in (4.58) can be expressed as

$$\hat{P}_{out}(R,\sigma) = 1 - \mathrm{E}\{\chi_\rho \hat{w}(\boldsymbol{\alpha})\}. \tag{4.60}$$

Considering an arbitrary duty cycle vector $\boldsymbol{\mu}$ in the class of probabilistic stationary memoryless power-allocation functions [55] satisfying the constraint $\mathrm{E}\left\{\sum \mu_i\right\} \leqslant \sigma$, we define the region

$$A(\boldsymbol{\alpha}, R) = \left\{\boldsymbol{\mu} \in \mathbb{R}_+^{K+1} : I_M(\boldsymbol{\alpha}, \boldsymbol{\mu}) \geqslant R\right\}. \tag{4.61}$$

Therefore the outage probability resulting from $\boldsymbol{\mu}$ is given by

$$P_{out}(R,\sigma) = 1 - \Pr\{\boldsymbol{\mu} \in A(\boldsymbol{\alpha}, R)\}. \tag{4.62}$$

We need to show that $\hat{P}_{out}(R,\sigma) \leqslant P_{out}(R,\sigma)$. Let χ_A denote the indicator function of $\{\boldsymbol{\mu} \in A(\boldsymbol{\alpha}, R)\}$ and define the weight function as

$$w(\boldsymbol{\alpha}) = E\{\chi_A | \boldsymbol{\alpha}\} \tag{4.63}$$

where expectation is with respect to $F(\boldsymbol{\mu}|\boldsymbol{\alpha})$ and $0 \leqslant w(\boldsymbol{\alpha}) \leqslant 1$. Then, we define a new power control law as

$$\boldsymbol{\mu'}(\boldsymbol{\alpha}) = \begin{cases} \chi_\rho \boldsymbol{\mu}^*(\boldsymbol{\alpha}), & \text{with probability } w(\boldsymbol{\alpha}) \\ 0, & \text{with probability } [1 - w(\boldsymbol{\alpha})] \end{cases} \tag{4.64}$$

Using the definition of $\boldsymbol{\mu}^*(\boldsymbol{\alpha})$, the outage probability $P'_{out}(R,\sigma)$ resulting from $\boldsymbol{\mu'}$ can be written as

$$
\begin{aligned}
P'_{out}(R,\sigma) &= 1 - \mathrm{E}\{\chi_\rho w(\boldsymbol{\alpha})\} \\
&= 1 - \mathrm{E}\{\chi_\rho E\{\chi_A|\boldsymbol{\alpha}\}\} \\
&= 1 - \mathrm{E}\{E\{\chi_A\chi_\rho|\boldsymbol{\alpha}\}\} \\
&= 1 - \mathrm{E}\{\chi_A\} \\
&= 1 - \Pr\{\boldsymbol{\mu} \in A(\boldsymbol{\alpha}, R)\} \\
&= P_{out}(R,\sigma) \qquad (4.65)
\end{aligned}
$$

where we can write $\chi_A\chi_\rho = \chi_A$, since χ_ρ is either equal to 1 or if $\chi_\rho = 0$ then no power control law can prevent from outage and thus $\chi_A = 0$ as well. Equation (4.65) shows that the newly defined power control law $\boldsymbol{\mu'}$ results in the same outage probability as $\boldsymbol{\mu}$ does. Moreover, we can show that $\boldsymbol{\mu'}$ satisfies the long-term power constraint. In fact, we can write

$$
\begin{aligned}
\sigma &\geqslant \mathrm{E}\left\{\sum \mu_i\right\} \\
&\geqslant \mathrm{E}\left\{\chi_A \sum \mu_i\right\} \\
&\geqslant^{a} \mathrm{E}\left\{\chi_A\chi_\rho \sum \mu_i^*\right\} \\
&= \mathrm{E}\left\{E\{\chi_A\chi_\rho \sum \mu_i^*|\boldsymbol{\alpha}\}\right\} \\
&=^{b} \mathrm{E}\left\{\chi_\rho \sum \mu_i^* E\{\chi_A|\boldsymbol{\alpha}\}\right\} \\
&= \mathrm{E}\left\{\chi_\rho \sum \mu_i^* w(\boldsymbol{\alpha})\right\} \\
&= \mathrm{E}\left\{\sum \mu_i'\right\} \qquad (4.66)
\end{aligned}
$$

where the inequality a follows by the fact that for all $\boldsymbol{\alpha}$ such that $\chi_A = \chi_A\chi_\rho = 1$, we have $\sum \mu_i^* \leqslant \sum \mu_i$ which results from the definition of μ_i^*. Furthermore, the equality b can be written by noting that μ_i^* is a deterministic function of $\boldsymbol{\alpha}$. Equation (4.66) implies that $\boldsymbol{\mu'}$ indeed satisfies the long-term power constraint.

Now, noting that the weight function $w(\boldsymbol{\alpha})$ satisfies the constraint of (4.59) (i.e., $\mathrm{E}\{\chi_\rho \sum \mu_i^* w(\boldsymbol{\alpha})\} \leqslant \sigma$), we can conclude $\mathrm{E}\{\chi_\rho w(\boldsymbol{\alpha})\} \leqslant \mathrm{E}\{\chi_\rho \hat{w}(\boldsymbol{\alpha})\}$ since $\hat{w}(\boldsymbol{\alpha})$ is the

solution of the maximization problem in (4.59). Therefore, recalling the definitions in (4.60) and (4.65), we have $\hat{P}_{out}(R,\sigma) \leqslant P_{out}(R,\sigma)$ which means that the power control law in the form of (4.58) can achieve outage probability lower or equal to that of any arbitrary power control law. □

Having the optimum form for the solution of (4.30) by Lemma 4.5, we need to obtain an explicit expression for the weight function $\hat{w}(\boldsymbol{\alpha})$ by Lemma 4.4 in order to write the solution of (4.30). Let $u = \sum \mu_i^*(\alpha_i)$ which is a continuous function $\mathbb{R}_+^{K+1} \to \mathbb{R}_+$. For a given continuous $F(\alpha)$, this power sum is a random variable with cdf of

$$F(u) = \Pr\left\{\sum\nolimits_{i=1}^{K+1} \mu_i^*(\alpha_i) \leqslant u\right\} \tag{4.67}$$

which remains continuous. Applying Lemma 4.4 to $u = \sum \mu_i^*(\alpha_i)$ to find $\hat{w}(\boldsymbol{\alpha})$ and ς^* and further using Lemma 4.3 and Lemma 4.5, we can simply write the explicit solution of (4.30) as in Proposition 4.1 (i.e., (4.33, 4.34, and 4.35)) where the region $\Re(\varsigma^*)$ in (4.33) corresponds to the union of the interval $u \leqslant \varsigma^*$ in (4.53) and the effect of indicator function χ_ρ in (4.58). Furthermore, knowing that $\mu_i^*(\alpha_i) = I^{-1}(\alpha_i, R)$ is continuous and non-increasing, we have $\Re(\varsigma) \subseteq \Re(\varsigma')$ for any $0 \leqslant \varsigma \leqslant \varsigma' \leqslant \infty$. □

4.4.5 Proof of Proposition 4.2

Proof. Since $I(\cdot,\mu)$ is an increasing continuous function with a range covering the whole $\mathbb{R}_+$, $I(\alpha,\mu) = R$ has a unique solution for all $\mu, R \in \mathbb{R}_+$. Therefore we can rewrite the objective function in (4.39) as

$$\Pr\{\alpha < f(\mu)\} = F(f(\mu)) \tag{4.68}$$

where $f(\mu) = I^{-1}(R,\mu)$ is the solution of $I(f(\mu),\mu) = R$ and $F(\cdot)$ is the cdf of the continuous fading parameter α. Note that the function $f(\mu) = I^{-1}(R,\mu)$ is the inverse of mutual information function with respect to the first argument and is different from

the inverse function given by (4.18). Following that cdf function $F(\cdot)$ is increasing, the outage minimization problem in (4.39) reduces to

$$\begin{aligned} \min \quad & f(\mu) = I^{-1}(R, \mu) \ , \\ \text{s.t.} \quad & \mu \leqslant \sigma/(K+1). \end{aligned} \tag{4.69}$$

Let us first consider the problem in (4.69) without constraint. We can find the derivative of $f(\mu)$ through the following differential equation

$$\frac{dI(f(\mu), \mu)}{d\mu} = \frac{dR}{d\mu} = 0. \tag{4.70}$$

Expanding (4.70), we can write the first derivative of $f(\mu)$ as

$$f'(\mu) = \frac{f(\mu)\left[1 - \ln(\mu f(\mu) + s)\right] - \zeta(f(\mu), s)}{\mu\left[\ln(f(\mu) + s) - \ln(\mu f(\mu) + s)\right]} \tag{4.71}$$

which implies that the function $f(\mu) : (0,\ 1) \to \mathbb{R}_+$ is differentiable and therefore continuous in its domain. To find the critical points of $f(\mu)$, we apply $f'(\mu) = 0$ and obtain

$$\mu f(\mu) - s\ln(\mu f(\mu) + s) + s\ln s = R/A \tag{4.72}$$

and after some algebra, we can express $f(\mu)$ in terms of Lambert-W function as

$$f(\mu) = \frac{-s}{\mu}\left[\mathrm{W}_{-1}\left(-\exp\left(-1 - \frac{R}{As}\right)\right) + 1\right]. \tag{4.73}$$

Applying $I(\cdot, \mu)$ to both sides of (4.73) and noting that $I(f(\mu), \mu) = R$, we have $R = I(\beta/\mu, \mu)$ or equivalently

$$\mu\zeta(\beta/\mu, s) = \frac{R}{A} - \zeta(\beta, s) \tag{4.74}$$

where the constant β is given by (4.42).

Taking the derivative of (4.71) and inserting $f'(\mu) = 0$ in the resulting expression, we can write the second derivative of $f(\mu)$ at its critical point(s) as

$$f''(\mu^*) = \frac{\alpha^2}{\mu^*(\mu^* f(\mu^*) + s) \ln\left(\frac{f(\mu^*)+s}{\mu^* f(\mu^*)+s}\right)} > 0 \tag{4.75}$$

which implies that the critical points of $f(\mu)$ can be only local minimum. Therefore, since $f(\mu)$ is differentiable throughout its domain and has no local maximum, it can only have a single local minimum at μ^*, i.e., solution of (4.74), which would be the global minimum as well. Furthermore, the function $f(\mu)$ is non-increasing within the interval $(0,\ \mu^*)$. Therefore, the solution to the constrained problem can be either at μ^* or at the upper limit of the feasible interval (i.e., $\sigma/(K+1)$) as stated in (4.40). $\square$

Chapter 5

Relay-Assisted Free-Space Quantum-Key Distribution

In this chapter, we study free-space quantum-key distribution (QKD) as a particular application of the FSO communication and propose a relay-assisted transmission technique to overcome the range limitations in the terrestrial free-space QKD systems. Our proposed relay-assisted QKD system employs passive relay(s). The relays are passive in the sense that they simply redirect the qubits without any detection or quantum measurement involved. These relays, which can be implemented by adaptive optics [58, 59, 60, 61, 62, 63], reconstruct the turbulence-degraded wave-front of the received beam and redirect the resulting collimated beam to the next relay or destination.

We investigate the efficiency of such relay-assisted systems to combat the range limitations in a terrestrial scenario. Based on a near-field analysis of the free-space optical systems, we derive an upper-bound on quantum bit error rate (QBER) as a performance criterion of QKD systems. Our results demonstrate that the relay-assisted scheme is able to outperform point-to-point direct transmission for long link ranges in which turbulence effects are particularly degrading.

5.1 Related Works

In today's world, wireless and wired communication networks transport huge volumes of data including highly confidential information. Therefore, the privacy of information and the security of the network are of the utmost concern. Conventional cryptosystems are able to offer only computational security within the limitations of computing power. Quantum cryptography, on the other hand, builds upon the basic principles of quantum mechanics and promises unconditional security between two legitimate parties.

In analysis, design, and optimization of QKD systems, a critical issue to consider is the operating environment. The common form of quantum channel which has been intensively studied so far is fiber optic. Although today's telecommunications networks based on optical fibers are very advanced, such channels may not always be available. With the recent commercialization successes, FSO technology has reached to a certain maturity for classical data transmission and is a reliable alternative to fiber optics in quantum cryptographic applications as well. In contrast to optical fibers, the dispersion (birefringence) effects of FSO links are negligible especially at the low-loss transmission windows of atmosphere (e.g., around wavelength of 770 nm) [32]. This guarantees the consistency of the propagating photon's polarization and makes FSO particularly attractive for QKD systems.

Previous studies on terrestrial free-space QKD systems have presented analytical approaches to characterize atmospheric effects [64, 65, 66] and demonstrated some experimental results [67, 68, 69]. A major drawback of QKD systems either operating through fiber optic or atmospheric links (free-space optical links) is the range limitation. In free-space QKD systems, this performance limitation is due to absorption, scattering, diffraction, and turbulence degradation experienced in atmospheric channels [64, 65, 66, 67, 68, 69].

Relay-assisted QKD has been originally proposed in [70] for fiber optic QKD systems. In the relaying scheme of [70] called as *quantum repeater*, long quantum channel is divided into shorter hops in which perfect entangled pairs are created. Connecting these individual entangled pairs though entanglement swapping leads to a single entangled pair which is used for QKD based on Ekert's protocol. The quantum repeaters

are able to improve the performance by overcoming the exponential path loss of signal. However, they require using quantum memory and entanglement purification to ensure creation of perfect entangled pairs in the individual hops.

In [71], a simpler relaying scheme has been proposed which avoids the use of quantum memory and entanglement purification. This scheme is not anymore able to mitigate the exponential loss of signal, but it still improves the performance of fiber optic QKD systems by suppressing the aggravated effect of detector dark counts experienced in long distance links. Unlike [70, 71], a class of quantum relays called as *trusted relays* have been further introduced in [72, 73] which are assumed sufficiently reliable to have partial or perfect knowledge of the distributing keys. For example, a trusted quantum relay may perform the well-known intercept/resend eavesdropping strategy to direct Alice's transmitted qubits to Bob without endangering the security of the QKD system [72].

Quantum relaying has been also studied over FSO channels, but the current results are mainly restricted to the satellite transmission [74, 75]. In [74], Hughes et al. have considered a relay-assisted QKD scenario for satellite communication between two terrestrial nodes without line-of-sight path to each other. A trusted relay in a satellite generates secure keys with the nodes and then reveals the exclusive disjunction (XOR) of the two keys [74]. To support the idea, a feasibility analysis is also reported in [74] based on the estimation of key generation capability of QKD system between a ground station and a low earth orbit (LEO) satellite. In [75], Aspelmeyer et al. have studied a similar satellite-based QKD set-up using quantum entanglement. They have investigated the link attenuation of surface/satellite-to-satellite systems to demonstrate the feasibility of their idea.

5.2 The Relay-Assisted QKD System

We consider a relay-assisted free-space QKD system in which the transmitted qubits by Alice travel through K relay nodes before detection by Bob. Conventional amplify-and-forward and decode-and-forward relaying schemes typically employed in wireless

communications are of no use for QKD systems[1]. Here, we consider passive relays which simply redirect the qubits to the next relay node or to Bob without performing any measurement or detection process. Therefore, any eavesdropping attempt which takes place either at the relay nodes or in the middle of the FSO link can be still detected by Alice and Bob during the error correction process of the BB84 protocol.

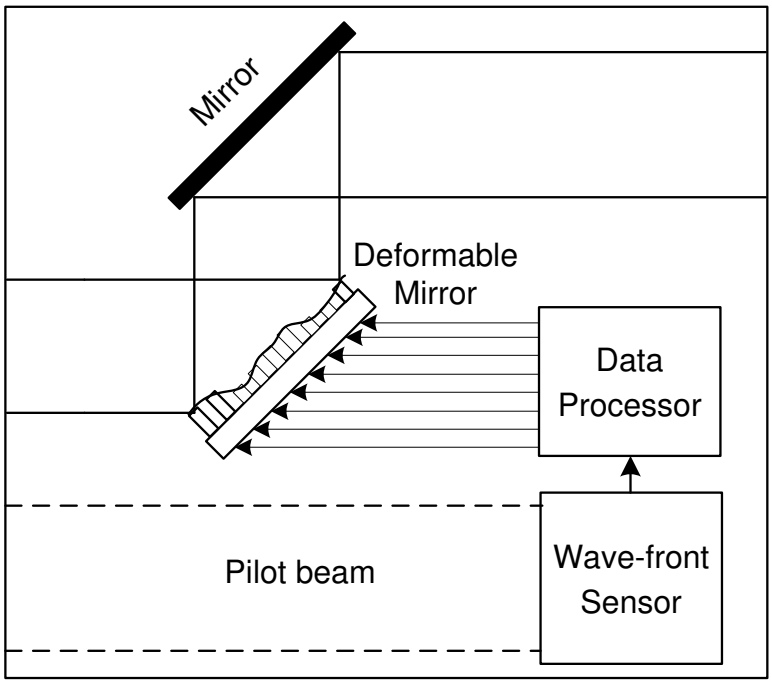

Figure 5.1: The schematic diagram of a typical adaptive optics system.

The relays receive the transmitted optical beam and reconstruct its turbulence-degraded wave-front using adaptive optics before pointing it to the next relay or Bob. Adaptive optics involves the use of a wave-front sensor and a deformable mirror as depicted in figure 5.1. The wave-front sensor estimates the effects of atmospheric turbulence by measuring the turbulence-induced distortions in the received pilot-beam wave-front at the beginning of each block of key transmission. The deformable mir-

[1]No amplification can be performed at relay nodes without perturbing the quantum system [32]. Furthermore, since the relays are not necessarily trusted, neither measurements nor detection can be performed.

ror then uses this information to correct the atmospheric wave-front distortions of the received qubit beam.

Different adaptive optics systems with full [59, 60, 61] and partial [62, 63] compensation are proposed in the literature. In a fully compensated adaptive optics system, the scale of the operating element (sub-aperture of the wave-front sensor and the actuator of the deformable mirror) matches the scale of the atmospheric correlation length ($\sim r_0$ given by (2.15)) which is inversely related to the link length. Since the proposed relay-assisted system divides the link range into shorter hops, adaptive optics can be implemented relatively easier with larger, therefore fewer, elements. Furthermore, we note that the atmospheric coherence time is inversely related to the link length [34]. Therefore, longer atmospheric coherence time can be experienced in the shorter hops decreasing the rate of required updates in the adaptive optics system.

The proposed relay-assisted QKD system uses BB84 protocol for key distribution as described in chapter 2. For each qubit, Alice generates a polarized optical pulse with an average photon number of n_s which is encoded with the corresponding polarization state of the qubit for a randomly chosen basis. Due to the atmospheric effects (i.e., diffraction, atmospheric turbulence, and absorption-and-scattering loss), the i^{th} relay node ($i = 1, 2...K$) collects only a random fraction γ_i of the transmitted photons in the i^{th} hop. The relay then redirects the received photons by pointing the light beam to the next relay node (or Bob) without performing any amplification/detection process. At the destination side, Bob collects a fraction γ_{K+1} of the transmitted photons from the last relay node which corresponds to an overall fraction $\gamma = \gamma_1\gamma_2\cdots\gamma_{K+1}$ of the originally transmitted photons from Alice[2].

In the i^{th} hop ($i = 1, 2, \cdots, K+1$), a spatial beam pattern $\xi_i(\vec{\rho})$ is assumed to be transmitted from a circular pupil R_i with diameter d_i located in the $z = 0$ plane[3]. A field pattern $\xi_i'(\vec{\rho}')$ is collected within the pupil R_i' with diameter d_i' in the $z = L_i$ plane where L_i is the length of i^{th} hop. The received field pattern by the i^{th} relay

[2]We assume negligible optics losses and perfect correction of wave-front turbulence-induced distortions by adaptive optics within the relay terminals.

[3]Without loss of generality, we assume that the coordinate system is properly transformed for each hop.

$(i = 1, 2, \cdots, K)$ or Bob $(i = K + 1)$ can be expressed similar to (2.2) as

$$\xi_i'(\vec{\rho}') = \int_{R_i} \xi_i(\vec{\rho}) h_i(\vec{\rho}, \vec{\rho}') e^{-aL_i/2} d\vec{\rho} \tag{5.1}$$

where a is the extinction coefficient determining the loss due to absorption and scattering and $h_i(\vec{\rho}, \vec{\rho}')$ denotes the Green's function for atmospheric propagation through clear turbulent air over the i^{th} hop which is given by (2.3). The fraction parameter [64] of the i^{th} hop γ_i $(i = 1, 2, \cdots, K + 1)$ is expressed in terms of transmit and receive beam patterns as

$$\gamma_i = \frac{\int_{R_i'} |\xi_i'(\vec{\rho}')|^2 d\vec{\rho}'}{\int_{R_i} |\xi_i(\vec{\rho})|^2 d\vec{\rho}}. \tag{5.2}$$

We assume that the relays and the destination collect an average number of n_{B0} background photons per polarization. Taking into account the background photons redirected by the relays, the total average number of background photons collected at Bob's receiver per polarization can be expressed as[4]

$$\begin{aligned} n_B &= n_{B0}(1 + \gamma_{K+1} + \gamma_K \gamma_{K+1} + \cdots + \gamma_2 \cdots \gamma_{K+1}) \\ &= n_{B0} \left(1 + \sum_{i=2}^{K+1} \prod_{j=i}^{K+1} \gamma_j \right). \end{aligned} \tag{5.3}$$

Besides the background noise, each of the single-photon detectors (APDs) at Bob's receiver registers an average number of n_D dark counts.

[4]Equation (5.3) overestimates the effect of redirected background photons for the relay-assisted system since the associated path loss is assumed to be as low as the path loss of the transmitted collimated beam.

5.3 Performance Analysis

We investigate the performance of the relay-assisted free-space QKD system through the derivation of an upper-bound on QBER. QBER is given by [32]

$$\text{QBER} = \frac{\Pr(\text{error})}{\Pr(\text{sift})} \tag{5.4}$$

where Pr(sift) and Pr(error) are probabilities of sift and error, respectively. Using the results from [64], we can express the conditional sift and error probabilities of the relay-assisted QKD system (conditioned on $\boldsymbol{\gamma} = \{\gamma_1, \gamma_2, \cdots \gamma_{K+1}\}$) as

$$\Pr(\text{sift}|\boldsymbol{\gamma}) = \eta \left(n_S\gamma/2 + 2n_N\right) \exp\left[-\eta \left(n_S\gamma + 4n_N\right)\right], \tag{5.5}$$

$$\Pr(\text{error}|\boldsymbol{\gamma}) = \eta n_N \exp\left[-\eta(n_S\gamma + 4n_N)\right] \tag{5.6}$$

where η is the quantum efficiency of Geiger-mode APDs and $n_N \triangleq n_B/2 + n_D$ denotes the average number of noise counts at each of Bob's detectors.

To obtain unconditional probabilities of sift and error, we first need to statistically characterize $\boldsymbol{\gamma} = \{\gamma_1, \gamma_2, \cdots \gamma_{K+1}\}$. We use the singular value decomposition of $h_i(\vec{\rho}, \vec{\rho}')$, $i = 1, 2, \cdots, K+1$, which is given by [64, 76]

$$h_i(\vec{\rho}, \vec{\rho}') = \sum_{n=1}^{\infty} \sqrt{\mu_i^n} \varphi_i^n(\vec{\rho}') \Phi_i^{n*}(\vec{\rho}) \tag{5.7}$$

where μ_i^n's are the eigenvalues which satisfy $1 \geqslant \mu_i^1 \geqslant \mu_i^2 \geqslant \mu_i^3 \geqslant \cdots \geqslant 0$. $\{\Phi_i^n(\vec{\rho})\}$ and $\{\varphi_i^n(\vec{\rho}')\}$ are, respectively, the input and output eigenfunction vectors which constitute complete orthonormal sets on R_i and R_i'. Let μ_i denote the largest eigenvalue in (5.7), i.e., $\mu_i \triangleq \mu_i^1$, and $\Phi_i(\vec{\rho})$ denote the corresponding input eigenfunction (i.e., $\Phi_i(\vec{\rho}) \triangleq$

$\Phi_i^1(\vec{\rho})$). Using (5.1), (5.2), and (5.7), an upper bound on the fraction parameter γ_i can be obtained as [64]

$$\gamma_i \leqslant \mu_i e^{-aL_i} \tag{5.8}$$

with equality when $\bar{\xi}_i(\vec{\rho}) = \Phi_i(\vec{\rho})$. Here, $\bar{\xi}_i(\vec{\rho})$ is the normalized transmit beam pattern of the i^{th} hop which can be expressed as

$$\bar{\xi}_i(\vec{\rho}) = \frac{\xi_i(\vec{\rho})}{\sqrt{\int_{R_i} |\xi_i(\vec{\rho})|^2 d\vec{\rho}}}. \tag{5.9}$$

Under atmospheric turbulence conditions which exhibit a slowly-varying nature, Alice and relay nodes can employ adaptive optics to generate the optimum transmit field pattern as

$$\xi_i(\vec{\rho}) = \left[\sqrt{\int_{R_i} |\xi_i(\vec{\rho})|^2 d\vec{\rho}}\right] \Phi_i(\vec{\rho}) \tag{5.10}$$

which guarantees that the equality in (5.8) is achieved yielding the optimum fraction parameter (i.e., maximum power transfer). Let μ denote the product of the individual largest eigenvalues, i.e., $\mu = \mu_1 \mu_2 \cdots \mu_{K+1}$ $(0 \leqslant \mu \leqslant 1)$. The optimum overall fraction parameter can be then written as $\gamma = \mu e^{-aL}$ where $L = L_1 + L_2 + \cdots + L_{K+1}$. Unfortunately, for near-field propagation, a statistical description of μ_i is not available in the literature. However, noting that $E\{\mu_i\}$ is the maximum average power transfer over the i^{th} hop obtained through the use of optimum beam pattern, it can be simply lower bounded by the average power transfer of any deterministic beam pattern, such as in [64, 76], as

$$E\{\mu_i\} \geqslant \hat{\mu}_i \equiv \frac{8\sqrt{D_f}}{\pi} \int_0^1 e^{-\frac{D_i(d_i x)}{2}} (\cos^{-1}(x) - x\sqrt{1-x^2}) J_1(4x\sqrt{D_f}) dx \tag{5.11}$$

where $J_1(\cdot)$ is the first-order Bessel function of the first kind, $D_i(\cdot)$ is the i^{th} hop's spherical-wave wave structure function given by $D_i(\nu) = 1.09k^2C_n^2L_i\nu^{5/3}$, and D_f is the Fresnel number product of the R_i and R_i' pupils given by $D_f = ((\pi d_i d_i')/4\lambda L_i)^2$.

5.3.1 Bound on the Sift Probability

Let $\boldsymbol{\mu} = \{\mu_1, \mu_2, \cdots \mu_{K+1}\}$ denote the vector of the largest eigenvalues (within each hop) and $V(\boldsymbol{\mu})$ be a function of $\boldsymbol{\mu}$ defined as

$$\begin{aligned} V(\boldsymbol{\mu}) &= \eta(n_S\gamma + 4n_N) \\ &= \eta\left[n_S e^{-aL}\prod_{j=1}^{K+1}\mu_j + 2n_{B0}\left(1 + \sum_{i=2}^{K+1}\prod_{j=i}^{K+1} e^{-aL_j}\mu_j\right) + 4n_D\right]. \end{aligned} \tag{5.12}$$

Using (5.12), we can rewrite (5.5) for the case of optimum beam transmission as

$$\Pr(\text{sift}|y) = \frac{V(\boldsymbol{\mu})}{2}e^{-V(\boldsymbol{\mu})} = \frac{(\alpha y + \beta)}{2}e^{-(\alpha y+\beta)} \tag{5.13}$$

where α, β, and y are given by[5]

$$\alpha = V(\boldsymbol{\mu} = \mathbf{1}) - V(\boldsymbol{\mu} = \mathbf{0}) = \eta\left[n_S e^{-aL} + 2n_{B0}\left(\sum_{i=2}^{K+1}\prod_{j=i}^{K+1} e^{-aL_j}\right)\right], \tag{5.14}$$

$$\beta = V(\boldsymbol{\mu} = \mathbf{0}) = \eta(2n_{B0} + 4n_D), \tag{5.15}$$

$$y = \frac{V(\boldsymbol{\mu}) - \beta}{\alpha}. \tag{5.16}$$

[5] $\mathbf{0}$ and $\mathbf{1}$ denote all-zero and all-one vectors, respectively.

Averaging (5.13) over y, we obtain the sift probability as

$$\Pr(\text{sift}) = \int_0^1 \frac{(\alpha y + \beta)}{2} e^{-(\alpha y+\beta)} p(y) dy \tag{5.17}$$

where $p(y)$ is the probability density function of y. Defining $f(y) \triangleq (\alpha y/2+\beta/2)e^{-(\alpha y+\beta)}$ and noting that it is a concave function for $0 \leqslant \alpha y + \beta < 2$, we can lower bound (5.17) as

$$\begin{aligned}\Pr(\text{sift}) &\geqslant \int_0^1 [f(0)(1-y) + f(1)y] p(y) dy \\ &= f(0)(1 - E\{y\}) + f(1)E\{y\}. \end{aligned} \tag{5.18}$$

Using (5.11), (5.12), (5.14), (5.15), and (5.16) and the fact that the elements of $\boldsymbol{\gamma}$ (and therefore the elements of $\boldsymbol{\mu}$) are statistically independent, $E\{y\}$ can be bounded as

$$E\{y\} \geqslant \hat{y} \triangleq \frac{n_S e^{-aL} \prod_{j=1}^{K+1} \hat{\mu}_j + 2n_{B0} \left(\sum_{i=2}^{K+1} \prod_{j=i}^{K+1} e^{-aL_j} \hat{\mu}_j \right)}{n_S e^{-aL} + 2n_{B0} \left(\sum_{i=2}^{K+1} \prod_{j=i}^{K+1} e^{-aL_j} \right)}. \tag{5.19}$$

Inserting (5.19) in (5.18) and noting that $f(y)$ is increasing for $0 \leqslant \alpha y + \beta < 1$, we have a lower bound on the sift probability as

$$\begin{aligned}\Pr(\text{sift}) &\geqslant f(0)(1-\hat{y}) + f(1)\hat{y} \\ &= (\beta/2)e^{-\beta}[1-\hat{y}] + (\alpha/2 + \beta/2)\, e^{-(\alpha+\beta)}\hat{y} \end{aligned} \tag{5.20}$$

under the practically reasonable condition $\eta(n_S e^{-aL} + 4n_N) < 1$.

5.3.2 Bound on the Error Probability

Ignoring the effects of diffraction and turbulence on the redirected background photons (from the relays), a pessimistic noise count at each of Bob's detectors (i.e., $\hat{n}_N = n_N|_{\boldsymbol{\mu}=\mathbf{1}}$) can be written as

$$\hat{n}_N = \frac{n_{B0}}{2}\left(1 + \sum_{i=2}^{K+1}\prod_{j=i}^{K+1} e^{-aL_j}\right) + n_D \tag{5.21}$$

which obviously satisfies $\hat{n}_N \geqslant n_N$. Therefore, we can bound (5.6) as

$$\Pr(\text{error}|\boldsymbol{\gamma}) \leqslant \eta\hat{n}_N e^{-\eta(n_S\gamma + 4\hat{n}_N)}. \tag{5.22}$$

Inserting $\gamma = \mu e^{-aL}$ in (5.22) and averaging the resulting expression over μ, we have

$$\Pr(\text{error}) \leqslant \int_0^1 \eta\hat{n}_N e^{-\eta(n_S\mu e^{-aL} + 4\hat{n}_N)} p(\mu)d\mu \tag{5.23}$$

where $p(\mu)$ is the pdf of μ. Defining $g(\mu) \triangleq \eta\hat{n}_N e^{-\eta(n_S\mu e^{-aL} + 4\hat{n}_N)}$ and noting that it is a convex function, we can further upper bound (5.23) as

$$\begin{aligned}\Pr(\text{error}) &\leqslant \int_0^1 [g(0)(1-\mu) + g(1)\mu]P(\mu)d\mu \\ &= g(0)(1 - E\{\mu\}) + g(1)E\{\mu\} \\ &\leqslant g(0)(1-\hat{\mu}) + g(1)\hat{\mu}\end{aligned} \tag{5.24}$$

where we define $\hat{\mu} = \hat{\mu}_1\hat{\mu}_2\cdots\hat{\mu}_{K+1}$. The first bound in (5.24) comes from the convexity of $g(\mu)$ and the last bound results from the bound in (5.11) assuming that μ_i's are

statistically independent and noting that $g(\mu)$ is a decreasing function. Expanding (5.24), we obtain

$$\Pr(\text{error}) \leqslant \eta\hat{n}_N e^{-\eta 4\hat{n}_N}[1-\hat{\mu}] + \eta\hat{n}_N e^{-\eta(n_S e^{-aL}+4\hat{n}_N)}\hat{\mu}. \tag{5.25}$$

Finally, replacing (5.20) and (5.25) in (5.4), we obtain an upper bound on QBER as

$$\text{QBER} \leqslant \frac{2\eta\hat{n}_N e^{-\eta 4\hat{n}_N}\left[(1-\hat{\mu}) + e^{-\eta n_S e^{-aL}}\hat{\mu}\right]}{\beta e^{-\beta}\,(1-\hat{y}) + (\alpha+\beta)\,e^{-(\alpha+\beta)}\hat{y}}. \tag{5.26}$$

It is important to note that, although at the beginning of this derivation we consider optimum beam shaping in (5.8) to achieve the equality, the derived bound in (5.26) is valid for non-optimized transmission as well. This is because, in (5.11), the lower-bound on average μ_i is based on the transmission of a deterministic beam pattern rather than the optimum one [64].

Finally, as a benchmark, to demonstrate the efficiency of the proposed relaying scheme in compensating the degrading effects of atmospheric turbulence, we consider a QKD system operating over non-turbulent air. The exact QBER of such a QKD system is given by [64]

$$\text{QBER} = \frac{2n_N}{n_S\mu_0 e^{-aL_{AB}} + 4n_N} \tag{5.27}$$

where L_{AB} is the length of line-of-sight link connecting Alice and Bob and μ_0 is the largest eigenvalue of the singular value decomposition of vacuum-propagation Green's function given in [77].

5.4 Performance Results and Discussions

In this section, we demonstrate the performance of relay-assisted QKD scheme under consideration and compare its performance with point-to-point direct transmission. We assume $\lambda = 0.77\,\mu$m, $C_n^2 = 1 \times 10^{-15}\,\mathrm{m}^{-2/3}$, and operation in clear weather conditions with visibility of 10 km which corresponds to the absorption and scattering loss of about 2 dB/km. Under the assumption that proper temporal, spectral, and spatial filters are employed, a constant average number of background count, $n_{B0} = 10^{-4}$ is assumed [67]. Bob's APD detectors are operated at the detection efficiency of $\eta = 0.5$ with average dark count of $n_D = 10^{-6}$ [64]. We also assume that all the receive and transmit pupils have the same diameter d and the relay nodes are located equidistant along the path connecting Alice and Bob, i.e., $L_{AB} = L$.

Before we illustrate QBER performance, we study the behavior of the overall fraction of collected photons at Bob's receiver, i.e., γ. We normalize γ by the total amount of absorption and scattering loss experienced in the direct path from Alice to Bob, i.e., $e^{-aL_{AB}}$. Based on the assumption made on the relay locations, we have $\gamma/e^{-aL_{AB}} = \mu e^{-aL}/e^{-aL_{AB}} = \mu$. Figure 5.2 plots the lower bound on the average of μ (i.e., $E\{\mu\} = \prod_i E\{\mu_i\}$) calculated from (5.11) for a relay-assisted QKD system operating over a turbulent atmosphere with pupil diameter of $d = 10\,$cm. We consider relay-assisted systems with different number of relays, i.e., $K = 1$, 2, and 3. The results for direct QKD systems operating over turbulent (i.e., $\hat{\mu}$, $K = 0$) and non-turbulent (i.e., μ_0 given in [77]) atmosphere are further included as benchmarks.

Comparing the performance curves of over the turbulent and non-turbulent atmosphere for the direct system in figure 5.2, we observe that atmospheric turbulence degrades the performance of QKD systems particularly over the long links where stronger turbulence effects are experienced. For example, the average number of photons collected over a 10 km non-turbulent atmospheric path is more than three times the average number of collected photons in the corresponding turbulent case.

It is obvious from figure 5.2 that, similar to the classical multi-hop FSO systems studied in the previous chapters, the relay-assisted QKD scheme takes advantage of the resulting shorter hops with weaker turbulence effects and improves the performance of

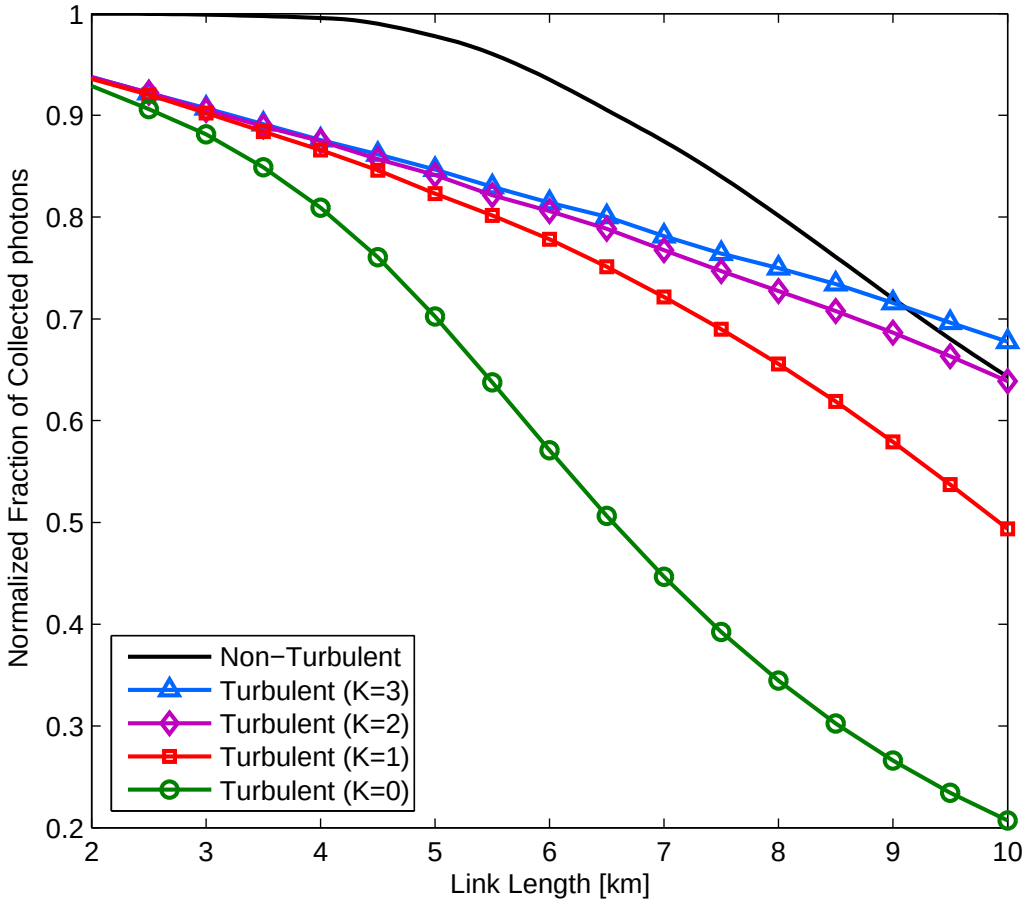

Figure 5.2: The normalized fraction of collected photons at Bob's receiver in relay-assisted QKD system for different number of relays ($d = 10$ cm).

the QKD system. For example, deployment of two relays would be sufficient to compensate the decrease in the average number of collected photons caused by turbulence for a 10 km link.

Figure 5.3 demonstrates the upper bound on QBER performance of the relay-assisted and direct QKD system operating over turbulent atmosphere as a function of the link range ($L_{AB} = L$) which are calculated through (5.26). We assume $d = 10\,\text{cm}$ and $n_s = 1$. As a benchmark, we include the QBER performance of direct QKD system

over non-turbulent atmosphere calculated through (5.27). It is observed from figure 5.3 that the relay-assisted scheme improves the QBER performance of the links longer than 5.5 km. For example, for a link with the length of 10 km, the presence of turbulence causes 193% increase in QBER of the direct QKD system. However, this degradation is drastically reduced to only 26% for a triple-hop ($K = 2$) relay-assisted QKD system.

Although the triple-hop relay-assisted QKD system can significantly improve the QBER performance, it should be emphasize that it cannot achieve the QBER perfor-

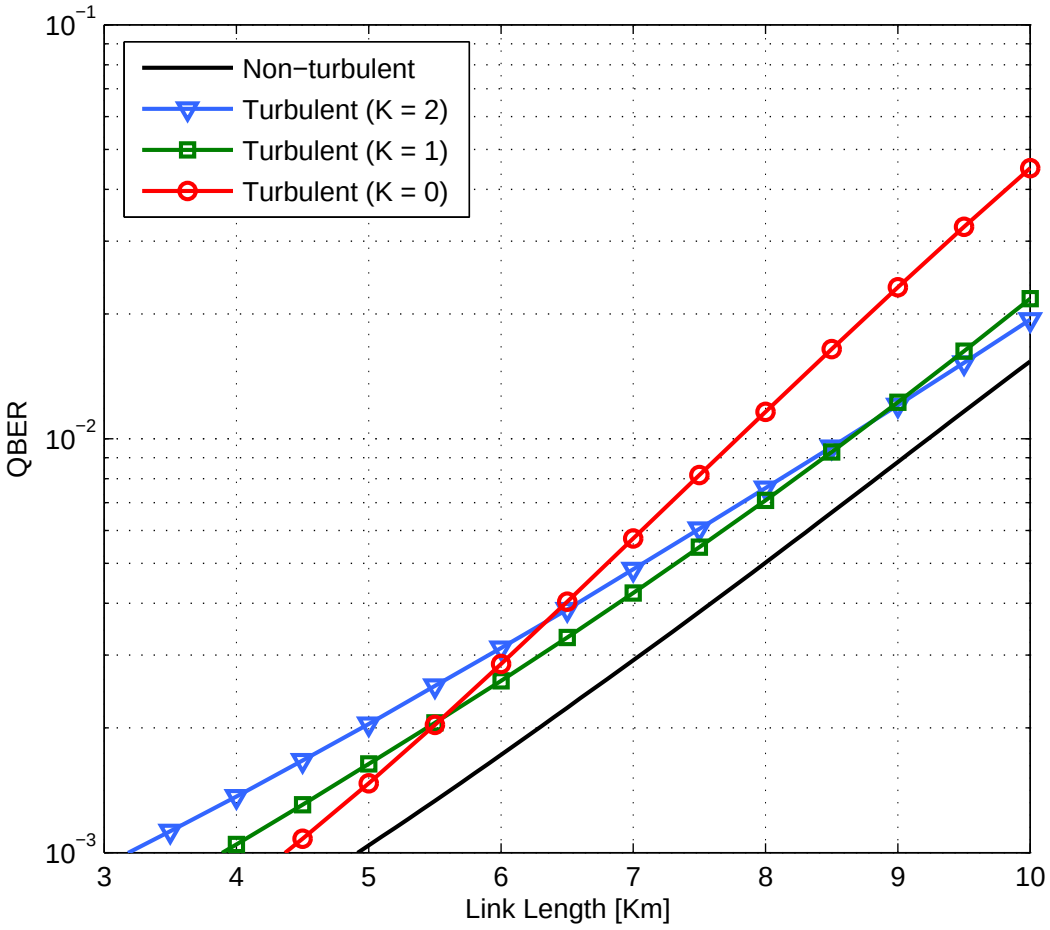

Figure 5.3: The QBER of the relay-assisted QKD system for different number of relays ($d = 10$ cm and $n_s = 1$).

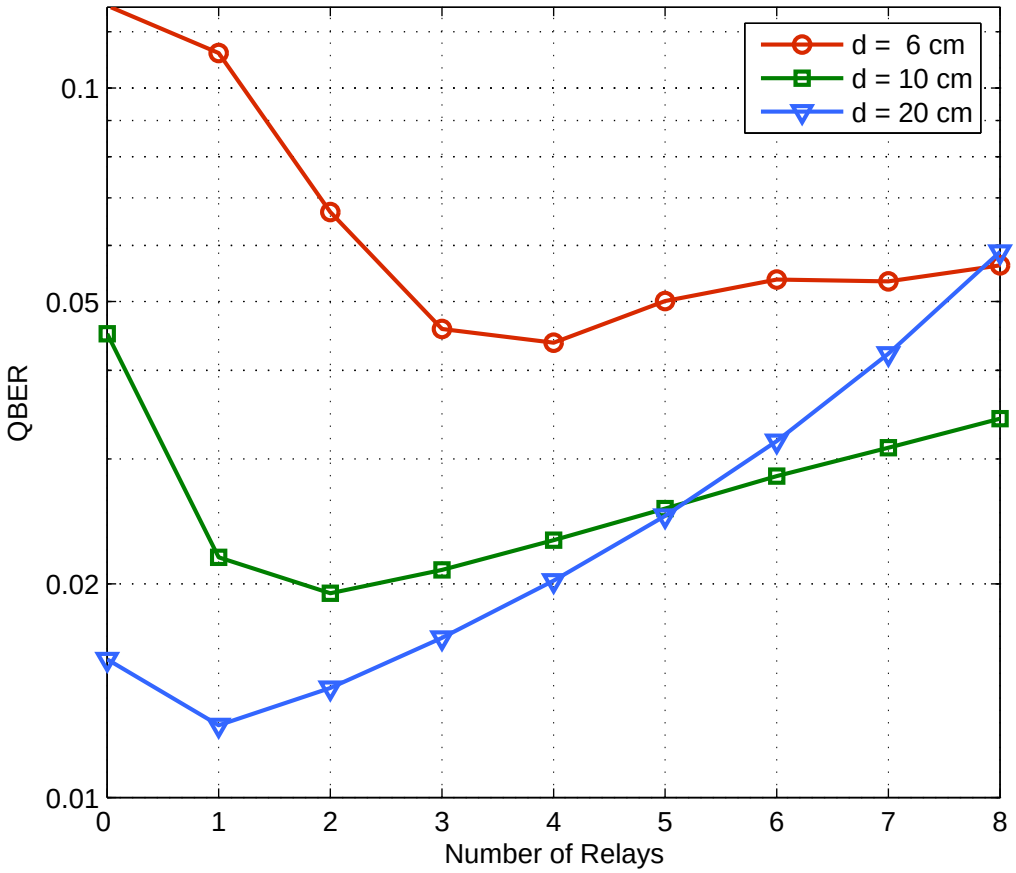

Figure 5.4: The QBER of the relay-assisted QKD system versus the number of relays with different pupil diameters ($L = 10$ km and $n_s = 1$).

mance of the direct non-turbulent case as it might be expected from figure 5.2. This is a result of the accumulation of background noise[6] redirected from relays to Bob's receiver. In other words, there are two reverse effects which need to be considered. The relay-assisted scheme increases the average number of collected photons coming from Alice, but it also results in an increase of the average number of background photons

[6]Note that, in our analysis, this effect has been exaggerated in the derivation of the upper bound on QBER of the relay-assisted system (c.f. equations (5.3) and (5.21)).

at Bob's receiver. It is therefore important to determine the optimum number of relays (in the sense of QBER minimization) to be deployed.

In figure 5.4, we demonstrate the upper bound on QBER of the relay-assisted QKD system with $n_s = 1$ versus the number of relays. We fix the link length as 10 km and consider different pupil diameters i.e., $d = 6\,\text{cm},\ 10\,\text{cm},$ and $20\,\text{cm}$. We find out that four, two and one relays are sufficient to minimize QBER respectively for $d = 6\,\text{cm},\ 10\,\text{cm},$ and $20\,\text{cm}$. It is observed that the optimum number of relays increases

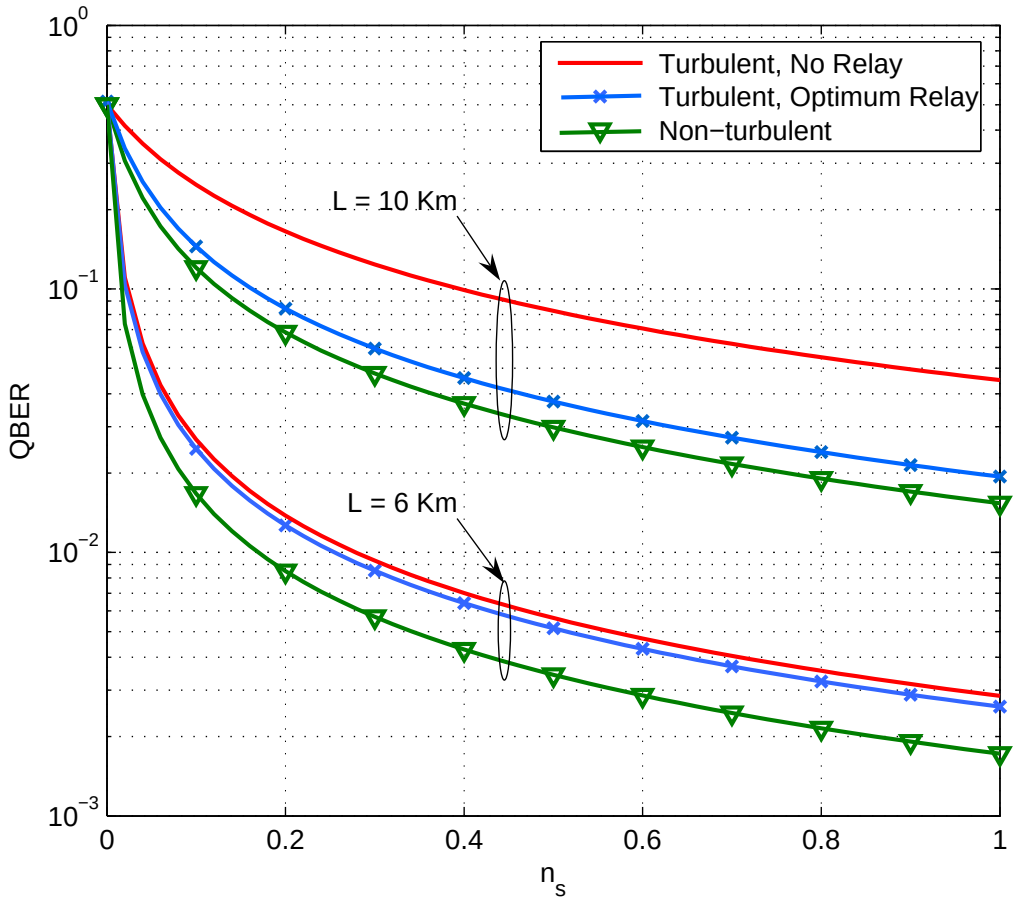

Figure 5.5: The QBER of the relay-assisted QKD system versus n_s for different link lengths ($d = 10$ cm).

as the pupil sizes decrease. This comes from the fact that for the system with smaller pupil sizes, shorter hops are required for effective compensation of the diffraction and turbulence effects.

In figure 5.5, we demonstrate the upper bound on QBER of the relay-assisted QKD system as a function of the average number of transmitted photons by Alice, n_s. We consider $L = 6\,\text{km}$ and $10\,\text{km}$ and assume $d = 10\,\text{cm}$. Note that the QBER performance improvements demonstrated in figures 5.3 and 5.4 were obtained for a fixed value of $n_s = 1$. From figure 5.5, we observe that decreasing the value of n_s does not considerably affect the amount of QBER improvement and therefore, similar conclusions can be also made for these lower values of n_s.

Chapter 6

Conclusions

In this thesis, we introduced the relay-assisted free-space optical system as a very promising technique to overcome atmospheric turbulence degradations whether employed over a classical or a quantum optical channel. FSO communication is a line-of-sight optical transmission technique through the atmosphere which provides a cost-effective and easy-to-install alternative to fiber optics. A major degrading factor in FSO communication links is the atmospheric turbulence degradations. To mitigate the degrading effect of turbulence-induced fading, different techniques such as spatial diversity have been proposed in the literature. However, they are not so effective in longer ranges where the atmospheric turbulence is most degrading. The contributions of this work can be summarized as follows.

6.1 Relay-Assisted FSO Communication over the Gaussian Channel

In chapter 3, we studied the relay-assisted FSO communication over a Gaussian channel model of the intensity modulation direct detection systems. We have investigated serial and parallel relaying, each of which operates either in amplify-and-forward or decode-and-forward mode. The fact that fading variance is distance-dependent in FSO systems

constitutes a major difference between wireless RF and wireless optical systems. This lets multi-hop FSO transmission smartly exploit the shorter distance in the resulting hops and brings substantial improvements against the degrading effects of turbulence-induced fading. As a possible alternative to serial relaying, we have also considered parallel relaying where an artificial broadcasting is obtained through the use of multiple transmitter apertures directed to relay nodes.

Through the derivation of outage probability and Monte-Carlo simulations, we have quantified the performance improvements obtained for both parallel and serial relaying schemes. Specifically, for a single-relay serial relaying scheme (i.e., dual-hop scheme), performance improvements of 12.2 dB and 18.5 dB at the outage probability of 10^{-6} have been obtained for serial relaying with AF and DF modes respectively. For a triple-hop scheme, the respective performance improvements climb up to 17.7 dB and 25.4 dB. In comparison to serial relaying, parallel relaying takes advantage of distance-dependency of fading log-normal variance to a lesser extent and is outperformed by its competitor as the number of relays increases.

We have also quantified the diversity gain of FSO communication systems operating in log-normal fading channels. We have derived so-called relative diversity orders defined based on the outage probability for FSO diversity systems. Specifically, we have demonstrated that diversity orders of $(K+1)^{11/6}$, and $2^{11/6}K$ are obtained, respectively, for serial and parallel DF relaying schemes employing K relay nodes. Comparing these expressions, we can state the diversity order of the relay-assisted FSO systems with DF relaying in a general form of $N_H^{11/6}N_D$ where N_H and N_D are respectively the number of hops and the number of diversity paths in the relaying configuration. It is observed that the serial relaying factor (i.e., $N_H^{11/6}$) in this diversity order expression is stronger than the parallel relaying factor (i.e., N_D). Therefore, we can confirm our previous finding that a parallel relaying scheme ($N_D \geqslant N_H$) is benefited from the distance-dependency of fading log-normal variance less than a serial relaying scheme ($N_H \geqslant N_D$) and therefore is outperformed by its counterpart as the number of relays increases.

6.2 Relay-Assisted FSO Communication over the Poisson Channel

In chapter 4, we have studied the outage behavior of multi-hop Poisson channel degraded by atmospheric turbulence. This is the suitable model for multi-hop FSO communication with shot-noise-limited direct detection receivers. In chapter 3, under a Gaussian channel model, we showed that such a serial relaying strategy can significantly outperform the parallel relaying and direct transmission counterparts. Therefore, we focused on the multi-hop relaying scheme in chapter 4.

We considered a decode-and-forward relaying strategy for the multi-hop FSO transmission where the turbulence-induced degradation is described by a block fading model. Under the assumption of perfect CSI at the receiver, the outage probability minimization problem has been solved and power control law (optimal duty cycle) has been presented under peak and average sum power constraints. A number of scenarios based on the availability or lack of CSI at the transmitter along with short or long-term power constraints have been investigated. Moreover, a simple and accurate sup-optimal solution with low complexity has been proposed for the case of perfect CSI with short-term power constraint.

Our numerical results have clearly demonstrated that relay-assisted transmission in a direct-detection Poisson channel significantly improves the outage probability and this improvement enhances as the number of relays increases. For example, an additional performance gain of about 18 dB is observed at the outage probability of 10^{-5} when the second relay is inserted. This is the result of the fact that multi-hop FSO system exploits the distance-dependency of the turbulence-induced fading variance by lowering the fading strength of the individual intermediate hops through the insertion of relay nodes.

We further observe that CSI at the transmitter is not useful for a single-hop Poisson fading channel with short-term constraint, but this information improves the outage probability over the single-hop Poisson fading channel with long-term constraint as well as that over the multi-hop Poisson fading channel with both short- and long-term

power constraints.

Furthermore, it is shown that the proposed sub-optimal solution yields an outage probability very close to the optimum values under short-term constraint for different multi-hop scenarios. Therefore, the sub-optimal power control law with much less complexity can perform almost the same as the more complicated optimal power control law.

6.3 Relay-Assisted Free-Space Quantum-Key Distribution

In chapter 5, we have applied the concept of relaying to a quantum FSO communication system to combat atmospheric turbulence degradation effects. Quantum cryptography builds upon the basic principles of quantum mechanics and promises unconditional security between two legitimate parties. In this technique, quantum-key distribution establishes a secure shared key between the two parties enabling them to encrypt their massages. A major drawback of QKD systems either operating through fiber optic or atmospheric links is the range limitation. To increase the link range, "quantum repeater" and "quantum relay" were proposed based on the idea of entanglement swapping which is not yet practical.

We proposed a terrestrial relay-assisted free-space quantum-key distribution system for long links operating over turbulent atmosphere. Our proposed relay-assisted free-space QKD system employs passive relays. These relays reconstruct the turbulence-degraded wave-front of the received beam using adaptive optics and redirect the resulting collimated beam to the next relay or destination. Based on a near-field analysis, we have derived an upper bound on QBER of the proposed system and presented extensive numerical results on the performance as a function of various system parameters including the number of relays, link range, pupil diameter, etc. Although the relay-assisted scheme results in an increase of the average number of background photons collected at the receiver, it is able to significantly decrease the photon loss caused by diffraction and turbulence. The net gain is an overall performance improvement particularly for

long link ranges.

The significance of this work lies on the ease of its implementation with respect to the alternative relaying strategies. Although use of adaptive optics increases hardware cost but it is a practical technique which can be conveniently implemented unlike the entanglement swapping technique which is required for the previously proposed schemes such as quantum repeater and quantum relay.

6.4 Future Works

In chapter 3, we assumed equal power allocation for the source and the relays. Therefore, optimal power allocation for the Gaussian FSO channel particularly for an unbalanced distribution of the relays can be investigated as a future work. Furthermore, our diversity gain analysis can be extended to the case of amplify-and-forward relaying systems. Investigating the performance of relay-assisted FSO communication employing coherent receivers can be also another topic for the future work.

In chapter 4, we showed that the availability of perfect CSI at the transmitters improves the performance of the relay-assisted FSO system. Although we studied the FSO communication over multi-hop Poisson channel in the case of no CSI at the transmitters, we assumed symmetric channel statistics for the multi-hop system. Therefore, a possible research subject could be the investigation of the effects of CSI imperfection on the performance of the power-optimized multi-hop FSO system in the case of unbalanced distribution of the relays. Moreover, the multi-hop turbulence-degraded Poisson channel can be studied based on the simpler amplify-and-forward relaying configuration.

In chapter 5, our results build upon the ideal assumption of perfect reconstruction of the wave-front using adaptive optics. Our preliminary results [78] suggest that the relay-assisted QKD system could be useful even in the case of partial adaptive correction. However, full investigation of this problem which requires an accurate analytical or numerical modeling of the residual errors induced by partial adaptive correction is the subject of a future work.

References

[1] R. M. Gagliardi and S. Karp, *Optical Communications*, John Wiley & Sons, New York, NY, USA, 1995. 1, 9, 13, 17

[2] R. G. Hunsperger, *Photonic Devices and Systems*, Marcel Dekker, New York, NY 1994. 1

[3] L. C. Andrews, R. L. Phillips and C. Y. Hopen, *Laser Beam Scintillation with Applications*, SPIE Press, 2001. 1, 16

[4] D. Kedar and S. Arnon, "Urban Optical Wireless Communication Networks: The Main Challenges and Possible Solutions", *IEEE Communications Magazine*, vol. 42, no. 5, p.s2-s7, May 2004. 1

[5] X. Zhu and J. M. Kahn, "Free-Space Optical Communication through Atmospheric Turbulence Channels", *IEEE Transactions on Communications*, vol. 50, no. 8, pp. 1293-1300, August 2002. 2, 24

[6] X. Zhu and J. M. Kahn, "Performance bounds for coded free-space optical communications through atmospheric turbulence channels", *IEEE Transactions on Communications*, vol. 51, no.8, p. 1233-1239, August 2003. 2

[7] M. Uysal, S. M. Navidpour, and J. Li, "Error Rate Performance of Coded Free-Space Optical Links over Strong Turbulence Channels", *IEEE Communications Letters*, vol. 8, no. 10, p.635-637, Oct. 2004. 2

[8] X. Zhu and J. M. Kahn, "Markov chain model in maximum-likelihood sequence detection for free-space optical communication through atmospheric turbulence

channels", *IEEE Transactions on Communications*, vol. 51, no. 3, p. 509-516, March 2003. 2

[9] S. M. Haas, *Capacity of and Coding for Multiple-Aperture Wireless Optical Communications*, Ph.D. Dissertation, Massachusetts Institute of Technology, 2003. 2, 3, 12, 16, 31

[10] E. Lee and V. Chan, "Part 1: Optical Communication over the Clear Turbulent Atmospheric Channel Using Diversity," *IEEE Journal on Selected Areas in Communications*, vol. 22, no. 9, pp. 1896-1906, 2004. 2, 3, 24, 32

[11] S.G. Wilson, M. Brandt-Pearce, Q. Cao and M. Baedke, "Optical repetition MIMO transmission with multipulse PPM." *IEEE Journal on Selected Areas on Communications*, vol. 23, no. 9, p.1901-1909, Sept. 2005. 2, 3, 25

[12] S. M. Navidpour, M. Uysal, and M. Kavehrad, "BER Performance of Free-Space Optical Transmission with Spatial Diversity", *IEEE Transactions on Wireless Communications*, vol. 6, no. 8, p. 2813-2819, August 2007. 2, 3, 45

[13] E. Bayaki, R. Schober, and R.K. Mallik, "Performance analysis of MIMO free-space optical systems in gamma-gamma fading," *IEEE Transactions on Communications*, vol. 57, Issue 11, pp. 3415-3424, Nov. 2009. 2, 3

[14] S. M. Haas, J. H. Shapiro, and V. Tarokh, "Space-time codes for wireless optical communications", *EURASIP Journal on Applied Signal Processing*, vol. 3, p. 1-11, March 2002. 2

[15] M. K. Simon and V. Vilnrotter, "Alamouti-type space-time coding for free-space optical communication with direct detection", *IEEE Transactions on Wireless Communications*, vol. 4, no. 1, p. 35-39, Jan. 2005. 3

[16] S. M. Alamouti, "A simple transmitter diversity scheme for wireless communications," *IEEE Journal on Selected Areas on Communications*, vol. 16, p. 1451-1458, Oct. 1998. 3

[17] M. Safari, and M. Uysal, "Do We Really Need OSTBC for Free-Space Optical Communication with Direct Detection?" *IEEE Transactions on Wireless Communications*, vol. 7, pp. 4445-4448, Nov. 2008. 3, 25

[18] J. N. Laneman and G. W. Wornell, "Energy-efficient antenna sharing and relaying for wireless networks," in *Proceeding of IEEE Wireless Communications and Networking Conf. (WCNC)*, Chicago, IL, Sept. 2000. 3

[19] N. Laneman, D. N. C. Tse, and G. W. Wornell, "Cooperative diversity in wireless networks: Efficient protocols and outage behavior," *IEEE Transactions on Information Theory*, vol. 50, no. 12, pp. 3062-3080, Dec. 2004. 3, 25

[20] A. Sendonaris, E. Erkip, and B. Aazhang, "User cooperation diversity-Part I: System description," *IEEE Transactions on Communications*, vol. 51, pp. 1927-1938, Nov. 2003. 3

[21] M. O. Hasna and M. S. Alouini, "Outage probability of multihop transmission over Nakagami fading channels," *IEEE Communication Letters*, vol. 7, pp. 216-218, May 2003. 3

[22] A. S. Acampora and S. V. Krishnamurthy, "A broadband wireless access network based on mesh-connected free-space optical links," *IEEE Personal Communications*, vol. 6, pp. 62-65, Oct. 1999. 3

[23] J. Akella, M. Yuksel, and S. Kalyanaraman, "Error analysis of multihop free-space optical communication," in *Proceeding of IEEE Internatioanl Conference on Communications 2005 (ICC'05)*, Seoul, Korea, May 2005. 3, 4

[24] T. A. Tsiftsis, H. G. Sandalidis, G. K. Karagiannidis, and N. C. Sagias, "Multihop Free-Space Optical Communications Over Strong Turbulence Channels," in *Proceeding of IEEE Internatioanl Conference on Communications 2006 (ICC'06)*, Istanbul, Turkey, June 2006. 3, 4

[25] G. K. Karagiannidis, T. A. Tsiftsis, H. G. Sandalidis, "Outage probability of relayed free space optical communication systems," *Electronics Letters*,Vol. 42, pp. 994-995, Aug. 2006. 3, 4

[26] M. Safari and M. Uysal, "Relay-Assisted Free-Space Optical Communication," *IEEE Transactions on Wireless Communications*, vol. 7, no. 12, pp. 5441-5449, Dec. 2008. 4

[27] M. Safari, and M. Uysal, "Diversity Gain Analysis of Free-Space Optical Communication Systems," in *proceeding of Canadian Conference on Electrical and Computer Engineering (CCECE'08)*, pp. 1239-1244, Niagara Falls, Canada, 2008. 4

[28] M. Safari, M.M. Rad, and M. Uysal, "Multi-Hop Relaying over Turbulent Atmospheric Poisson Channel," under revision in *IEEE Transactions on Communications*. 4

[29] M. Safari and M. Uysal, "Relay-assisted free-space quantum-key distribution," *Journal of Lightwave Technology*, vol. 27, pp. 4508-4515, Oct. 2009. 4

[30] M. Safari, and M. Uysal, "Cooperative Diversity over Log-Normal Fading Channels: Performance Analysis and Optimization," *IEEE Transactions on Wireless Communications*, vol. 7, pp. 1963-1972, 2008. 5, 40, 41

[31] G. Van Assche, *Quantum Cryptography and Secret-Key Distillation*, Cambridge University Press, Cambridge, 2006. 6

[32] N. Gisin, G. Ribordy, W. Tittel and H. Zbinden, "Quantum cryptography," *Reviews of Modern Physics*, vol. 74, p. 145, 2002. 6, 20, 21, 22, 87, 89, 92

[33] J. H. Shapiro, "Imaging and optical communication through atmospheric turbulence," in *Laser Beam Propagation in the Atmosphere*, J. W. Strohbehn, Ed, Berlin, Germany: Springer-Verlag, 1978, ch. 6.E. 10, 11

[34] G. R. Osche, *Optical Detection Theory for Laser Applications*, John Wiley & Sons, New York, NY, USA, 2002. 14, 15, 16, 90

[35] D. L. Fried, "Optical Heterodyne Detection of an Atmospherically Distorted Signal Wave Front," in *Proceeding of IEEE*, vol. 55, pp. 57-67, 1967. 15

[36] J. H. Churnside and S. F. Clifford, "Log-normal Rician Probability Density Function of Optical Scintillations in The Turbulent Atmosphere," *Journal of Optical Society of America*, Vol. 4, No. 10, Oct. 1987, pp. 1923-1930. 16

[37] L. C. Andrews and R. L. Phillips, "I-K distribution as a Universal Propagation Model in Atmospheric Yurbulence," *Journal of Optical Society of America*, Vol. 2, No. 2, Feb. 1985, p. 160. 16

[38] G. Vernam, "Cipher printing telegraph systems for secret wire and radio telegraphic communications," *Journal of American Institute of Electrical Engineers*, vol. 45, pp. 109-115, 1926. 20

[39] C. H. Bennett and G. Brassard, "Quantum cryptography: Public key distribution and coin tossing," in *Proceeding of IEEE International Conference on Computer Systems and Signal Processing*, Bangalore, India, p. 175-179, 1984. 20, 21

[40] A. K. Ekert, "Quantum cryptography based on bell's theorem," *Physical Review Letters*, vol. 67, p. 661-663, 1991. 21

[41] F. C. Leone, L. S. Nelson, and R. B. Nottingham, "The folded normal distribution," *Technometrics*, vol. 3, pp. 543-550, 1961. 29

[42] S. Dolinar, D. Divsalar, J. Hamkins and F. Pollara, "Capacity of pulse-position modulation (PPM) on Gaussian and Webb channels," *JPL TMO Progress Report*, vol. 42-142, pp. 1-31, Apr.-June 2000. 31

[43] E. Biglieri, J. Proakis, and S. Shamai, "Fading channels: Information theoretic and communications aspects," *IEEE Transactions on Information Theory*, vol. 44, no. 6, pp. 2619-2692, Oct. 1998. 31, 55

[44] L. F. Fenton, "The sum of lognormal probability distributions in scatter transmission systems," *IRE Transactions on Communications*, vol. COM-8, pp. 57-67, Mar. 1960. 34

[45] M. K. Simon and M-S. Alouini, *Digital Communication over Fading Channels*, John Wiley & Sons, 2000. 40

[46] S. Verdu, "Poisson communication theory," presented at *the International Technion Communication Day in Honor of I. Bar-David*, Invited Talk, March 1999. Available at http://www.princeton.edu/∼verdu/. 53

[47] Y. M. Kabanov, "The capacity of a channel of a Poisson type," *Theory of Probability and its Application*, vol. 23, pp. 143147, 1978. 53

[48] M. H. A. Davis, "Capacity and cutoff rate for the Poisson-type channels," *IEEE Transactions on Information Theory*, vol. IT-26, pp. 710715, Nov. 1980. 53

[49] A. D. Wyner, "Capacity and error exponent for the direct detection photon channel-Parts 1 & II," *IEEE Transactions on Information Theory*, vol. 34, pp. 1449-1471, Nov. 1988. 53, 56, 57, 58, 68

[50] S. Shami (Shitz) and A. Lapidoth, "Bounds on the capacity of a spectrally constrained Poisson channel," *IEEE Transactions on Information Theory*, vol. 39, pp. 19-29, Jan. 1993. 53, 57

[51] S. M. Haas and J. H. Shapiro, "Capacity of wireless optical communications," *IEEE Journal on Selected Areas in Communications*, vol. 21, pp. 1346-1357, Oct. 2003. 53

[52] K. Chakraborty and P. Narayan, "The Poisson fading channel," *IEEE Transactions on Information Theory*, vol. 53, pp. 2349-2364, Jul. 2007. 53, 56, 58, 60, 68

[53] K. Chakraborty, S. Dey, and M. Franceschetti, "Outage Capacity of the MIMO Poisson Fading channels," *IEEE Transaction on Information Theory*, vol. 54, pp. 4887-4907, Nov. 2008. 53, 60

[54] V. W. S. Chan, "Coding for the turbulent atmosphere optical channel," *IEEE Transactions on Communications*, vol. 30, pp. 269-275, Jan. 1982. 55

[55] G. Caire, G. Taricco, and E. Biglieri, "Optimum power control over fading channels," *IEEE Transactions on Information Theory*, vol. 45, pp. 1468-1489, Jul. 1999. 57, 63, 79, 81

[56] R. M. Corless, G. H. Gonnet, D. E. G. Hare, D. J. Jeffrey, and D. E. Knuth, "On the Lambert W function," *Advances in Computational Mathematics*, vol. 5, pp. 329-359, 1996. 59

[57] T. M. Cover and J. A. Thomas, *Elements of Information Theory*, John Wiley & Sons, New York, NY, USA, 1991. 59

[58] J. W. Hardy, *Adaptive Optics for Astronomical Telescopes*, Oxford University Press, Oxford, 1998. 86

[59] J. W. Hardy, J. E. Lefebvre, and C. L. Koliopoulos, "Real-time atmospheric compensation," *Journal of Optical Society of America*, vol. 67, pp. 360-369, 1976. 86, 90

[60] J. R. P. Angel, "Ground-based imaging of extrasolar planets using adaptive optics," *Nature*, vol. 368, pp. 203-207, 1994. 86, 90

[61] B. M. Levine, E. A. Martinsen, A. Wirth, A. Jankevics, M. Toledo-Quinones, F. Landers, and T. L. Bruno, "Horizontal line-of-sight turbulence over near-ground paths and implications for adaptive optics corrections in laser communications," *Applied Optics*, vol. 37, pp. 4553-4560, 1998. 86, 90

[62] P. Nisenson and R. Barakat, "Partial atmospheric correction with adaptive optics," *Journal of Optical Society of America A*, vol. 4, pp. 2249-2253, 1987. 86, 90

[63] M. C. Roggemann, "Limited degree-of-freedom adaptive optics and image reconstruction," *Applied Optics*, vol. 30, pp. 4227-4233, 1991. 86, 90

[64] J. H. Shapiro, "Near-field turbulence effects on quantum-key distribution," *Physical Review A*, vol. 67, no. 2, p. 022309, 2003. 87, 91, 92, 93, 97, 98

[65] M. Gabbi and S. Arnon, "Quantum key distribution by free space MIMO system," *IEEE/OSA Journal of Lightwave Technology*, vol. 24, no. 8, pp. 3114-3140, August 2006. 87

[66] G. Gilbert and M. Hamrick, "Practical quantum cryptography: A comprehensive analysis (part one)," *MITRE Technical Report*, preprint quant-ph/0009027, September 2000. 87

[67] R. J. Hughes, J. E. Nordholt, D. Derkacs, C. G. Peterson, "Practical free-space quantum key distribution over 10 km in daylight and at night," *New Journal of Physics*, vol. 4, p. 43, 2002. 87, 98

[68] M. Gabbi and S. Arnon, "The effect of turbulence on a quantum-key distribution scheme based on transformation from the polarization to the time domain: laboratory experiment," *Optical Engineering*, vol. 44, no. 4, p. 045002-10-45002-6, April 2005. 87

[69] K. J. Resch, M. Lindenthal, B. Blauensteiner, H. R. Bohm, A. Fedrizzi, C. Kurtsiefer, A. Poppe, T. Schmitt-Manderbach, M. Taraba, R. Ursin, P.Walther, H. Weier, H. Weinfurter, and A. Zeilinger, "Distributing entanglement and single photons through an intra-city, free-space quantum channel," *Optics Express*, vol. 13, pp. 202-209, 2005. 87

[70] H. J. Briegel, W. Dr, J. I. Cirac, and P. Zoller, "Quantum Repeaters: The Role of Imperfect Local Operations in Quantum Communication," *Physical Review Letters*, vol. 81, pp. 5932 - 5935, 1998. 87, 88

[71] B. C. Jacobs, T. B. Pittman, and J. D. Franson, "Quantum relays and noise suppression using linear optics," *Physical Review A*, vol. 66, p. 052307, 2002. 88

[72] C. Elliot, "Building the quantum network," *New Journal of Physics*, vol. 4, p. 46.1-46.12, 2002. 88

[73] H. Bechmann-Pasquinucci and A. Pasquinucci, "Quantum key distribution with trusted quantum relay," eprint *quant-ph/0505089*, 2005. 88

[74] R. J. Hughes, W. T. Buttler, P. G. Kwiat, S. K. Lamoreaux, G. L. Morgan, J. E. Nordholt, and C. G. Peterson, "Free-space quantum key distribution in daylight," *Journal of Modern Optics*, vol. 47, pp. 549-562, 2000. 88

[75] M. Aspelmeyer, T. Jennewein, M. Pfenningbauer, W. R. Leeb, and A. Zeilinger, "Long-distance quantum communication with entangled photons using satellites," *IEEE Journal of Selected Topics in Quantum Electronics*, vol. 9, pp. 1541-1551, 2003. 88

[76] J. H. Shapiro, "Normal-Mode Approach to Wave Propagation in the Turbulent Atmosphere," *Applied Optics*, vol. 13, p. 2614, 1974. 92, 93

[77] D. Slepian, "Analytic solution of two apodization problems," *Journal of Optical Society of America*, vol. 55, p. 1110-1115, 1965. 97, 98

[78] M. Safari and M. Uysal, "Relay-Assisted Free-Space Quantum-Key Distribution with Partial Phase Compensation", in *proceeding of Conference on Lasers and Electro-Optics/Quantum Electronics and Laser Science Conference (CLEO/QELS'10)*, San Jose, California, USA, May 2010. 108